

# **A Novel Adaptive Method for Robotic Wheelchair Navigation Using Brain Signals**

脳信号によるロボット車椅子の適応型  
ナビゲーションシステムの研究

by

**Marsel Mano**

B.Sc., Polytechnic University of Tirana, Tirana, Albania, 2004

M.Sc., Beihang University (BUAA), Beijing, China, 2008

*A thesis submitted in partial fulfillment of the requirements for the degree of  
**Doctor of Philosophy***



Graduate School of Science and Engineering for Education

Faculty of Engineering

University of Toyama

August 9, 2013

Advisor: *Prof.* Genci Capi

Copyright © Marsel Mano, 2013



## **Declaration**

I hereby declare that this submission is my own work and that, to the best of my knowledge and belief, it contains no material previously published or written by another person nor material which to a substantial extent has been accepted for the award of any other degree or diploma of the university or other institute of higher learning, except where due acknowledgment has been made in the text.

Name: Marsel Mano

Date: 2013/08/09

**The Evaluation Committee for Marsel Mano Certifies that this is the approved  
version of the following dissertation:**

**A Novel Adaptive Method for Robotic Wheelchair  
Navigation Using Brain Signals**

脳信号によるロボット車椅子の適応型  
ナビゲーションシステムの研究

**Evaluation Committee:**

印  
\_\_\_\_\_  
Prof. Genci Capi, Advisor

印  
\_\_\_\_\_  
Prof. Iwata Sakagami

印  
\_\_\_\_\_  
Prof. Koichi Ogawa

印  
\_\_\_\_\_  
Prof. Masato Tajima

印  
\_\_\_\_\_  
Prof. Shigenori Kawahara

## Acknowledgments

First, I'd like to express my deepest appreciation to my advisor Prof. Genci Capi, for the time he spent consulting and helping me on my ideas. He provided me with the opportunity to work with his research group. His constant support, guidance, enthusiasm and encouragement were invaluable throughout my PhD studies.

I also would like to thank the rest of the members of the evaluation committee: Prof. Koichi Ogawa, Prof. Iwata Sakagami, Prof. Masato Tajima, and Prof. Shigenori Kawahara for their insightful comments, questions and especially for carefully evaluating my work.

My sincere thanks go to Dr Hideki Toda and Dr Mitsuki Kitani for offering their support during my time at the University of Toyama.

I thank my fellow lab members at the intelligent robotics laboratory of University of Toyama, who volunteered for the BMI experiments. Their help was indispensable in the achievements of my research.

I'd like to express my deepest gratitude to my parents Pandi and Fidella Mano and my sister Etleva for supporting my choices throughout my life, for their dedication, encouragement, advice, and the many years of support. Their unconditional love has been a very strong motivation during all my life.

Most importantly, I'd like to thank my wife Estela whose continued patience and encouragement was what made it all possible. Without her continuous support and comprehension, I'd not have been able to find the drive and willingness to finish my PhD.



## Dedication

*To my unborn daughter and my wife*



## **Abstract**

A brain machine interface (BMI) is a direct communication pathway between the brain and an external device (i.e. robot). The BMI ability to directly communicate with machines and bypass the peripheral nerves and muscles is often used to assist or repair human sensorimotor functions in severely disabled or locked-in syndrome affected humans. Therefore, the BMI coupled with the assistive technology is seen as a promising approach to restore mobility in disabled people. A very important application in rehabilitation technology is the BMI based navigation of robotic wheelchairs. The aim of this application is to restore some mobility independence to paralyzed patients.

Navigating a robotic wheelchair by using only brain signals is a very challenging task. Since only brain signals and no other means can be used to control the wheelchair, the safety requirements are higher than standard wheelchairs. Proximity sensing data are usually used to detect objects and avoid collisions to improve wheelchair navigation safety.

BMI is a low-bit communication channel. This means, the subject has to perform a high amount of mental tasks for a relatively long period of time, even for simple navigation scenarios. This makes the navigation task tiring and long for the BMI subject. Shared control between subject's mental intentions and intelligent robots is usually proposed as a solution of these problems. Shared control generally improves the navigation experience but also restricts the subject's control over the robot. Also prior environment training and/or goal location information are required to assist the robot during navigation.

In this thesis, we present a novel adaptive method that improves the navigation of a brain controlled robotic wheelchair. We employ a synchronous brain machine interface to

retrieve mental intentions from the subject at specific points in time. Furthermore, we have developed two modules to assist the robotic wheelchair navigation. The first module is capable of navigating the wheelchair autonomously following assistive information (tactile paving for visually impaired people) on the floor captured by the visual sensor in real time. The second module uses a laser range finder sensor to detect and avoid objects in the navigation path. The adaptive platform integrates the brain signals, the robot sensing and the navigation modules in order to provide the subject with context based navigation choices through acoustic and visual queries.

Based on environment conditions the subject can choose to navigate the robot turn-by-turn or give high-level control commands, and allow the robot to navigate autonomously following the assistive information. The subject is able to accept or reject the assistance by using only brain signals.

Experimental results show that the proposed adaptive navigation, the robotic wheelchair is able to navigate on a shorter trajectory, avoid potential collisions and reduce the navigation time. The number of mental tasks required is reduced significantly when the assistive information is used. As a consequence of a reduced mental workload the subject is more relaxed and is able to perform better mental tasks, which lead to a higher BMI classification accuracy during adaptive navigation.

# Table of Contents

Declaration .....	i
Acknowledgments .....	iii
Dedication .....	v
Abstract .....	vii
Table of Contents .....	ix
List of Figures .....	xiii
List of Tables .....	xvii
List of Abbreviations .....	xix
1 Introduction .....	1
1.1 Thesis Objectives .....	2
1.2 Overview of Proposed Method and Contributions .....	3
1.3 Thesis Structure .....	4
2 Background .....	7
2.1 Human Brain Anatomy .....	7
2.2 Measuring Neural Activity .....	11
2.2.1 Overview of Brain Activity Measurement Methods .....	12
2.2.2 Invasive BMI Methods .....	12
2.3 Electroencephalography .....	13
2.3.1 Recording EEG .....	14
2.3.1.1 Brain Rhythms .....	16

2.3.1.2	EEG Signal Quality.....	18
2.3.2	Electrophysiological Signals Suitable for BMI.....	19
2.3.3	Sensorimotor Rhythms.....	20
2.3.4	Conclusion.....	21
3	Brain Machine Interface.....	23
3.1	BMI Diagram.....	23
3.2	Definitions.....	25
3.3	BMI Applications.....	26
3.3.1	Communication and Control.....	26
3.3.2	Gaming, Entertainment and Virtual Reality.....	28
3.3.3	Motor Recovery.....	29
3.3.4	Motor Substitution.....	29
3.3.4.1	Grasping.....	29
3.3.4.2	Assistive Mobility.....	30
4	Developed BMI System.....	33
4.1	EEG Signal Acquisition.....	33
4.2	Offline EEG Recording Sessions.....	35
4.3	Signal Processing.....	36
4.3.1	Signal Pre-processing.....	37
4.3.2	Spatial Filtering.....	39
4.3.2.1	Common Spatial Patterns.....	40
4.3.2.2	Spec-CSP Algorithm.....	41
4.3.3	Feature Extraction.....	44
4.3.4	Implementation, Feature Selection and Dimensionality Reduction.....	45
4.4	Classification.....	46
4.4.1	Linear Discriminant Analysis.....	47
4.4.2	Regularized and Multi-Class LDA.....	49
4.5	Online Predictive Module.....	50
5	Robotic Wheelchair and Navigation Modules.....	53

5.1	Robotic Wheelchair .....	53
5.1.1	Laser Range Finder Sensor .....	54
5.2	Navigation Assistive Modules .....	56
5.2.1	Direct Control Module .....	56
5.2.2	Collision Detection Module .....	56
5.2.3	Autonomous Navigation Module .....	60
5.3	Adaptive Navigation Platform .....	62
5.3.1	Control Mode Transitions and Finite State Machine .....	65
5.4	Environment and Experimental Setup.....	68
6	Results .....	71
6.1	Offline BMI Results .....	71
6.1.1	Preprocessing .....	72
6.1.2	Filtering Model.....	74
6.2	Online BMI results .....	77
6.3	Robot Navigation Results.....	78
6.3.1	Collision Detection and Avoidance Performance .....	78
6.3.2	Autonomous Navigation Performance .....	79
6.3.3	Adaptive Robotic Navigation Results .....	80
7	Conclusions .....	85
	Appendices .....	87
A	Brain Activity Measurement Techniques.....	88
B	Other Electrophysiological Signals Used in BMI .....	89
B.1	Slow Cortical Potentials .....	89
B.2	Common Evoked Potentials Used in BMI Systems.....	89
B.2.1	Visual Evoked Potentials .....	89
B.2.2	Event Related Potentials .....	90
C	BMI Classifiers .....	92
C.1	Classifiers Used in BMI .....	92
C.2	Classifier Combination.....	93

D	Offline BMI Method Evaluation .....	96
D.1	Datasets .....	96
D.1.1	BCI Competition iii & iv Datasets .....	96
D.1.2	BCILAB Datasets.....	97
D.1.3	Intelligent Robotics Laboratory Datasets.....	97
D.2	Results of LTI Filtering.....	98
D.3	Classification Results .....	99
	Bibliography .....	103

# List of Figures

<i>Figure 2-1 Brain sagittal section (adopted from Wikimedia)</i> .....	8
<i>Figure 2-2 Brain cognitive functions location map (adopted from AlianaHealth)</i> .....	10
<i>Figure 2-3 Primary motor cortex function mapping (adopted from StudyBlue)</i> .....	11
<i>Figure 2-4 Structure of a neuron (adopted from (Sanei and Chambers 2007))</i> .....	14
<i>Figure 2-5 Multi-electrode EEG recordings (adopted from Wikipedia)</i> .....	14
<i>Figure 2-6 International 10–20 electrode placement system</i> .....	17
<i>Figure 2-7 Brain rhythms (adopted from Wikipedia)</i> .....	17
<i>Figure 2-8 Event Related De-synchronization and Event Related Synchronization (ERD/ERS) (adopted from (Lemm, Müller, and Curio 2009))</i> .....	21
<i>Figure 3-1 Generic diagram of a BMI system</i> .....	24
<i>Figure 3-2 The text entry system ‘Hex–O–spell’ interface (adopted from (Blankertz, Dornhege, Krauledat, Schroder, et al. 2006))</i> .....	27
<i>Figure 3-3 BMI navigation in a virtual street (adopted from (Leeb, Friedman, Slater, et al. 2007))</i> .....	28
<i>Figure 4-1 (a) the electrode cap, and (b) the electrode placements positions</i> .....	34
<i>Figure 4-2 Electrode box (adopted from Mitsar Co., Ltd website)</i> .....	34
<i>Figure 4-3 BMI subject during offline data recording session</i> .....	35
<i>Figure 4-4 Trial structure</i> .....	36
<i>Figure 4-5 Offline training cues: (a) Left hand (b) Right hand (c) Foot (d) Relax and (e) Start</i> .....	36
<i>Figure 4-6 Epoch extraction interval</i> .....	37
<i>Figure 4-7 Best class projection</i> .....	48
<i>Figure 4-8 Online Predictive Module flow chart</i> .....	51

Figure 5-1 Robotic Wheelchair.....	54
Figure 5-2 Servo motor wheel system components (adopted from Yamaha Motor website) .....	54
Figure 5-3 The “URG-04LX-UG01” model LRF sensor; all the values in the drawings are in mm (adopted from Hokuyo Automatic website).....	55
Figure 5-4 Sensor reading snapshots (a) before and (b) after area restriction to $0^{\circ} - 180^{\circ}$ .....	58
Figure 5-5 Sensor measuring subareas: left ( <b>SL</b> ), forward ( <b>SF</b> ) and right ( <b>SR</b> ) subarea .....	58
Figure 5-6 Web camera used on our system.....	60
Figure 5-7 Assistive information: (a) line (b) decision point with 3 lines (c) decision point with 2 lines .....	60
Figure 5-8 Processed image frame representation.....	61
Figure 5-9 Block diagram of the BMI-based robotic wheelchair control system using ANP.....	63
Figure 5-10 (a) Activate ANM popup GUI, (b) Change Navigation Mode popup GUI, and (c) Main GUI of the system.....	65
Figure 5-11 FSM diagram .....	67
Figure 5-12 FSM diagram during unassisted control mode.....	68
Figure 5-13 Experimental environment .....	69
Figure 6-1 Raw 15 channel EEG signal recordings during an offline trial .....	71
Figure 6-2 Single trial power spectrum.....	72
Figure 6-3 Mean log power spectrum of a continuous 15 channel EEG dataset: (a) without LTI filtering, and (b) with LTI filtering .....	73
Figure 6-4 The C3 and C4 Electrode (channel) signal averaged over trials, after preprocessing in the time interval [0.5, 1.5] seconds after the cue during: (a) Left Hand tasks and (b) Right Hand tasks.....	74
Figure 6-5 Scalp topographic maps of the spatial patterns for the three biggest & smallest eigenvalues of the MI pair: (a) Left Hand v. Right Hand, (b) Left Hand v. Foot and (c) Right Hand v. Foot .....	75
Figure 6-6 Frequency filters $\alpha$ corresponding to the three biggest & smallest eigenvalues of the MI pair: (a) Left Hand v. Right Hand, (b) Left Hand v. Foot and (c) Right Hand v. Foot.....	76
Figure 6-7 BMI classification accuracy distribution over experimental sessions .....	77
Figure 6-8 Collision detection results over experimental sessions .....	79
Figure 6-9 Collision avoidance results over experimental sessions.....	79
Figure 6-10 Assistive information extraction from the real-time image processing algorithm of a line (captured image in (a) and its result in (b)) and a decision point (captured image in (c) and its result in (d)) .....	80

*Figure 6-11 Mental task results over experimental sessions* ..... 81

*Figure 6-12 Trial time results over experimental sessions* ..... 81

*Figure 6-13 Robot navigation metric improvement during assisted navigation* ..... 82

*Figure 6-14 A navigation trial conducted in (a) assisted mode (b) unassisted mode* ..... 83

*Figure A-1 ERP component's approximate positions relative to the event or stimulus* ..... 91

*Figure A-2 An EEG waveform showing typical ERP components (adopted from Wikipedia)* ..... 91

*Figure A-3 Electrode placement labels/positions* ..... 98

*Figure A-4 Single channel mean activity log power spectrum of subset OFC4: a) left hand MI trials, and b) right hand MI trials* ..... 99



## List of Tables

<i>Table 4-1 Mitsar-EEG 201 technical specifications (adopted from Mitsar Co., Ltd website).....</i>	<i>34</i>
<i>Table 4-2 Filtering Model.....</i>	<i>46</i>
<i>Table 4-3 Statistical definitions .....</i>	<i>48</i>
<i>Table 4-4 Classification Model.....</i>	<i>50</i>
<i>Table 5-1 The “URG-04LX-UG01” model LRF sensor technical specifications (adopted from Hokuyo Automatic website) .....</i>	<i>55</i>
<i>Table 5-2 OPM output translations into real time robot direction change in assisted and unassisted control modes .....</i>	<i>64</i>
<i>Table 6-1 The mean and the standard deviation of the BMI misclassifications and the BMI accuracy during each experimental session.....</i>	<i>77</i>
<i>Table 6-2 CDM Performance .....</i>	<i>78</i>
<i>Table 6-3 Navigation Metrics .....</i>	<i>81</i>
<i>Table A-1 Brain Activity measuring methods and their main distinctive features.....</i>	<i>88</i>
<i>Table A-2 ERP component properties .....</i>	<i>91</i>
<i>Table A-3 Properties of classifiers used in BMI research (adopted from (Lotte et al. 2007)) .....</i>	<i>94</i>
<i>Table A-4 Classification accuracies (mean and standard deviation) obtained for each dataset for the standard CSP and Spec-CSP, with and without <math>f1, -1</math> filtering .....</i>	<i>100</i>
<i>Table A-5 Classification accuracies (mean and standard deviation) obtained for each dataset collected in the intelligent robotics lab, for the standard CSP and Spec-CSP, with and without <math>f1, -1</math> filtering .....</i>	<i>101</i>
<i>Table A-6 Classification accuracies (mean, standard deviation and train loss) of the online feedback experiments .....</i>	<i>102</i>



## List of Abbreviations

ANM: Autonomous Navigation Module .....	4
ANN: Artificial Neural Networks.....	92
ANP: Adaptive Navigation Platform .....	4
BMI: Brain Machine Interface.....	1
CDM: Collision Detection Module.....	4
CSP: Common Spatial Patterns .....	38
DCM: Direct Control Module.....	3
ECoG: Electrocorticography.....	12
EEG: Electroencephalography .....	1
EP: Evoked Potential .....	19
ERD: Event Related De-synchronization .....	20
ERP: Event Related Potential .....	19
ERS: Event Related Synchronization .....	20
FES: Functional Electrical Stimulation .....	29
fMRI: Functional Magnetic Resonance Imaging.....	12
FSM: Finite State Machine .....	66
GUI: Graphical User Interface.....	64
LRF: Laser Range Finder.....	4
LTI: Linear Time Invariant.....	3
MEG: Magnetoencephalography .....	12
MI: Motor Imagery .....	2
MLP: Multi-Layer Perceptron.....	92
NIRS: Near Infrared Spectroscopy .....	12

OPM: Online Predictive Module .....	3
PET: Positron Emission Topography.....	12
RLDA: Regularized Linear Discriminant Analysis .....	3
SCP: Slow Cortical Potentials .....	20
SNR: Signal-to-Noise Ratio.....	36
Spec-CSP: Spectrally Weighted Common Spatial Patterns .....	38
SSVEP: Steady-State Visual Evoked Potentials.....	89
SVM: Support Vector Machine .....	46
TTD: Thought Translation Device.....	27
UART: Universal Asynchronous Receiver/Transmitter .....	53
USB: Universal Serial Bus.....	33
VEP: Visually Evoked Potentials .....	89

# 1 Introduction

Brain Machine Interfaces (BMI) are often directed at assisting, augmenting, or repairing human cognitive or sensorimotor functions (Wolpaw et al. 2000). BMI systems enable humans to send commands to an external device (generally a computer or robot), by using only brain signals recorded while performing voluntary mental activity (Wolpaw et al. 2002; Birbaumer 2006). BMI is thought to be particularly useful in restoring communication to locked-in syndrome affected patients (Kübler et al. 2001) or restore mobility to paralyzed patients (Pfurtscheller et al. 2003).

Commonly, electroencephalography (EEG) is used to record the brain activity. The first experiments of recording EEG on humans date back in 1929 and they were carried out by researcher Hans Berger (Berger 1929).

EEG measures micro currents generated by brain activity on scalp. By decoding EEG signals, we can understand the brain activity to a certain degree. The first attempt to create an EEG based BMI dates back in 1973 (Vidal 1973).

Despite some early attempts (Farwell and Donchin 1988), it is only in the last two decades that BMI research has gained significant popularity, involving a lot of research which is at present being conducted in an increasing number of laboratories around the world. Together with the BMI applications, the methods and technologies used for measuring the brain activity have increased and become more sophisticated. BMI designs and applications have particularly shown promising results in the medical domain (Rebsamen et al. 2007; Shih, Krusienski, and Wolpaw 2012), but also in other areas (Nijholt, Bos, and Reuderink 2009; Blankertz et al. 2010). Unfortunately, most of the results acquired in research laboratories seem to have had small or no impact on commercial and real life applications yet.

## 1.1 Thesis Objectives

The work presented in this thesis belongs to the research and development of BMI controlled robots. More precisely, it focuses on the study of BMI controlled robotic wheelchair applications for disable people. Despite some valuable and promising achievements already obtained in the literature, the field of brain controlled robotic wheelchair applications remains a relatively new research field and there is still a long way to go until the final goal of making these wheelchairs available to disable patients for everyday use is reached. Up to now, all the results and applications are limited to research laboratories experimenting in simulated and/or virtual environments and also some indoor experimental environments. Real life applications are still far in the horizon.

The research on intelligent robotics is focused on building assistive modules for shared navigation. The BMI community has emphasized the need for shared (collaborative) navigation and intelligent wheelchairs in order to compensate the BMI imperfections (Carlson and del R. Millan 2013; Millan et al. 2010; Carlson, Leeb, Chavarriaga, et al. 2012; Leeb and Millan 2013; Lopes, Pires, and Nunes 2013).

In this thesis, we propose a novel adaptive method for the task of navigating a robotic wheelchair by using brain signals collected and decoded through BMI system based on the motor imagery (MI) mental activity (Section 2.3.3) measured by EEG. Among the numerous possible improvements, we are going to address the following topics:

- 1- Improve BMI classification by applying de-noise filtering to the EEG brain signals
- 2- Reduce the mental workload of the BMI subject by offering autonomous navigation
- 3- Improving robot navigation by introducing real time adaptive navigation assistance

The above topics are widely discussed and addressed as being important and necessary research topics for the improvement of BMI technology in general and BMI based wheelchair navigation technology in particular (McFarland et al. 2006; Kübler 2006; Wolpaw et al. 2002; Allison, Wolpaw, and Wolpaw 2007; Millan et al. 2010; Shih, Krusienski, and Wolpaw 2012; Green and Kalaska 2011; Cabrera, Farina, and Dremstrup 2010; Leeb and Millan 2013; Carlson and del R. Millan 2013).

In the next section we are going to introduce the main methods and the contributions of this thesis with regard to the three topics shown above.

## 1.2 Overview of Proposed Method and Contributions

In order to address the topics raised in the previous section, we conducted an in-depth review and investigation process of different BMI approaches; then, we decided to select the MI generated electrophysiological process for the EEG signal based BMI system in our experiments. The selected BMI system allows the subject to voluntarily control the mental activity (voluntary MI tasks) in order to achieve brain machine communication. Furthermore, previous research on MI based BMI has already shown to achieve sustainable communication capabilities (Mason et al. 2007).

In order to improve BMI communication, it is very important to have a high brain signal classification rate. EEG signals are very noisy, which makes the classification task challenging (Section 2.3.1.2). In order to remove noise from EEG signals, we propose a linear time invariant (LTI) filtering during the signal pre-processing step, and then we apply spatial and temporal filters (Section 4.3). These filters enable emphasize important discriminatory features of the pre-processed EEG signals, while reducing irrelevant ones.

Linear classifiers are very fast and robust for real time applications. In our implementation, we propose a regularized linear discriminant analysis (RLDA) classifier (Section 4.4.2) which is trained with the data acquired during offline recording sessions. The performance of the above filtering and classification methods are tested with offline datasets from 36 subjects and the results are shown in Appendix D.

Prior to the robot real time navigation sessions, we conducted an offline data recording session. Typical offline sessions involve the subject staring at the screen, and repeatedly perform MI tasks according to the cues presented on screen. In order to minimize the subject's fatigue and mental workload, we reduce the duration of the offline session to approximately 15 minutes. Based on the offline recording we built a feature extraction model (Section 4.3.4) and a classification model (Section 4.4.2) and we integrated both in the online predictive model (OPM). The OPM (Section 4.5) was used to retrieve, pre-process, filter, classify and send the subject's mental intentions to the robot in real time during navigation. The OPM is very fast and offers high classification accuracy.

To reduce the subject's mental workload and improve the real time robot navigation, we have developed assistive modules for direct navigation, autonomous navigation and collision detection (Section 5.2). The direct control module (DCM) is capable to

navigate the robot turn-by-turn. The collision detection module (CDM) uses laser range finder (LRF) sensor data to detect and avoid potential collisions. The autonomous navigation module (ANM) uses a camera to capture assistive information on the floor and navigates the robot autonomously.

The above navigation modules are integrated with the OPM by using an adaptive navigation platform (ANP). The proposed ANP (Section 5.3) adaptively assists the subject during navigation by offering autonomous navigation or direct control navigation, based on the environment context.

In order to evaluate the impact of our method in the robot navigation performance, the experiments were conducted in a comparative manner. During each session, the experimental trials were conducted in assisted and unassisted navigation mode. In assisted mode, the ANP was able to offer collision detection (and avoidance) and autonomous navigation assistance to the subject. The subject was able to accept or reject it by using brain signals. In unassisted mode the ANP was only able to offer collision detection and avoidance assistance.

Experimental results show that when robot navigates in assisted mode using full assistance from ANP, the number of mental tasks per trial, the trial navigation time and the maximal number of collisions detected in a trial, are reduced significantly (Section 6.3). This indicates that the assistance from ANP improves the navigation capabilities of the wheelchair and facilitates the usage of BMI controlled wheelchairs.

The proposed adaptive method not only improves navigation, but also it improves the overall real time BMI classification. By allowing the subject to relax during autonomous navigation, he is able to perform better mental tasks and with greater focus. This improves the BMI classification.

### 1.3 Thesis Structure

The rest of this thesis is organized into 6 chapters and four appendices. The content of each chapter and the appendices are shown below:

**Chapter 2** contains a general background of the human brain anatomical construction and functionality. Then it offers a background of the methods that are used to measure the electromagnetic signals generated from brain activity. The major part of this chap-

ter is used to explain the EEG signal measurement methods and the electro-physiological signals that are most suitable for BMI systems. This includes observations about the EEG signal quality and the brain rhythms that are present in EEG signals. Special attention is paid to the sensorimotor rhythms of the brain, more precisely to MI activity generated rhythms, since these are the rhythms that are used by the BMI system in our experiments.

**Chapter 3** reviews the BMI applications. It starts with an introduction of the most important definitions of BMI systems. Then it continues with a review of the BMI application areas, their importance and it introduces some famous BMI applications. A significant part of this chapter is used to introduce the development status of the BMI robotic wheelchair applications for disable people.

**Chapter 4** describes in detail the theory and the algorithms that we have used to build our BMI system. It contains a detailed description of the data acquisition hardware and software. Furthermore, it details the offline recording procedure and the offline EEG signal processing including, offline session description, signal pre-processing, spatio-temporal filter construction, feature selection criteria, linear classifier training and it finishes with the OPM, which is used to generate the robot control commands during online robot navigation.

**Chapter 5** describes in detail the hardware and the software components of the robotic wheelchair that we have built in our lab and used for the experiments. It contains a detailed description of the sensing and actuating equipment of the robot including the LRF sensor, the web camera, AC servomotors, etc. Furthermore, all software modules that we have developed for assisting robot navigation, the ANP that integrates these modules with the BMI system and the functionality of the BMI controlled robotic wheelchair system as a whole, are described in this chapter. The experimental environment and the experimental protocol for the real time navigation are shown in the last section.

**Chapter 6** shows the results of our experiments. It is divided in three parts, the offline BMI, the online BMI and the robot navigation results. Section 6.1 shows the results of the offline EEG signals: the pre-processing, filtering and the OPM construction. The results of BMI classification during real time robot navigation sessions are shown in Section 6.2. Section 6.3 shows the performance of different assistive modules and the

overall performance of the ANP during real time robotic wheelchair navigation experiments.

**Chapter 7** concludes the thesis. It emphasizes the main contributions of this thesis by explaining the advantages of our method in comparison to previous works in the field of BMI controlled robotic wheelchairs.

The last part of the thesis contains four appendices. Appendix A summarizes the features and properties of most popular brain activity measurement techniques. Appendix B introduces the electrophysiological signals used to establish BMI communication. Appendix C gives a review of the classification methods used in BMI systems. Last, appendix D shows the classification results obtained by applying our BMI system offline in datasets obtained in our lab and also datasets downloaded from public domains of the BMI community.

## 2 Background

This chapter gives background information about the human brain anatomy, followed by an overview of some popular brain activity measurement methods. Emphasis will be put on electroencephalography (EEG) since this is the most widely used method for non-invasive BMI applications and it is the method used in the work presented in this thesis. Further, electrophysiological signals used in BMI will be described with a primary focus on the sensorimotor rhythms.

### 2.1 Human Brain Anatomy

The human central nervous system is made of the brain and the spinal cord which is the continuation of the brain. The brain is the most complex organ of the human body. An adult brain is made of more than  $10^{11}$  highly compressed and interconnected (through approximately  $5 \times 10^{14}$  synapses) neurons into a very complex compound of mass (Sanei and Chambers 2007). Although single neuron functions are fully understood, the vast amount of neurons, and the dynamic inter-neural connections make it quite impossible to fully understand the right workflow principles of the brain and how certain information is processed dynamically involving different brain parts.

For more than two centuries, neuroscientists have used the spatial approach, which maps the brain into functionally distinct parts. This is mainly based on the principle that neurons serving a similar function are likely to be interconnected with each other, thus be in the same region of the brain.

The brain has a symmetric, bilateral structure with three main regions, the fore brain, the mid brain and the hind brain; and it is connected to the spinal cord through the

hind brain. Each brain region shown above has different parts (Figure 2-1) that are responsible for specific functions.

**Spinal Cord** – is partly responsible for controlling limb movement and the trunk. Furthermore, it processes sensory information from the skin, joints and their associated muscles.

**Hind Brain** consists of medulla oblongata, pons and cerebellum.

- **Medulla Oblongata** – is an extension of the spinal cord into the brain. It contains tracts from and to higher portions of the brain, and also is responsible for vital functions like respiration and heart rate. The upper part of the medulla (reticular formation) is the regulatory system for sleep, waking, and alertness.
- **Pons** (“bridge” in Latin) serves as a connection pathway between: a) the lower cerebellum and spinal cord and b) the higher parts of the brain like the cerebrum and mid brain. It is responsible for providing movement information originating from the cerebral hemispheres to the cerebellum.
- **Cerebellum** (“little brain” in Latin), is shaped like a small brain, and it is primarily responsible for coordinating involuntary movement, walking balance, etc. It is also responsible for precision and fine control of the voluntary movements. It is believed that, when you learn complex motor tasks, the details are stored in the cerebellum.

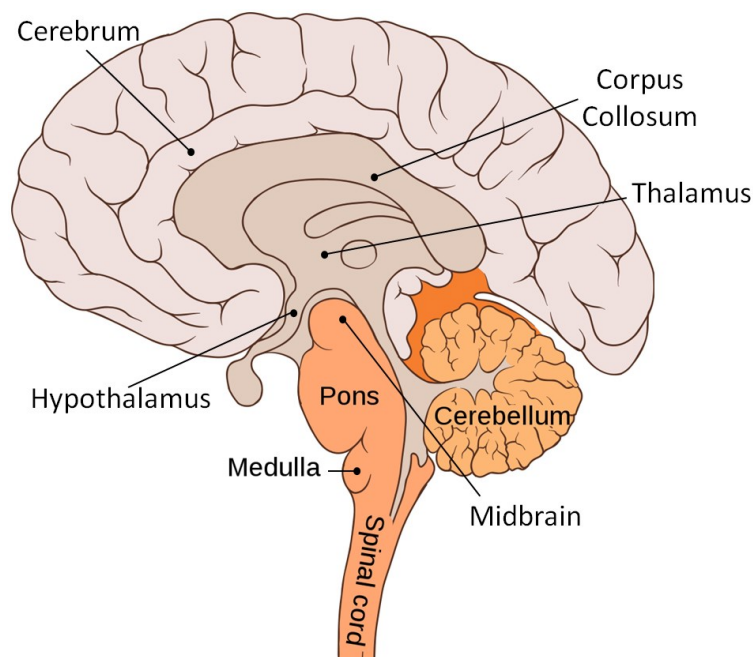


Figure 2-1 Brain sagittal section (adopted from [Wikimedia](#))

**Midbrain** is the smallest part of the human brain and connects the hindbrain to the forebrain. It contains important pathways for hearing and vision; furthermore, it is involved in processing and controlling a variety of sensory and motor functions (e.g. eye movements), and coordinates auditory and visual reflexes.

**Fore Brain** consists of the diencephalon (hypothalamus and thalamus) and cerebrum.

- **Thalamus** is responsible for processing sensory and motor information and then relays it to the corresponding part of the cortex.
- **Hypothalamus** is responsible for the taste and smell, it controls the heart rate, blood pressure, body temperature, etc. It also controls mood and emotions.
- **Cerebrum** is the largest and the most developed part of the brain. It is made of two symmetrical cerebral hemispheres connected by the **corpus callosum**. The surface of the cerebrum is called the *cortex* and consists of layers of neuron cells. It appears grey in color; hence it is usually called the “grey matter”. The inner part is called the *medulla* and it consists of trillions of neuron connection fibers. It is white in color; hence it is called the “white matter”. The *cortex* is highly convoluted to increase its surface area. It is believed that higher convolutions lead to higher intelligence. Cerebrum is responsible for the intelligence, personality, thinking, memory, consciousness, will power, producing and understanding language, interpretation of sensory impulses, motor functions, planning etc.

Supposedly, all cognitive functions are processed through the electrical activity of the neuron cells located in the structures of the cortex layer of the brain. Specific cortex areas are responsible for sensory, motor or intellectual processing. Brain mapping is used to associate different brain functions with different areas. This mapping is done by associating similar function classes in a large area and then specific sub-class of functions into smaller subareas. Theoretically, this mapping can go up till single neuron function level. Practically, it is impossible to associate every specific neuron cell with a brain function; instead, neural populations are mapped as responsible for specific brain activity.

The cortex has **sensory areas**, **association areas** and **motor areas**. The sensory areas receive the messages from the sensing organs, the association areas associate this information with other sensory information and the motor areas are responsible of the control of the voluntary muscles. The cortex has four distinct lobes: frontal, parietal, temporal and occipital (Figure 2-2).

**Frontal Lobes** are located at the front of each hemisphere, anterior to the neighboring parietal lobe and above the temporal lobe. Some of their most distinctive functions are associated with behavior, planning, motivation, long-term memory and attention. Here are located the areas responsible for motor functions (Figure 2-3).

**Parietal Lobes** function is primarily associated with multimodal sensory information integration especially for navigation and object manipulation. The most distinctive function is to visually map in space and time a perceived object's position, relative to the body. Specific parts of the parietal lobes are associated with language processing functions.

**Temporal Lobes** are located on both sides of the brain mainly associated with auditory processing, language processing and some visual processing. In this region of the cortex is also located the hippocampus which plays an essential role in converting short-term memory into long-term memory.

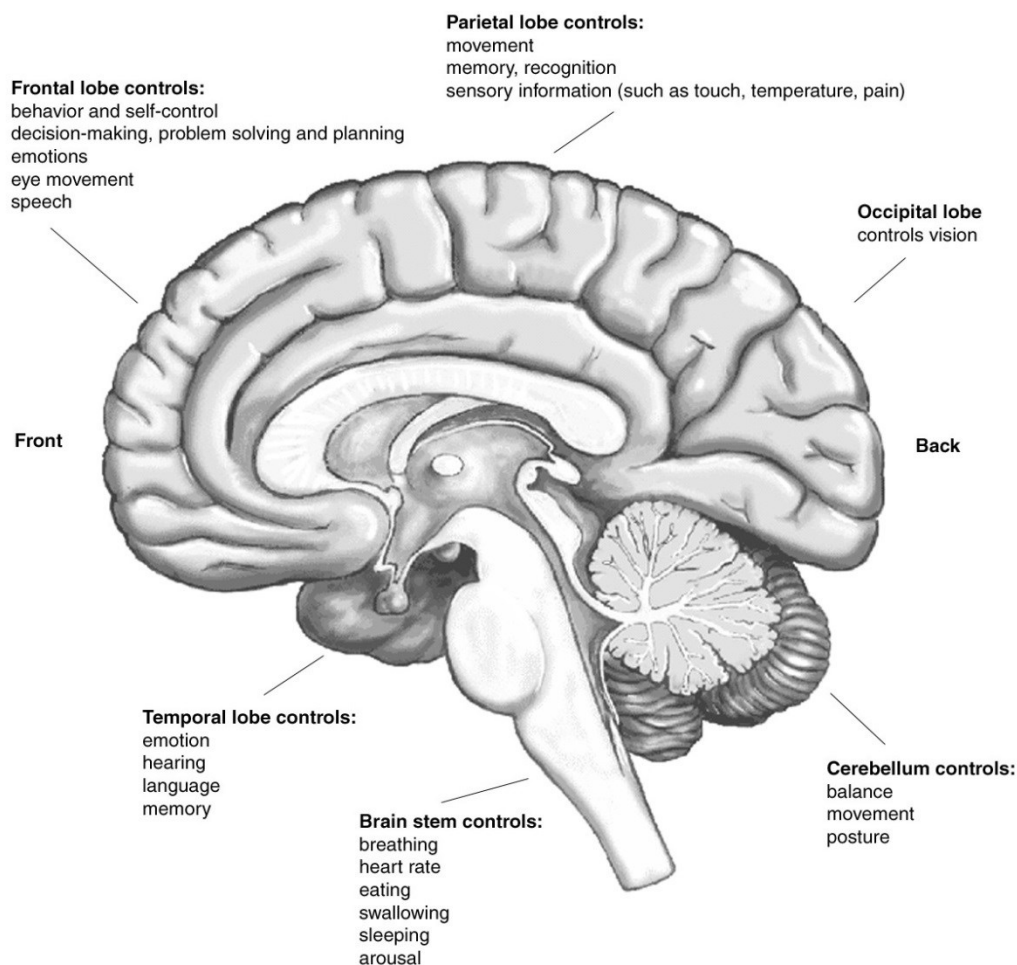
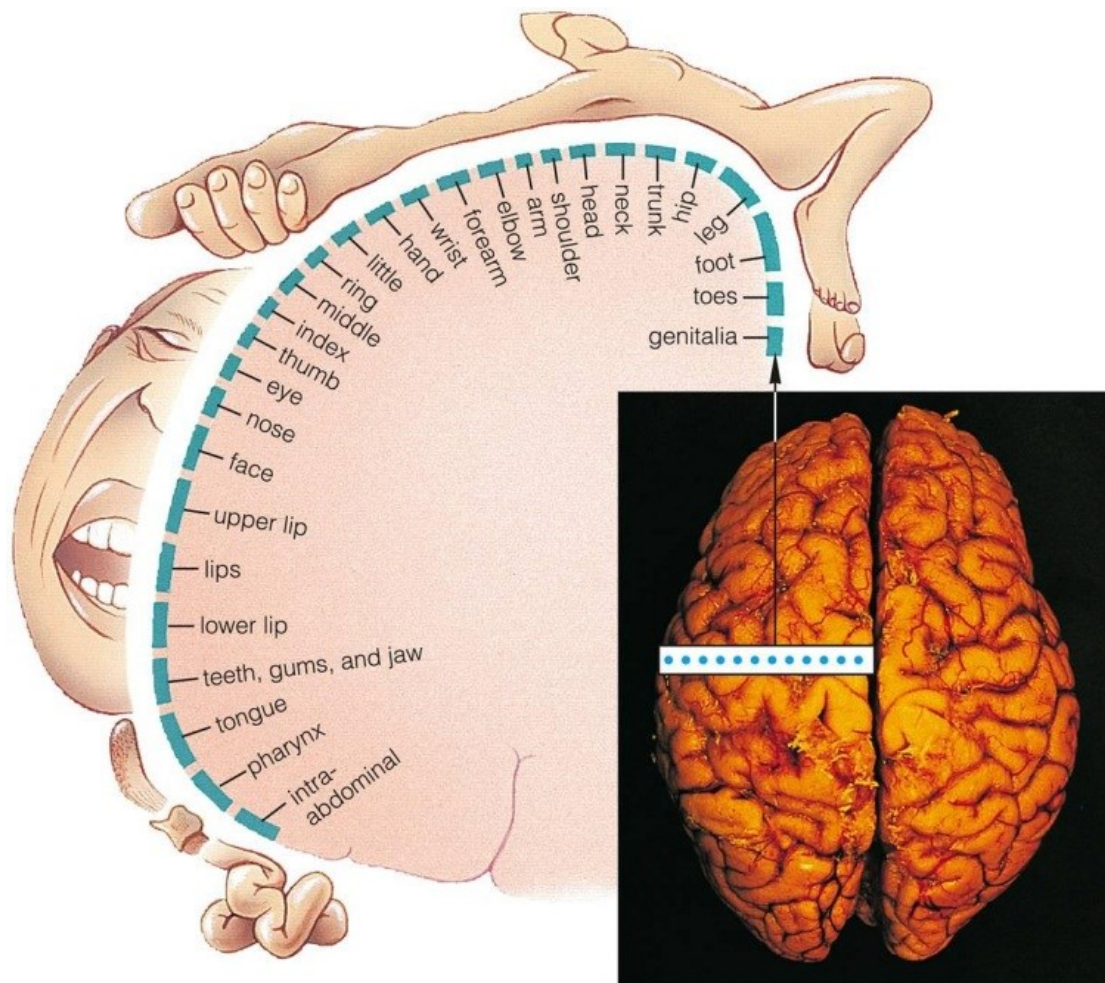


Figure 2-2 Brain cognitive functions location map (adopted from [AlianaHealth](#))



**Figure 2-3 Primary motor cortex function mapping (adopted from [StudyBlue](#))**

**Occipital Lobes** are located at the back of the head. Their function is almost exclusively associated to visual processing; including sub-areas specialized for color or edge direction detection. The back of the lobes are arranged in such a way as to reflect the retinal field as a spatial map.

The motor cortex is subdivided into distinct areas associated with different body parts (Figure 2-3). In this thesis, we will mainly focus on the brain activity of the motor cortex and the signals generated from this area of the brain, more precisely to the signals corresponding to the control of limbs.

## 2.2 Measuring Neural Activity

BMIs operate based on the subject's measured brain activity. In this section, we will describe different available methods for measuring brain activity. Then we will identify the brain signals that are commonly used to drive the BMI.

### 2.2.1 Overview of Brain Activity Measurement Methods

Researchers have identified around a dozen different kinds of brain signals as suitable for a BMI (Wolpaw et al. 2002). Based on the signal and the targeted brain activity different measurement methods are used (Wolpaw et al. 2006). These methods are divided into three categories:

- 1- Non-invasive methods, which include methods that measure the magnetic field changes, the Magnetoencephalography (MEG) (Bianchi et al. 2010; Mellinger et al. 2007; Besserve et al. 2007; Pfurtscheller and Lopes da Silva 1999) or the electrical field changes, the EEG.
- 2- Other non-invasive methods that measure metabolic processes of the brain like Functional Magnetic Resonance Imaging (fMRI) (Weiskopf et al. 2004; Minati et al. 2012), Near Infrared Spectroscopy (NIRS) (S. M. Coyle, Ward, and Markham 2007; Sagara, Kido, and Ozawa 2009), or Positron Emission Topography (PET) (Bernhard Graimann, Pfurtscheller, and Allison 2010).
- 3- Invasive methods like Electrocorticography (ECoG) or implanted electrodes placed inside the cortex (Leuthardt et al. 2011; Krusienski and Shih 2011; Chapin et al. 1999; Velliste et al. 2008; Mano et al. 2013).

The most popular non-invasive measurement method used in BMI applications is EEG (Wolpaw et al. 2006). More details about other techniques used for brain activity measurement are shown in Appendix A.

Recently, EEG devices have become more affordable (although still expensive for personal use), more portable and provide a relatively good signal resolution. Furthermore, EEG based measurement methods are entirely non-invasive and easier to set up, compared to invasive and other complicated non-invasive methods. Consequently, most of current BMI systems are using EEG to measure brain activity. In this thesis, we have focused our work on EEG-based BMI.

### 2.2.2 Invasive BMI Methods

Invasive BMI is very promising and rapidly growing research field. Invasive BMI uses signals acquired from electrodes (sensors) implanted inside specific parts of the brain, to measure targeted neural populations' activity (Lebedev and Nicolelis 2006;

Friehs et al. 2004; Hochberg et al. 2006; Nicolelis 2001; Schwartz et al. 2006). Obviously, it is by far less popular than EEG for the very difficulties and risks that the surgery for implanting the electrodes carries. Most of invasive BMI system applications are designed and evaluated in primates (Lebedev and Nicolelis 2006; Nicolelis 2001; Velliste et al. 2008) or rats (Chapin et al. 1999; Mano et al. 2013). However, examples of invasive BMI in humans exist and have shown some promising results (Yanagisawa et al. 2012; Collinger et al. 2013).

When it comes to signal quality, invasive BMI offers the best spatial resolution and signal quality. The recording electrodes are implanted in the target neural area (e.g. motor cortex) and acquire better signal compared to the cluttered, multi-sourced and noisy EEG signal recorded on scalp. For instance, electrodes implanted into the motor cortex area, which is responsible for left hand movement, will record a much higher neural activity when a left hand movement occurs opposed to a right hand movement. The signal measured with EEG electrodes on the scalp is very noisy, comes from multiple approximately same distance neural sources and it is attenuated from the skull.

Nevertheless, the signal quality in invasive BMI comes with a high price. The use of implanted electrodes might be dangerous for the health of the subjects. Implanting electrodes requires neurosurgical operation. Furthermore, electrodes have a limited lifetime, which requires regular surgery operations for electrode replacements. Moreover, the body may resist the electrodes, which makes the whole risky procedure go in vain.

### 2.3 Electroencephalography

An EEG signal is the measurement of currents that flow during synaptic excitations of the dendrites of many pyramidal neurons in the cerebral cortex. When brain cells (neurons) are activated, the synaptic currents are produced within the dendrites (Figure 2-4). This current generates a magnetic field measurable by electromyogram measuring devices and a secondary electrical field over the scalp measurable by EEG measuring devices (Sanei and Chambers 2007).

A typical multi-electrode EEG recording is shown on Figure 2-5. EEG measurements have been conducted on human subjects for almost a century since the first recordings in 1924 by Hans Berger. It is at that time that he named it “electroencephalogram”. Anyway, in the last 20 years there has been a rapid increase of EEG usage.

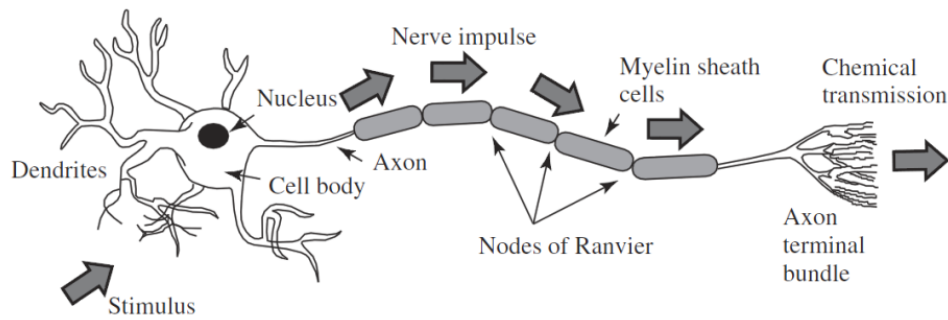


**Figure 2-4 Structure of a neuron (adopted from (Sanei and Chambers 2007))**



**Figure 2-5 Multi-electrode EEG recordings (adopted from [Wikipedia](#))**

### 2.3.1 Recording EEG

EEG signals are measured by using specific EEG electrodes placed on the scalp of a human subject. The number of recording electrodes varies from few to about 256. Usually, these electrodes come pre-mounted on elastic caps.

To improve conductivity (i.e. reduce electrode impedance), which leads to the acquisition of better signal resolution, the contact between the electrodes and the skin is generally enhanced by using ethanol, conductive gel or paste (Sanei and Chambers 2007). As a general rule, the best signal is acquired when impedance is below  $3k\Omega$ . In order to achieve good performance, each electrode's impedance needs to be carefully checked and

the gel needs to be applied thoroughly. This makes the electrode montage procedure generally tedious and lengthy. Furthermore, electrodes need to be placed as close to the scalp as possible which may lead to headache caused by pressure. Recently, dry electrodes have been introduced to the market (e.g. *g.SAHARA*<sup>1</sup>). However, the signal acquired with this electrodes results in lower BMI performance, compared to the performance of BMI based on signals acquired with gel electrodes.

EEG measures voltage differences, generally with an amplitude range of 100 microvolts (Sanei and Chambers 2007). It is thus necessary to amplify these signals before digitizing and processing them. Usually, EEG signals are amplified up to 100.000 times, which equals up to 100dB voltage gain. In order to obtain voltage differences, usually one electrode or a combination of electrodes are used as reference. The most popular referencing methods include:

**Common Reference** – Usually the *reference electrode* is placed in one or both ear lobes, or in the right/left mastoid. Then, each EEG signal channel is yielded from the difference of each *recording electrode* with the common *reference electrode*.

**Common Average Reference** – Here the *reference* is not just an electrode but is the average value of all recordings electrodes. Then, similar to common reference, each EEG signal channel is yielded from the difference of each *recording electrode* with the common average *reference*.

**Bipolar Reference** – This is very different from the above methods. In bipolar reference, each EEG channel is the result of the difference between two electrodes. They are arranged as linked serial pairs since the reference electrode of the first channel is the active electrode of the next channel.

EEG electrode placement is very important since the signal recorded in one site is different from another. In order to standardize the placements and thus, make it easier to compare the recordings, the standard model “10–20 international system” is used (Klem et al. 1999).

The standard electrode placement (Figure 2-6) uses two fixed reference locations, the nasion and the inion, to define the size of the head. The distance from nasion to inion is divided into 10% and 20% intervals in the horizontal and vertical plane. Each elec-

---

<sup>1</sup> A product of [g.tec](#)

trode location has a unique label assigned in a systematic manner. Depending on the electrode location, the first character of each label can be one of the following letters: ‘O’ for occipital lobe, ‘T’ for temporal lobe, ‘P’ for parietal lobe or ‘F’ for frontal lobe. The second character can be the letter ‘z’, which denotes the midline, or a number. Labels ending with odd numbers are located on the left hemisphere while those ending with even numbers are located on the right hemisphere. Further, the distance of the location to the midline can be determined by its trailing number. The smaller the electrode number, the closer its location to the midline.

### 2.3.1.1 Brain Rhythms

The signals recorded with EEG consist of different oscillations named “rhythms” (Sanei and Chambers 2007). These rhythms are very distinctive in terms of spatial and spectral localization. There are 6 classical brain rhythms (Figure 2-7):

- 1- **Delta rhythm** is usually observed in adults during sleep. It is a slow rhythm (1–4 Hz), with relatively large amplitude.
- 2- **Theta rhythm** is usually observed during drowsiness and in young children. It is faster than delta rhythm (4–7 Hz).
- 3- **Alpha rhythm:** These are oscillations, located in the 8–12 Hz frequency band, which appear mainly in the posterior regions of the head (occipital lobe) when the subject has closed eyes or is in a relaxation state.
- 4- **Mu rhythm:** These are oscillations in the 8–13 Hz frequency band, believed to be originated in the motor and sensorimotor cortex. The amplitude of this rhythm varies when the subject performs movements. Consequently, this rhythm is also known as the “sensorimotor rhythm” (Pfurtscheller and Neuper 2001).
- 5- **Beta rhythm:** This is a relatively fast rhythm, belonging approximately to the 13–30 Hz frequency band. It is a rhythm which is observed in awoken and conscious persons. This rhythm is also affected by the performance of movements, in the motor areas (Pfurtscheller and Neuper 2001).
- 6- **Gamma rhythm:** This rhythm concerns mainly frequencies above 30 Hz. This rhythm is sometimes defined with a maximal frequency around 80 Hz or 100 Hz and is associated with various cognitive and motor functions.

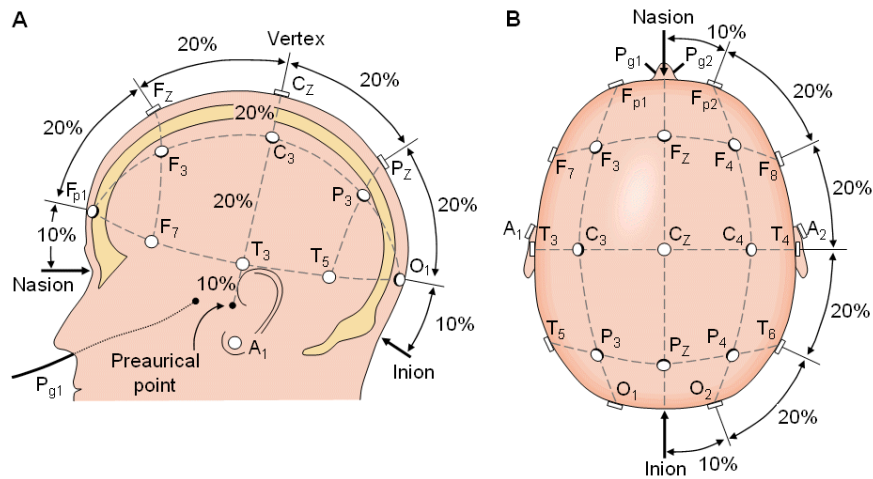


Figure 2-6 International 10–20 electrode placement system

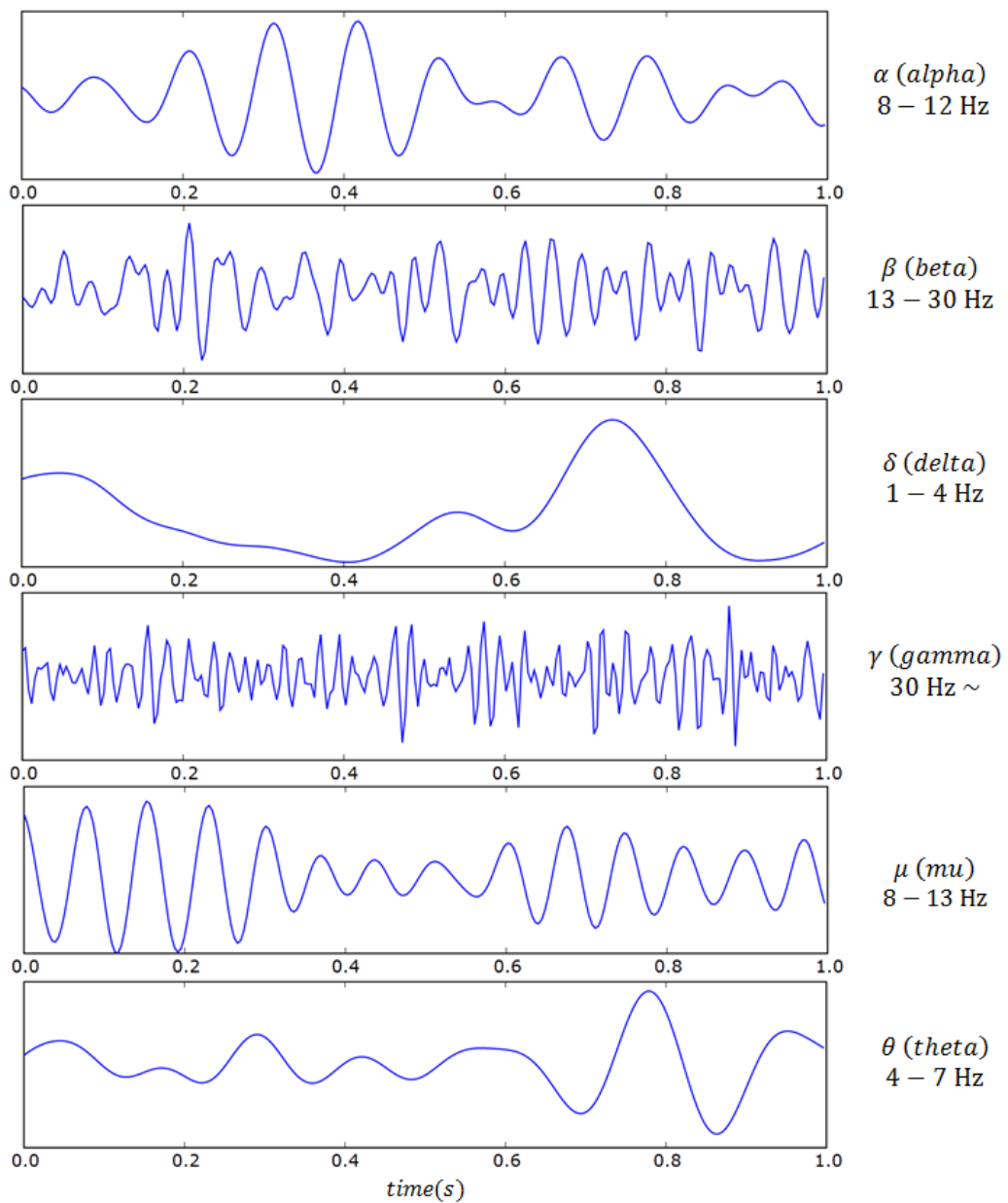


Figure 2-7 Brain rhythms (adopted from [Wikipedia](#))

### 2.3.1.2 EEG Signal Quality

A common problem with the signal measured with EEG is the high level of noises, which in the BMI community are commonly called artifacts. These artifacts are divided in two groups: 1) artifacts that do not originate from the subject, called subject independent, and 2) artifacts that originate from the subject (brain and/or muscle), called subject dependent.

The first group includes artifacts from the environment and the recording devices, including but not limited to: the power line, computers and computer screens, electrode amplifiers, cellphones, etc. An artifact source present in all EEG recordings is the noise induced by the EEG amplifier's power supply. The EEG signals are very weak and they can be easily disturbed by strong environment signals.

The second group includes signals generated from brain activity not related to the specific task performed for BMI, and capable to mask and or affect the EEG signal. For instance, alpha rhythms occur in the same frequency as the P300 component (Appendix B.2.2). With strong alpha activity the P300 diminishes as it gets masked by the higher amplitudes of the alpha rhythm. In the second group are included also signals coming from muscular activity, these artifacts may originate from: a) increased muscle tension (Electromyographical artifacts), especially head or neck muscles may corrupt the EEG with heavy signal disturbances of high amplitudes; b) electrical activity of the heart muscle (cardiac artifacts); c) limb or other body movements (motion artifacts) may disturb recording electrodes; d) eye blinking and eye movements (Oculographic artifacts) are easily visible in EEG and have higher amplitude than most of BMI significant electrophysiological signals.

Commonly, before every BMI operation the subject's scalp and the electrodes are cleaned, and gel is added to reduce impedance. Good grounding, reference and EEG signal electrode impedance leads to reduction of artifacts. Furthermore, the subjects, which in the research laboratories are usually healthy and able to move all their muscles, are advised to make as little movement as possible to reduce the artifacts. Reducing the amount of electronic equipment usually results in improved signal quality.

Besides artifacts, there are further limitations of EEG signals far more difficult to overcome. An EEG recording offers low spatial resolution; indeed, the signal recorded from an electrode is not just from one location. No matter where the electrode position is,

---

electrical activity from close proximity sources is simultaneously recorded. The number of these sources is unknown and dynamically changes in time. Moreover, neural population's electrical activity in the targeted brain area is impossible to measure on the scalp due to the attenuation ability of the skull. All dipole neurons of the area must be synchronized and must be oriented perpendicular towards the scalp with their dendrites aligned in parallel to maximize the amplitude of the electrical field in order to penetrate the skull (Niedermeyer and Silva 2005; Sanei and Chambers 2007).

### 2.3.2 Electrophysiological Signals Suitable for BMI

BMI communication is based on the identification of specific neural activity generated signals. In the case of EEG based BMI, the communication is established by using electrical brain signals (or electrophysiological signals). Based on the assumption that similar neural activity generates similar electrophysiological signal patterns (or features), the BMI goal is to identify specific neural activities by decoding the brain signals and associating them with previously known signal patterns (or features).

Current BMI systems use various electrophysiological signals to establish BMI communication. Based on the subject's role during the generation of these signals, there are two main categories (Curran and Stokes 2003; Wolpaw et al. 2002):

**Evoked Signal or Evoked Potential (EP)** are automatically generated in specific brain areas when an external stimulus (e.g. visual) is perceived by the subject. These signals, also referred to as event related potentials (ERPs), are typically generated in response to peripheral or external stimulations, and appear as somatosensory, visual, and auditory brain potentials, or as slowly evolving brain activity observed before voluntary movements or during anticipation of conditional stimulation (Sanei and Chambers 2007). The most commonly used signal class in this category is the Steady State Evoked Potentials (SSEP) and the P300. Since they are automatically generated, little or no subject training is required to operate the BMI system (Diez et al. 2013; Wolpaw et al. 2002). Nevertheless, an initial tuning based on offline recorded signals is still needed. The drawback of these signals is that they cannot be controlled by the subject, but only by the external stimulus device (e.g. monitor).

**Spontaneous Signals** are voluntarily generated by the subject following a voluntary cognitive process (i.e. mental activity). In this category, the most commonly used sig-

nals are the *motor* and *sensorimotor rhythms*. Other spontaneous signals used for BMI include, *Slow Cortical Potentials* (SCP) (Hinterberger, Schmidt, et al. 2004; Birbaumer 2006) and *non-motor cognitive task* generated signals like mental mathematical computations, mental rotation of geometric figures, visual counting, mental generation of words, music imagination, etc., (Cabrera, Farina, and Dremstrup 2010; Chai et al. 2012).

A description of the most popular electrophysiological signals acquired with EEG and used for BMI is shown in Appendix B. In this thesis, we will focus on spontaneous signals generated by *motor* and *sensorimotor rhythms*, which will be addressed in the next section.

### 2.3.3 Sensorimotor Rhythms

These brain rhythms are believed to be originated in the motor and sensorimotor cortex during a motor movement (e.g. hand movement) or imagination, by the subject. They are mainly generated in the  $\mu$  and  $\beta$  rhythm frequency bands, which are present in most healthy adults (Pfurtscheller and Berghold 1989). It is possible for a human to voluntarily control these rhythms. This feature makes these rhythms very attractive for BMI usage. In the following, we are going to explain two traditional approaches used to communicate through BMI by using sensorimotor rhythms:

**Operant Conditioning** – In this approach, the subject learns to voluntarily modify the amplitude of his sensorimotor rhythms through a (very) long training procedure using real time feedback (Wolpaw and McFarland 2004; Wolpaw et al. 1991; Vaughan et al. 2006; Wolpaw 2007). After training the subject is able to generate easily detectable sensorimotor rhythms.

**Motor Imagery** – During an EEG recording session if the subject performs a motor movement (or imaginary motor movement), a power decrease in  $\mu$  and  $\beta$  rhythms can be noticed over the corresponding motor cortex part of the imagined limb. This process is called Event Related De-synchronization (ERD). After the MI task is finished there is a recovery in the power of  $\mu$  and  $\beta$  rhythms known as Event Related Synchronization (ERS) (Lemm, Müller, and Curio 2009; Pfurtscheller and Lopes da Silva 1999; Pfurtscheller et al. 1998). The dynamic of the above electrophysiological activity is shown in Figure 2-8.

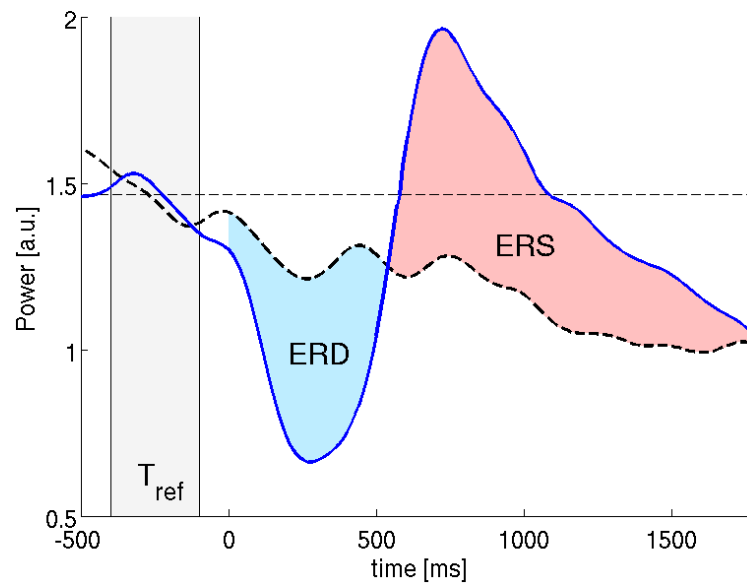


**Figure 2-8 Event Related De-synchronization and Event Related Synchronization (ERD/ERS)**  
(adopted from (Lemm, Müller, and Curio 2009))

The ERD/ERS process starts around one second before the actual movement or the imaginary movement. This is commonly referred to as *Readiness Potential* or *Pre-Motor Potential*. This potential is associated with pre-motor cortical activity that happens in the planning area of motor cortex. The ERD/ERS generated from MI is broadly used for BMI communication. Usually up to three MI tasks are used in BMI, each associated with a command or a control action (Wolpaw et al. 1991; Blankertz, Dornhege, Krauledat, Müller, et al. 2006; Pfurtscheller et al. 1997).

### 2.3.4 Conclusion

There exist successful BMI implementations with all the signals presented in this section. Depending on a specific application every signal has its advantages and its disadvantages, this makes the selection of the signals closely related to the application. EP can be operated without subject training, but they require continuous usage of external stimuli which can be tiring for the subjects. For instance, it has been reported that the P300 amplitude elicited by the mental task decreases over time due to mental and physical fatigue (Ullsperger, Metz, and Gille 1988; Sanei and Chambers 2007).

In the case of robot control, spontaneous signals are more natural and comfortable to use since they do not rely on external stimuli, but they generally require a long training time. Commonly, before using a MI based BMI system online (i.e. to control a robot in

real time), few training sessions are required to tune the BMI in order to become reliable (Pfurtscheller, Graimann, and Neuper 2006). In this direction, recent machine learning and signal processing methods have shown to significantly reduce the training time while still keeping good BMI communication quality (Blankertz, Dornhege, Krauledat, Müller, et al. 2006; Krauledat et al. 2008; Blankertz et al. 2007). Anyway, there remains the need for the subjects to be able to concentrate on the mental task, and with no doubt trained subjects perform better than untrained ones.

In this thesis, we will focus on the detection of MI brain activity generated electro-physiological signals, for the task of BMI based navigation of a robotic wheelchair in real time.

## 3 Brain Machine Interface

This chapter gives a general overview of BMI systems. It starts with the introduction of the generic diagram of a BMI system (Section 3.1). Then, it continues with some important definitions of the BMI systems (Section 3.2). The last part of this chapter (Section 3.3) contains a literature review of the BMI system applications in different research fields including, communication and control, gaming and virtual environments, motor recovery, and motor substitution.

### 3.1 BMI Diagram

BMI is a relatively new, multidisciplinary research field that involves computer science, signal processing, intelligent robotics, neuroscience, etc. The BMI systems are usually used to control assistive robots (Perrin et al. 2010; Mano and Capi 2013), communicate with computers (Birbaumer et al. 2000), play games (Lotte 2011; Nijholt, Bos, and Reuderink 2009), etc.

Since there are many ways to establish a BMI communication and the BMI applications cover a wide area of different fields, there does not exist a unified standard diagram for BMI. Anyway, a conceptual generic diagram of a BMI system that controls a robotic wheelchair in real time is shown in Figure 3-1. A BMI system usually follows six steps during online operation: signal acquisition, signal processing, feature extraction, classification, robot control command and feedback (Mason and Birch 2003):

- 1- **Signal Acquisition (brain activity measurement)** is done by using different types of sensors that measure brain activity (Shih, Krusienski, and Wolpaw 2012). In this thesis, we will focus on the electrophysiological brain signals measured by EEG.

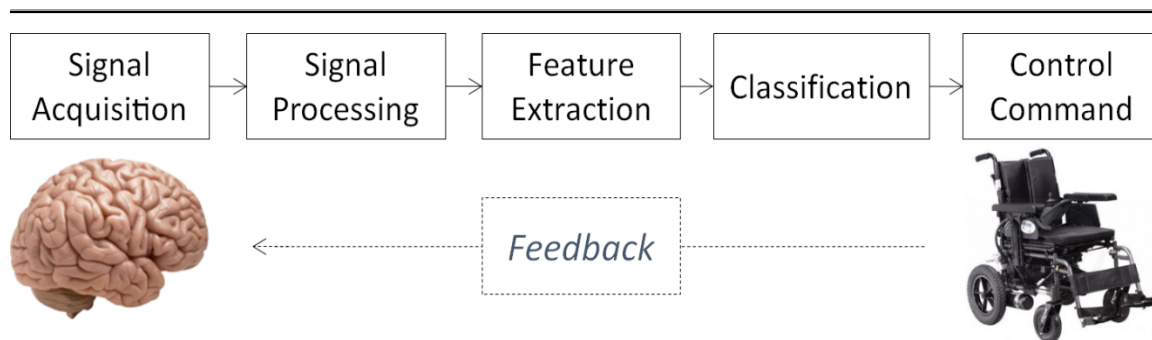


**Figure 3-1** Generic diagram of a BMI system

- 2- **Signal Processing** is used to remove signal noise, while preserving or even enhancing important information that is embedded within the recorded brain signals (Bashashati et al. 2007).
- 3- **Feature Extraction** (in some BMI application is also considered as part of the signal processing step) has the goal of extracting the values or features of the brain signals that best describe the targeted mental activity.
- 4- **Classification** assigns a “class” to the features extracted from the previous step (Lotte et al. 2007). In BMI, “class” refers to a specific mental state or mental activity which is used to establish BMI communication.
- 5- **Robot Control Command.** The output of the classifier is usually associated with a control command (i.e. turn left or turn right) that is used to actuate a robot (Wolpaw et al. 2006).
- 6- **Feedback** is used to notify the subject with the results of the classifier (mental state classification output). It is a common belief that subjects can, at some level, control and adapt their brain signals in order to achieve better BMI performance (Wolpaw et al. 2002). Feedback can be visual or auditory (Wolpaw et al. 2002; Hinterberger, Neumann, et al. 2004; Brumberg, Guenther, and Kennedy 2013).

As mentioned in Section 2.3.4, offline recording session(s) are used to calibrate the signal processing, classification and feature extraction algorithms of the BMI system. During offline session(s), the BMI subject is asked to repeat some predefined mental tasks for a certain amount of time while brain activity is monitored, recorded and stored in a computer.

The offline sessions are crucial to the BMI system performance. Since every subject’s mental activity has unique characteristics, then the BMI must be calibrated with the specific subject brain activity recordings (Pfurtscheller and Neuper 2001).

## 3.2 Definitions

A brain computer/machine interface is a direct communication pathway between the brain and an external device (Wolpaw et al. 2000) that does not depend on the brain's normal output channels of peripheral nerves and muscles (Wolpaw et al. 2002). This communication is based on the principle of decoding the brain activity produced while the BMI subject performs specific mental tasks. BMI systems are usually distinguished by three main features:

**Dependence** – A dependent BMI (Lalor et al. 2005; Allison, Graimann, and Gräser 2007) uses some level of motor control from the subject, whereas an independent BMI relies only in the online measured brain activity (Allison, Wolpaw, and Wolpaw 2007). By using motor functions, a dependent BMI system offers higher communication and control capabilities compared to an independent BMI system. But, in the case of BMI applications targeted at disabled people, residual motor functions are not always available, thus the independent BMI systems are the only solution.

**Invasiveness** – Depending on the placement of the signal acquisition electrodes (or sensors) that measure the brain activity, a BMI system can be classified as invasive, partially invasive or non-invasive. If the electrodes used for brain activity measurement are placed within the cortex, the BMI system is called invasive or fully invasive (Moritz, Perlmutter, and Fetz 2008; Mano et al. 2013). If the electrodes are placed inside the skull but outside the cortex area, the BMI system is called partially invasive. Last, if the measurement electrodes are placed outside the head (i.e. on the scalp) the BMI system is called non-invasive (Wolpaw et al. 2002; Shih, Krusienski, and Wolpaw 2012). With an invasive BMI it is possible to acquire better signal quality and thus improve overall communication performance, but invasive BMIs are very risky, expensive and require brain surgery.

**Device Synchronization** – Depending on the subject's interaction with the system, there are two types of BMIs: synchronous (device-paced) and asynchronous (self-paced). When using a synchronous BMI, the subject can interact with the robot or the BMI application only when notified by the system through a visual or auditory signal, called device stimuli. This interaction involves the subject performing a certain voluntary mental task, or the BMI system detecting itself an involuntary mental activity, for a predefined amount of time. Before the stimulus and after the mental task time ex-

pires, the communication channel is closed. In contrast, asynchronous BMIs do not use any device synchronization. In an asynchronous BMI, the subject is able to communicate with the device by voluntarily performing one or several predefined mental activities for the BMI communication, or choose not to interact by not performing any of the above activities (Mason et al. 2006; Bashashati 2007; Scherer et al. 2007; Pfurtscheller, Graimann, and Neuper 2006; Pfurtscheller et al. 2010). An asynchronous BMI system is ideally the best solution, but technically it is very challenging to design and build reliable asynchronous BMI systems that offer high level of accuracy. Recently, BMI applications in this direction have started to emerge (Tsui, Gan, and Hu 2011; H. Zhang et al. 2012).

### 3.3 BMI Applications

For more than 20 years, research on BMI systems has attracted a great deal of attention, and applications in different research fields have emerged. The first and most important BMI applications fall in the medical domain, aimed at assisting disable people (Shih, Krusienski, and Wolpaw 2012), but there exist applications in other domains like video games and virtual reality, that although primarily aimed for the development of BMI systems for disable people, can be used by healthy people as well (Bonnet, Lotte, and Lecuyer 2013; Leeb, Friedman, Slater, et al. 2007; D. Coyle et al. 2011)

The existing BMI applications can be divided into four major categories (Millan et al. 2010). Each of these categories will be explained in a separate subsection in the following this chapter.

#### 3.3.1 Communication and Control

This category includes applications that assist severely disable individuals to communicate with other people and/or to control their environment. Examples of such applications are spelling devices (Cecotti 2011), computer cursor control, etc. Here we are going to introduce three classical examples of BMI speller devices.

**The P300 speller** is an application used to spell words by utilizing the fact that rare events in the oddball paradigm elicit the P300 component of the ERP (Appendix B) in brain signals measured by EEG (Farwell and Donchin 1988; Donchin, Spencer, and

Wijesinghe 2000). This application could enable a subject to spell up to 7.8 letters per minute with approximately 80% accuracy. The advantage of this BMI application lies in the fact that almost any subject who is able to control his gaze, can use it without needing prior training. There exist also other BMI applications based on a similar principle that have been developed more recently (Piccione et al. 2006; Sellers and Donchin 2006; Hoffmann et al. 2008).

The “**Thought Translation Device**” (TTD) aims at enabling paralyzed individuals to spell words by using their spontaneous variations of the brain SCP (Appendix B) signal amplitude. The subjects using this BMI application must learn to control their SCP through a long training procedure before being able to use it. This TTD system enables disabled people to communicate with a speed approximately one letter every 2 minutes (Birbaumer et al. 2000).

**Hex-O-Spell** is an asynchronous BMI application that uses MI brain activity generated signals and is capable to achieve an information transfer rate up to 7.6 letters per minute (Blankertz, Dornhege, Krauledat, Schroder, et al. 2006). The system has two cascade levels (Figure 3-2). At level 1, the subject selects a hexagon cell containing 5 letters, by using right hand MI to rotate the green arrow until it points to the desired cell. Then, by using foot MI is able to select the cell. At level 2, the subject does the same procedure to select the cell with the desired letter.

BMI applications in communication also include web browsing (Karim et al. 2006; Bensch et al. 2007; Mugler et al. 2008), computer cursor control (Wolpaw et al. 1991; Wolpaw and McFarland 2004; Vaughan et al. 2006) virtual keyboards (Mayaud et al. 2013) and speech communication (Brumberg et al. 2010).

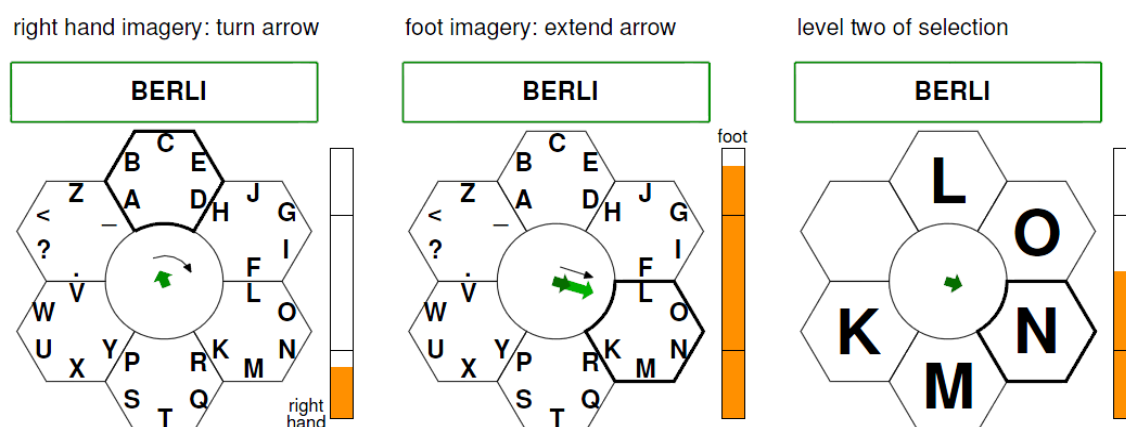


Figure 3-2 The text entry system ‘Hex-O-spell’ interface (adopted from (Blankertz, Dornhege, Krauledat, Schroder, et al. 2006))

### 3.3.2 Gaming, Entertainment and Virtual Reality

In addition to medical applications, there is an increasing number of BMI applications for entertainment, such as 2D/3D video games and virtual reality based BMI prototypes (Lecuyer et al. 2008; Hasan and Gan 2012; Lotte 2011). Virtual reality offers a convenient test bed for BMI applications. It allows research and development of different BMI systems behaviors, in different virtual scenery, environments and situations within the same place, thus avoiding the expense and risks of conducting those experiments in real world.

Early work on virtual reality includes use of BMI for flight simulators (Nelson et al. 1997; Middendorf et al. 2000; Bayliss and Ballard 2000). Other applications include, healthy and paralyzed adults exploring and/or walking in virtual environments (Leeb, Lee, et al. 2007; Scherer et al. 2008), controlling virtual cars (Zhao, Zhang, and Cichocki 2009), manipulating virtual objects (Lalor et al. 2005), and avatars (Faller et al. 2010).

Leeb et al. has shown a virtual reality BMI based wheelchair navigation controlled by a spinal cord injured patient. In this study, the subject was able to navigate the wheelchair in a virtual street populated with other avatars (Figure 3-3) by using an asynchronous BMI system based on a single bipolar recording of his centrally localized beta oscillations, generated from the movement imagination of his paralyzed feet. In average, the subject was able to navigate the wheelchair from one position in a virtual street to another with 90% accuracy (Leeb, Friedman, Slater, et al. 2007).

Recently, some interesting BMI based video game applications have been developed. They include single user based video games like bacteria hunt (Mühl et al. 2010) or BMI controlled spaceship video game (D. Coyle et al. 2011), and also multiple user games like playing soccer (Bonnet, Lotte, and Lecuyer 2013).



Figure 3-3 BMI navigation in a virtual street (adopted from (Leeb, Friedman, Slater, et al. 2007))

### 3.3.3 Motor Recovery

The modern approach of neuroscience-based rehabilitation aims to use BMI protocols (i.e. limb MI tasks) as an opportunity to improve motor function recovery by stimulating and guiding brain plasticity phenomena after stroke. Current rehabilitation therapies can directly benefit from BMI by reinforcing and increasing more effective usage of impaired brain areas and connections (Ward and Cohen 2004; Gerloff et al. 2006; Nudo 2006; Millan et al. 2010; Shih, Krusienski, and Wolpaw 2012).

Furthermore, combining BMI with functional electrical stimulation (FES) or assistive robotics may aid motor relearning in stroke patients. Using BMI to assist rehabilitation therapy may also reduce the cost of rehabilitation process by reducing the need for the presence of a rehabilitation therapist. Anyway, within the BMI community this topic is at a very preliminary stage (for a detailed review see (Birbaumer, Murguialday, and Cohen 2008; Daly and Wolpaw 2008; Mak and Wolpaw 2009; Millan et al. 2010; Shih, Krusienski, and Wolpaw 2012)).

### 3.3.4 Motor Substitution

The unique ability to communicate with machines only by mere thought (i.e. brain signals), makes the combination of BMI systems with assistive technologies a very attractive choice to provide solutions that can benefit patients with motor disability, when no other means are possible.

BMI usage to support human's motor disability is a very important application field within BMI community. Two main areas that have seen a significant development include the BMI systems that are used to: 1) substitute grasp function and 2) provide some mobility functions to paralyzed patients (Millan et al. 2010). Examples of applications in both areas are shown in the following.

#### 3.3.4.1 Grasping

FES has the potential to partially restore lost motor functions in disable individuals. A crucial motor function, that can significantly improve the quality of life in disabled patients, is hand grasping (K. D. Anderson 2004). The currently developed neuroprosthet-

ic arms that are aimed at restoring grasp function in disable individuals mainly fall into four categories:

The first category of neuroprosthetic arms relies on other residual motor functions, not related to grasping (i.e. forearm muscles), to restore grasp function (Kameyama et al. 1999; Mangold et al. 2005; Memberg, Crago, and Keith 2003).

The second category, involves non-invasive BMI neuroprosthetic arms, aimed at severely paralyzed patients that do not have other residual motor functions available (Müller-Putz et al. 2006; Tavella et al. 2010).

The third category is the combination of the first two. In this category non-invasive BMI and FES systems combined applications are used to restore grasp, wrist and elbow motor functions (Pfurtscheller et al. 2003; Müller-Putz et al. 2005; Leeb et al. 2010; Pfurtscheller et al. 2005).

The fourth category is the invasive BMI prosthesis. Isolated motor cortex neural recordings have shown the possibility of controlling prosthetic limbs (Moritz, Perlmutter, and Fetz 2008; Velliste et al. 2008; Chapin et al. 1999).

However, the use of BMI and FES in the field of motor recovery needs to be investigated more extensively (Millan et al. 2010; Leeb and Millan 2013).

#### 3.3.4.2 Assistive Mobility

BMI technology can provide motor substitution by assisting subject's mobility with brain controlled wheelchairs (Galán et al. 2008; Philips et al. 2007) or with remote brain controlled telepresence robots (Tonin et al. 2010). A third option is to provide sophisticated lower limbs to restore walking abilities in disable individuals. Due to the complexity of the walking process and the restricted capabilities of the BMI systems at the current state of their development, the third option has not been thoroughly investigated yet.

In this thesis, the case of mobility assistance provided by brain controlled wheelchairs is considered. There are two BMI aspects that make the task of controlling a wheelchair very challenging. First, it is the low-bitrate nature of the BMI communication channel. BMI can efficiently classify only up to three or four mental tasks, which limits the subject's available actions and affects directly the control performance. Second, the

brain signals change from one mental state of a human to another (Sanei and Chambers 2007) and from one human to another human. This makes the generalized BMI models inefficient for mental task classification, which directly affects the BMI communication quality. These aspects have been previously investigated in BMI based control of either real wheelchairs (Perrin et al. 2010; Urdiales et al. 2011; Carlson, Leeb, Monnard, et al. 2012; Lopes, Pires, and Nunes 2013) or simulated wheelchairs (Gentiletti et al. 2009; Galán et al. 2008).

In order to deal with the individuality and the dynamic nature of brain signals, subject's specific predictive models are commonly acquired prior to BMI operation. Furthermore, during online BMI operation, the subjects are required to follow the same mental task dynamics repeatedly. This usually leads to a high subject's mental workload and makes the whole navigation experience tiring.

A common ground used to address the above BMI controlled wheelchair challenges, is the combination of BMI systems with intelligent robotic wheelchairs (Wolpaw et al. 2000). The shared control or shared autonomy approach (Perrin et al. 2010; Galán et al. 2008; Philips et al. 2007) is proposed as an effective way to deal with the low bitrate nature of the BMI. In this approach, the robotic wheelchair is equipped with different assistive modules to complement BMI and assist robot navigation, based on robot intelligence and environment situation (Philips et al. 2007).

In general, the shared control approach allows a dynamic autonomous control level between the subject and the robot, which can be defined either by the subject or the robotic wheelchair system. In one approach, changing the control level (control mode) requires the subject to be able to control an extra switch or button (Katevas et al. 1997; Bourhis and Agostini 1998; Prassler, Scholz, and Paolo Fiorini 2001; Parikh et al. 2004; Yanco 1998). This approach offers a very complicated operation procedure and requires manual intervention, which is only possible when the subjects have residual motor functions. In a second approach, the shared control system automatically switches from one mode to another without requiring any subject intervention (Levine et al. 1999; Röfer and Lankenau 2000). This approach restricts the subjects control and offers navigation assistance only in a predefined manner, which makes the navigation strictly environment dependent. In a third approach, the BMI navigation system estimates the subject's mental intent and provides appropriate assistance for navigation of the wheelchair based on the environment and a predefined level of assistance priority (Vanacker et al. 2007; Galán et

---

al. 2008; Millan et al. 2009; Tonin et al. 2010). This approach, which is actually an improvement of the second approach, autonomously navigates the robot and switches assistance based on the subject mental activity using the BMI system. Theoretically, the third approach is the most suitable, but also the hardest to achieve.

When attempting to provide a shared control with a synchronous BMI (Lopes, Pires, and Nunes 2013) the subject's get easily tired, since continuous focus is needed on the stimuli screen. On the other hand attempts to provide an "asynchronous" BMI control either ignore the subject intentions during autonomous navigation or require the subject to continuously control its mental state, which leads to a very high mental workload (Galán et al. 2008; Philips et al. 2007; Perrin et al. 2010; Leeb, Friedman, Müller-Putz, et al. 2007; Vanacker et al. 2007). Furthermore, modules used to assist navigation require specific prior environment information (e.g. the goal location for orientation recovery module) and in some cases need environment training, which makes the BMI navigation closely environment dependent (Lopes, Pires, and Nunes 2013; Perrin et al. 2010). A typical example of the semi-autonomous strategy is introduced by Perrin et al. (Perrin et al. 2010). This method reduces subject's mental workload, by autonomously navigating the robot, and by requiring subject involvement for simple yes or no decisions. The subject get involved only when a navigation choice has to be done, and doesn't have any control (BMI based) over navigation otherwise.

The adaptive wheelchair navigation method proposed in this thesis, reduces the mental workload of the subject while still allowing full control over navigation. The subject is able to accept or reject assistance offered by the ANP at any time only by using his brain activity measured by EEG. Furthermore, no prior environment training or environment information (e.g. goal position, layout map, etc.) is used for robot navigation.

## 4 Developed BMI System

This chapter introduces in detail all the methods and techniques that we have used to design the BMI system for our experiments. As such, it details the different processing steps in our BMI system, including measurement of brain activity in Section 4.1, offline data recording in Section 4.2, signal processing and feature extraction in Section 4.3 and classification in Section 4.4. Finally, Section 4.5 describes the online predictive module that we will use for robot control.

### 4.1 EEG Signal Acquisition

The EEG signals were recorded on scalp by using  $d$  EEG electrodes ( $d = 15$ ) mounted on an electrode cap positioned as shown in Figure 4-1 ( $F7, F8, F3, F4, C3, C4, P3, P4, T3, T4, T5, T6, Cz, Fz, Pz$ ). The electrode cap was connected to the Mitsar–EEG 201 electrode box/amplifier (Figure 4-2). The technical specifications of the electrode box are shown in Table 4-1. Before starting signal acquisition, the electrode impedance was adjusted by applying conductive gel until the impedance meter showed below  $3k\Omega$  for every single electrode including reference and earth.

The EEG channels from the electrode box were collected on a personal computer by using an USB interface. Then, they were digitized in Matlab at a sampling rate of 250 Hz. The EEG signals were acquired by referencing the digitized EEG channels with the ear electrode average ( $A1$  and  $A2$ ).

In order to build the BMI predictive model for real time robot navigation, at first we conducted an offline recording session. In the next section we will explain the method used to acquire the offline EEG signals.

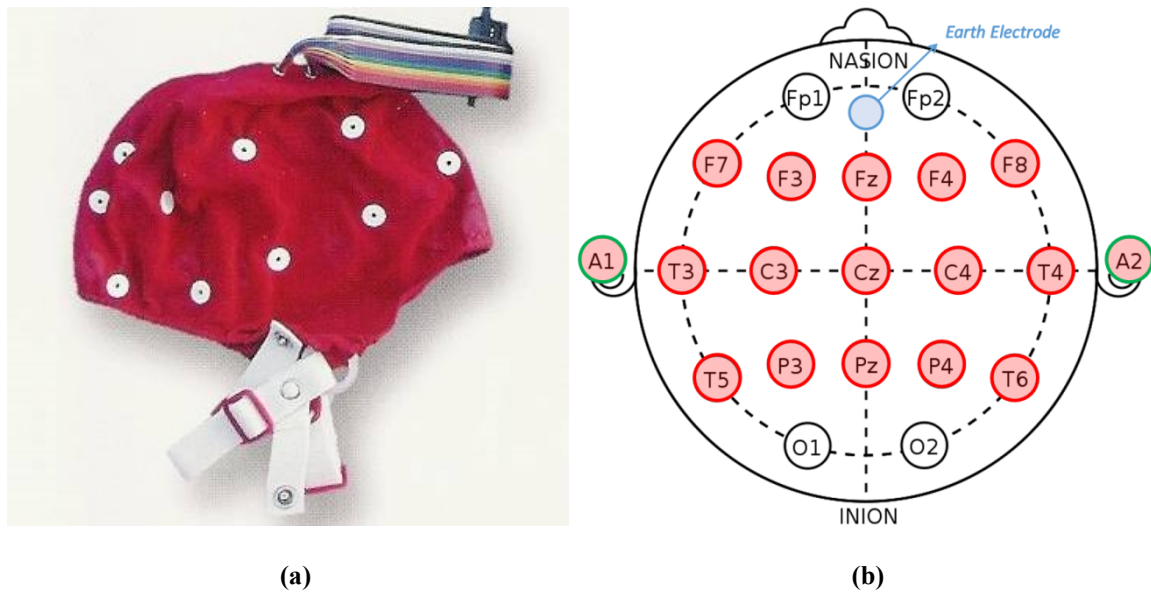


Figure 4-1 (a) the electrode cap, and (b) the electrode placements positions

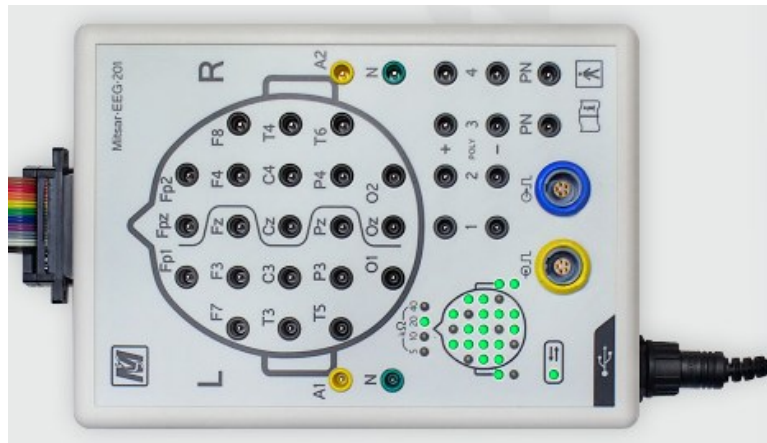


Figure 4-2 Electrode box (adopted from Mitsar Co., Ltd [website](#))

Table 4-1 Mitsar-EEG 201 technical specifications (adopted from Mitsar Co., Ltd [website](#))

<b>Channels</b>	21 EEG + 1 or 4 active/reference pair
<b>Frequency band</b>	0,16 – 70 Hz
<b>Analog to digital conversion</b>	16 bit ADC
<b>Sampling and rate</b>	500 Hz/channel
<b>Input impedance</b>	> 200 MOhm
<b>Input range</b>	5000 $\mu$ V peak to peak
<b>Noise</b>	< 1,5 $\mu$ V peak to peak
<b>Interface</b>	USB
<b>Power Supply</b>	USB powered
<b>Dimensions</b>	Head box: 185x135x45 mm
<b>Weight</b>	900 g (with batteries)

## 4.2 Offline EEG Recording Sessions

During the offline session, EEG brain signals were recorded while the subject performed MI tasks. The BMI subject was seated on a comfortable chair in a relaxed position (Figure 4-3) and looked at the computer screen during the whole session. The duration of an offline session is approximately 15 minutes. In total, an offline session has 120 trials, divided equally between three MI tasks (40 trials per task).

A trial consists of multichannel EEG recordings of the subject while performing one single MI task. The structure of one trial is shown on Figure 4-4, and the cues that appear on the screen during one trial are shown on Figure 4-5.

The subject is notified by the start cue, to prepare for the mental task and after one second the specific MI mental task cue would appear on the screen (*Left Hand*, *Right Hand* or *Foot*). The duration of a MI task is 3 – 5 seconds, followed by a relax time of 2 – 3 seconds. Then, the start cue will appear again on the screen to notify the subject to prepare for the next task.



Figure 4-3 BMI subject during offline data recording session

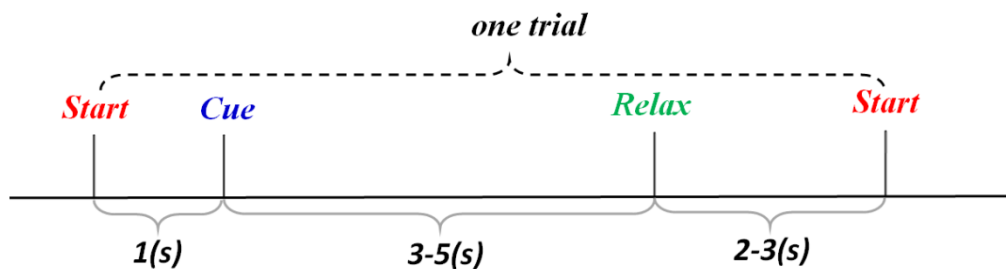


Figure 4-4 Trial structure

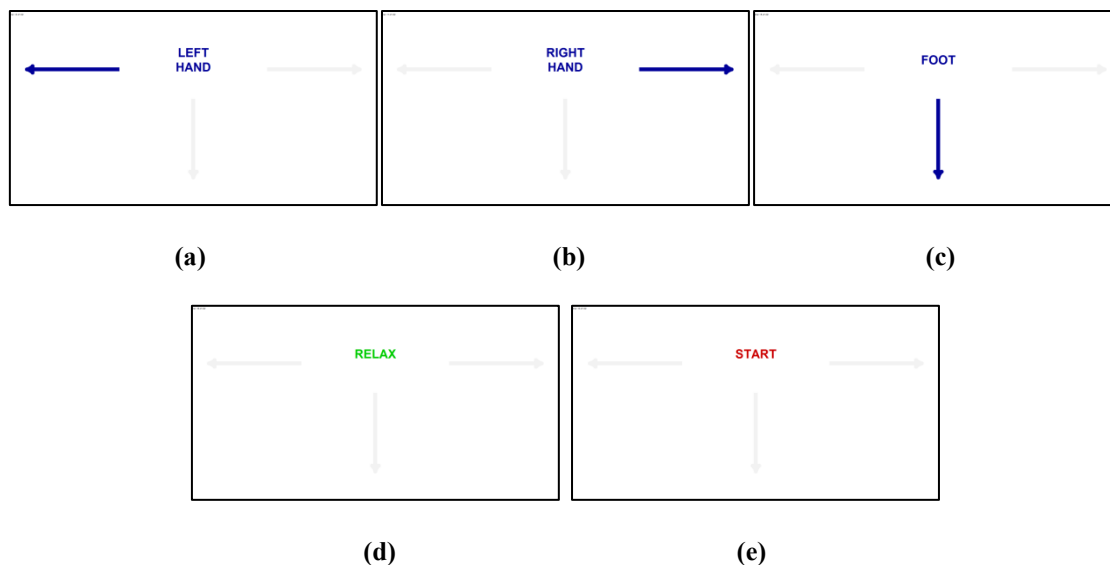


Figure 4-5 Offline training cues: (a) Left hand (b) Right hand (c) Foot (d) Relax and (e) Start

If we denote the signal coming from one electrode  $E_l$ , where  $l \in \{F7, F8, \dots, Pz\}$  is the electrode label, and  $Ref = (A1 + A2)/2$  is the reference channel (Section 4.1). Then, the EEG signal channels are calculated from:

$$x_i = E_{l_i} - Ref \quad \forall i \in \{1, 2, \dots, d\} \quad 1$$

The offline data session is represented by matrix  $X$ , with rows  $x_i$  ( $i \in \{N^+ | i < 16\}$ ) corresponding to the signal channels acquired from Eq. 1. Along with the EEG signal data, event data were also collected simultaneously. Their occurring time and type were saved together with the EEG signals in a data structure for further processing.

### 4.3 Signal Processing

As mentioned early in Section 2.3.1, the signals collected by EEG are very noisy and have a low signal-to-noise ratio (SNR). Signal processing is used to clean (de-noise)

the EEG signals and/or to enhance the target information within these signals. Common sources of the signal noise are muscle artifacts, which generally have higher amplitude than brain signals.

The background brain activity (i.e. brain activity not related to the electrophysiological signals used for BMI) is also considered as noise and it is present with similar amplitude and sometimes similar frequency as well. Furthermore, additional noise comes from other sources like the power network, EEG devices, computers, etc. These “noise” signals make the task of cleaning and extracting the desired electrophysiological signal very challenging. Indeed, the BMI research community has paid a great deal of attention to the EEG signal processing, since it affects the whole BMI performance.

In BMI community, the signal processing step is sometimes regarded as filtering since most of the signal processing techniques used to improve SNR of the EEG signal are temporal, spatial or spectral filters, and combinations of the above (McFarland et al. 1997; Ramoser, Müller-Gerking, and Pfurtscheller 2000; Besserve, Garnero, and Martinerie 2007). In addition, simple signal processing steps are used prior or after filtering, such as moving average filtering, subsampling, baseline correction or local averaging (Rakotomamonjy, Alain et al. 2005). Below, we are going to describe the signal processing methods used in our BMI system.

### 4.3.1 Signal Pre-processing

At first, we will resample the signal originally collected at 250 Hz. The new sampling rate will be 100 Hz. The offline EEG signals are marked with timed events (Section 4.2). Each event represents the cues that appear to the BMI subject during the offline recording session. We will extract epochs in the interval [0.5, 3] seconds after any of the three MI task cues used in our experiments (Figure 4-6).

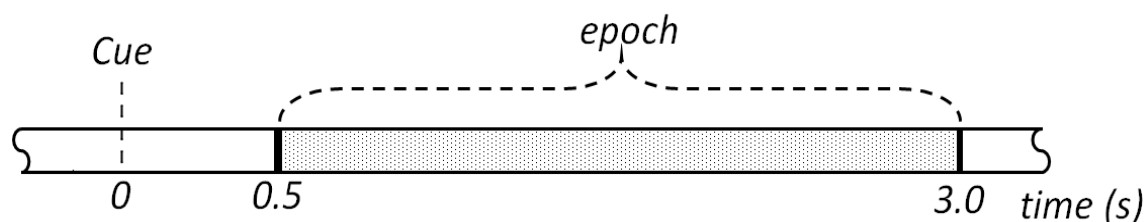


Figure 4-6 Epoch extraction interval

Frequency filters used for EEG signals include, low-pass, high-pass or band-pass filters. In order to frequency filter the EEG signals, first we use Discrete Fourier Transform. Then, we use brickwall filters to band-pass filter the signal spectrum in the [8, 30] Hz frequency band (Oppenheim, Schaffer, and Buck 1999). The brain activity recorded in this frequency band ( $\mu$  and  $\beta$  rhythms) is believed to be generated from the motor and somatosensory cortex areas during motor or MI activity (Section 2.3.1.1).

The band-pass filtered signal is again filtered using a LTI filter and then we use a Common Spatial Patterns (CSP) based method that involves spatial, temporal and spectral filtering. This method will be explained in the following.

#### ❖ LTI filtering

LTI filtering has been investigated before as an effective way to reduce noise and improve SNR. Leem et al. uses simple frequency filters with one delay operator for every signal channel and then optimizes spatial filters for both signals (Lemm et al. 2005). This method doubles the number of data channels and increases the computation load without gaining a significant improvement. Following this idea, a general LTI filtering is proposed for signal filtering before optimizing the spatial filters by Dornhege et al. (Dornhege et al. 2006). If we denote  $x^{(t)}$  the values of  $X$  at time point  $t$  then the LTI filtered EEG signal  $y^{(t)}$  is given as:

$$a_1 y^{(t)} = b_1 x^{(t)} + b_2 x^{(t-1)} + \dots + b_{n_b} x^{(t-n_b-1)} - a_2 y^{(t-1)} - \dots - a_{n_a} y^{(t-n_a-1)} \quad 2$$

In this method, the filter parameters ( $a_i$  and  $b_j$ ) are chosen manually; this makes the procedure of selecting the best parameters long and inconvenient.

The reason for using LTI filtering is to eliminate artifacts, reduce noise and improve SNR in EEG signals, while hoping that discriminative information will not be suppressed (Blankertz, Tomioka, et al. 2008).

Tomioka et al. introduces a simultaneous way to find the optimal spatial filters and to optimize the LTI filter (Tomioka, Dornhege, Aihara, et al. 2006), instead of adjusting it manually (Lemm et al. 2005; Dornhege et al. 2006). The method, called spectrally weighted CSP (Spec-CSP), has shown to significantly improve signal filtering by adding spectral weighting coefficients to simultaneously optimize the spatial and spectral information in the multichannel EEG signal. Nevertheless, the results found by this method are

not perfect. As we will show later in this chapter, the Spec-CSP method extracts the filters based on signal's frequency properties. The stationary background noise in the same frequency range resides within the signal and it is reflected in the final filters.

In our method, we propose a simple LTI filtering step, denoted as " $f^{1,-\bar{1}}$ ", before applying Spec-CSP. If we substitute  $a_1 = 1$ ,  $b_1 = 1$ ,  $b_2 = -\bar{1}$ ,  $b_{i>2} = 0$  and  $a_{j>1} = 0$  (where:  $\bar{1} = 1/(\text{sampling rate})$ ) then, from Eq. 2, we gain the new LTI filtered signal:

$$y^{(t)} = f^{1,-\bar{1}}[x^{(t)}] = x^{(t)} - x^{(t-\bar{1})} \quad 3$$

The de-noising filter  $f^{1,-\bar{1}}$  serves as a signal pre-processing step to remove the additive stationary noise from the EEG signals. The signals gained from Eq. 3 are used by the Spec-CSP to jointly optimize spatial and temporal filters.

### 4.3.2 Spatial Filtering

Spatial filters are used to extract important signal information by selecting the most relevant contributions from different spatial locations (electrode positions) (McFarland et al. 1997). The simplest way to do that is by manually selecting the most relevant electrodes and ignoring the others. Other popular spatial filters used for noise suppression include: Common Average Reference and the Surface Laplacian filters (McFarland et al. 1997). More advanced and more efficient filtering methods include independent component analysis, inverse solution and CSP based signal filtering methods.

**Independent component analysis** is a popular method used for the blind source separation problem (Stone 2005; Jutten and Herault 1991; Hyvärinen and Oja 2000; Belouchrani et al. 1997). It has been increasingly popular in the EEG signal processing and BMI community for quite a while. Theoretically, it is possible to isolate the sources of EEG signals into separate components and then filter only the desired sources (e.g. motor cortex sources in MI), or isolate the undesired sources (e.g. artifacts) and then remove those sources from further processing. Practically, it is impossible to know all the available sources of the EEG signal, thus the method performs better with a very high number of electrodes (i.e. 32 to 256). This results in a very high computational load, required for independent components extraction. Nevertheless, this method has shown to increase SNR in offline EEG signal processing (Delorme and Makeig 2004;

Naeem et al. 2006; Makeig et al. 2000; Kachenoura et al. 2008; Hoya et al. 2003; Hammon and de Sa 2007).

**Inverse solution's** goal is to reconstruct brain activity in a 3D head model based on scalp measurements (Michel et al. 2004; Baillet, Mosher, and Leahy 2001). Usage in BMI community is limited (Lotte, Lecuyer, and Arnaldi 2007; Noirhomme, Kitney, and Macq 2008). A distinguishing characteristic of this method is its usage in both signal processing (Grave de Peralta Menendez et al. 2005; Babiloni et al. 2007; Noirhomme, Kitney, and Macq 2008) and feature extraction (Qin, Ding, and He 2004).

#### 4.3.2.1 Common Spatial Patterns

CSP and its variations are the most popular filtering methods used for MI based BMI. The CSP method is based on the data-driven decomposition of the EEG signals into spatial patterns. For that purpose spatial filters are constructed in such a way that enables the maximization of the difference between two classes (Ramoser, Müller-Gerking, and Pfurtscheller 2000; Popescu et al. 2007; Blankertz et al. 2007; Blankertz, Müller, Krusienski, Schalk, et al. 2006; Sajda et al. 2003; Blankertz et al. 2004; Müller-Gerking, Pfurtscheller, and Flyvbjerg 1999; Dornhege et al. 2004a; Blankertz, Tomioka, et al. 2008). Variants of CSP include spatial filter extraction methods such as invariant CSP (Blankertz, Kawanabe, et al. 2008), Principal Component Analysis (PCA) (Smith Lindsay I. 2002; Lee and Choi 2003) or Common Subspace Spatial Decomposition (CSSD) (Wang et al. 2004; D. Zhang et al. 2007) as well as spectro-spatial filters (Dornhege et al. 2006; Lemm et al. 2005; Tomioka, Dornhege, Aihara, et al. 2006).

Let us consider the typical binary classification problem of two MI tasks where the two classes (i.e. *right hand* and *left hand*) are denoted by  $R$  for right and  $L$  for left. A single trial of the filtered EEG signal with  $d$  electrodes (channels) and with  $T$  sampled time points is denoted by  $Y \in \mathbb{R}^{d \times T}$ . The goal here is to find whether the unknown single trial  $Y$  belongs to class  $R$  or  $L$ . The CSP technique is used to simplify the classification of  $Y$  by identifying spatial filters that maximize the variance (signal power) of spatially filtered signal for one class while minimizing the variance for the other class(es) (Ramoser, Müller-Gerking, and Pfurtscheller 2000; Blankertz, Tomioka, et al. 2008). So basically the CSP aims an optimal discrimination of signal's band power (Ramoser, Müller-Gerking, and Pfurtscheller 2000). To achieve that mathematically, the CSP

method is used to find the spatial filters  $\omega$  which maximize/minimize the following function:

$$\mathcal{J}(\omega) = \frac{\omega^* Y_L Y_L^* \omega}{\omega^* Y_R X_R^* \omega} = \frac{\omega^* Cov_L \omega}{\omega^* Cov_R \omega} \quad 4$$

where,  $*$  denotes transpose<sup>1</sup>,  $Y_{c \in \{R,L\}}$  is calculated as the average over all trials belonging to each class separately, and  $Cov_{c \in \{R,L\}}$  is the respective class spatial covariance matrix. The optimal spatial filters  $\omega$  that maximize/minimize the function  $\mathcal{J}(\omega)$  are the eigenvectors  $\omega_i$  corresponding to the biggest/smallest eigenvalues  $\lambda_i$  of the matrix  $\bar{\Gamma} = Cov_R^{-1} Cov_L$  (Lotte and Guan 2011). The problem now is to calculate matrix  $\bar{\Gamma}$  based on offline recordings and to extract the filters/eigenvectors  $\omega_i$ .

The CSP filtering method has shown to be successful, but the spatial filtering offered by simple CSP does not take into consideration temporal and spectral discrimination between the two classes. Indeed, the covariance matrix  $Cov_c$  estimates the power density in the entire spectrum. The Spec–CSP shown in the next section takes into consideration spectral power along with spatial discrimination.

#### 4.3.2.2 Spec–CSP Algorithm

The Spec–CSP algorithm is an extended variant of CSP that introduces a simultaneous way to find the optimal spatial filters  $\omega$  and optimize a LTI temporal filter  $\mathbf{A} \in \mathbb{R}^{TxT}$  (Tomioka, Dornhege, Aihara, et al. 2006). Instead of the covariance matrix  $Cov_c$ , the sensor covariance  $\Gamma_c(\mathbf{A}) := \langle Y_c \mathbf{A} \mathbf{A}^* Y_c^* \rangle^c$  will be considered. The sensor covariance is the covariance between channels averaged over trials and over time. The brackets  $\langle \rangle^c$  denote the mean of class  $c \in \{L, R\}$  trials.

Since any LTI temporal filter is diagonal in the frequency domain and  $\mathfrak{F}^* \mathbf{A} \mathfrak{F} = \text{diag}(\alpha_1, \dots, \alpha_T)$ , then we can write<sup>2</sup>:

<sup>1</sup> Later on  $*$  will be used to denote conjugate transpose as well

<sup>2</sup>  $\mathfrak{F} := \{\frac{1}{\sqrt{T}} e^{-2\pi i k/T}\}_k \in \mathbb{C}^{TxT}$  is the discrete Fourier transformation  $\Rightarrow \mathfrak{F}^T \mathfrak{F} = I_T$

$$\Gamma_c(\alpha) := \sum_{k=1}^{T'} \alpha_k \langle V_k \rangle_c := \sum_{k=1}^{T'} \alpha_k \langle \hat{y}_k \hat{y}_k^* \rangle_c = Y_c \mathfrak{F} \mathfrak{F}^* \mathbf{A} \mathbf{A}^* \mathfrak{F} \mathfrak{F}^* Y_c^* = \Gamma_c(\mathbf{A}) \quad 5$$

where:  $\hat{y}_k \in \mathbb{C}^d$  is the  $k$ -th frequency component,  $V_k := 2 \cdot \text{Re} [\hat{y}_k \hat{y}_k^*]$  and  $\langle V_k \rangle_c \in \mathbb{R}^{d \times d}$  is the real part of the  $k$ -th frequency component in the cross spectrum<sup>1</sup>.

If we apply the LTI filter  $\mathbf{A}$  to the EEG signal trials than Eq. 4 becomes:

$$\mathcal{J}(\omega, \alpha) = \frac{\omega^* \langle Y_L \mathbf{A} \mathbf{A}^* Y_L^* \rangle \omega}{\omega^* \langle Y_R \mathbf{A} \mathbf{A}^* Y_R^* \rangle \omega} = \frac{\omega^* \Gamma_L(\mathbf{A}) \omega}{\omega^* \Gamma_R(\mathbf{A}) \omega} = \frac{\omega^* \Gamma_L(\alpha) \omega}{\omega^* \Gamma_R(\alpha) \omega} \quad 6$$

The optimal filters that maximize/minimize  $\mathcal{J}(\omega, \alpha)$  are the  $\omega_i$  eigenvectors corresponding to the biggest/smallest eigenvalues  $\lambda_i(\alpha)$  of the matrix  $\bar{\Gamma}(\alpha) = \Gamma_R^{-1}(\alpha) \Gamma_L(\alpha)$ , where the number of eigenvalues of matrix  $\bar{\Gamma}$  is  $i \leq d$ . This is the same problem with the one introduced in previous section (Eq. 4), but here we simultaneously optimize the coefficients  $\alpha = \{\alpha_k\}_{k=1}^{T'}$  to improve the power distribution discriminability. This optimization problem is formulated as follows:

$$\max_{\alpha} \frac{\langle \bar{Y}(\omega, \alpha) \rangle_L - \langle \bar{Y}(\omega, \alpha) \rangle_R}{\sqrt{\text{Var}[\bar{Y}(\omega, \alpha)]_L + \text{Var}[\bar{Y}(\omega, \alpha)]_R}}, \quad s. t. \alpha_k \geq 0 \quad (\forall k = 1, \dots, T') \quad 7$$

where,  $\bar{Y}(\omega, \alpha) := \sum_{k=1}^{T'} \alpha_k \bar{Y}_k(\omega) := \sum_{k=1}^{T'} \alpha_k \omega^* V_k \omega$ , is the spatio-temporally filtered signal and  $\text{Var}[\bar{Y}(\omega, \alpha)]$  is its variance. Eq. 7 can be viewed as the signed square root of the Rayleigh quotient used in Fisher's discriminant analysis with an additional constraint that all coefficients must be positive; therefore, if we exchange the labels Eq. 7 yields a different solution. In this way, we take the maximum for the "L" class and the minimum for the "R" class, just like choosing CSP projections from both ends of the eigenvalue spectrum. Then, the optimal coefficients are explicitly written as follows:

$$\alpha_k^{(L,R)opt} \propto \begin{cases} \frac{\langle \bar{Y}(\omega, \alpha) \rangle_{L,R} - \langle \bar{Y}(\omega, \alpha) \rangle_{R,L}}{\text{Var}[\bar{Y}(\omega, \alpha)]_{L,R} + \text{Var}[\bar{Y}(\omega, \alpha)]_{R,L}} & \langle \bar{Y}_k(\omega) \rangle_{L,R} - \langle \bar{Y}_k(\omega) \rangle_{R,L} \geq 0, \\ 0 & \text{otherwise,} \end{cases} \quad 8$$

<sup>1</sup> Only the  $T' = \lfloor \frac{n_{FFT}+1}{2} \rfloor$  independent frequency components below the Nyquist frequency are taken into the sum.

where,  $Var[\bar{Y}(\omega, \alpha)]_c = \sum_{k=1}^T \alpha_k^2 Var[\bar{Y}(\omega)]_c$ , since the filtered signal  $\bar{Y}(\omega, \alpha)$  is linear with respect to  $\{\alpha_k\}_{k=1}^T$  and the signal is assumed to be a stationary Gaussian process<sup>1</sup>. Since the norm of the vector  $\alpha$  cannot be determined from Eq. 7, in practice the coefficients are normalized to sum to one. Furthermore, Eq. 8 could be generalized to introduce selective spectrum:

$$\alpha_k^{(c)} = \left( \alpha_k^{(c)opt} \right)^q \cdot (\beta_k)^p \quad 9$$

where,  $\{\beta_k\}_{k=1}^{T'}$  denotes the spectrum selection, which is specific to a problem.

To summarize, the optimal spatial filters  $\omega$  are the eigenvectors of the matrix  $\bar{\Gamma}(\alpha)$  and the optimal spectral filter  $\alpha$  is the solution to the problem in Eq. 4 which is explicitly written in Eq. 8. Moreover, we could introduce selective spectrum by using Eq. 9.

In our implementation, we've already band-pass filtered the signal in the frequency [8, 30] Hz, thus the prior spectrum selection is in the same frequency band. The values of  $p$  and  $q$  are set equal to '1'. The Spectrum selection  $\{\beta_k\}_{k=1}^{T'}$  is calculated as follows:

$$\beta_k = I_k^{[8,30]} \frac{\langle \bar{Y}_k(\omega) \rangle_L + \langle \bar{Y}_k(\omega) \rangle_R}{2} \quad 10$$

where,  $T' = (30 - 8) * T/100$  and  $\{I_k^{[8,30]}\}_{k=1}^{T'}$  equals value '1' in the selected frequency band and value '0' otherwise, and the second term is the average activity. If we substitute the values of  $\beta_k$ ,  $p$  and  $q$ , then Eq. 8 becomes:

$$\alpha_k^{(L,R)} \propto I_k^{[8,30]} \begin{cases} \left( \frac{\langle \bar{Y}_k \rangle_{L,R} - \langle \bar{Y}_k \rangle_{R,L}}{Var[\bar{Y}_k]_{L,R} + Var[\bar{Y}_k]_{R,L}} \right) (\langle \bar{Y}_k \rangle_L + \langle \bar{Y}_k \rangle_R) & \langle \bar{Y}_k \rangle_{L,R} - \langle \bar{Y}_k \rangle_{R,L} \geq 0, \\ 0 & otherwise \end{cases} \quad 11$$

Since both the optimal spatial and spectral filters depend on each other, an iterative method that starts from conventional CSP (solving Eq. 4 *s.t.*  $\forall k, \alpha_k = 1$ ) and updates one while fixing the other alternately is used (Tomioka, Dornhege, Nolte, et al. 2006).

<sup>1</sup> The frequency components are independent to each other for a given class.

### 4.3.3 Feature Extraction

Measuring brain activity through EEG leads to the acquisition of a large amount of data. Indeed, EEG signals are generally recorded with a number of electrodes varying from 1 to 256 and with a sampling frequency varying from 100 Hz to 1000 Hz. In order to obtain the best possible performances, it is necessary to work with a smaller amount of values which describe the most relevant properties of the EEG signals. These values are known as “features”. Identifying and extracting good features from EEG signals is a crucial step in the BMI design. The enclosed information in the EEG signal features is used to describe the neurophysiological activity employed in BMI. Carefully selected features lead to higher discriminability when identifying the mental state of the subject.

Due to the fact that in some methods there is not a clear distinction between filtering and feature extraction, this step is may also be considered as part of the signal processing. Feature extraction methods are separated in three major classes:

**Temporal feature extraction methods** investigate the possibility of retrieving information from features or time locked variations of the signal in the time domain. The features exploited include, signal amplitude, autoregressive parameters, etc.

**Frequency feature extraction methods** investigate the possibility of retrieving important information from the frequency domain representation of the signal. The features exploited include band power features and power spectral density features.

**Time–frequency feature extraction methods** are combinations of the above. They include short–time Fourier transform, wavelets, Wigner–Ville distributions, adaptive Gaussian representations, etc.

In our implementation, we use *band power features*. In order to extract features with close to normal distribution log–transform of the signal band power is taken into account (Pfurtscheller and Neuper 2001). With the spatial filters  $\omega$  and temporal filters  $\mathbf{A}$  found by Spec–CSP algorithm in the previous section, we filter the signal of a single trial  $Y$  and extract its log–power features following Eq. 12.

$$\phi_f(Y; \omega_f, \mathbf{A}_f) = \log \omega_f^* Y \mathbf{A}_f \mathbf{A}_f^* Y^* \omega_f, \quad \forall f \in \{1, 2, \dots, d\} \quad 12$$

The feature vector  $\Phi^{L \leftrightarrow R} := \{\phi_f\}_{f=1}^d$  is the outcome of the signal processing and feature extraction, and it contains the discriminatory information between classes  $L$  and  $R$ .

The temporal filters  $\mathbf{A}_f$  and the spatial filters  $\omega_f$  are arranged according their corresponding eigenvalue. For instance,  $\omega_1$  and  $\mathbf{A}_1$  belong to the biggest eigenvalue  $\lambda_1 = \max(\lambda_i)$ ,  $\omega_2$  and  $\mathbf{A}_2$  belong to the second biggest eigenvalue; following this rule, filters  $\omega_d$  and  $\mathbf{A}_d$  belong to the smallest eigenvalue  $\lambda_d = \min(\lambda_i)$  of matrix  $\bar{\Gamma}$ .

#### 4.3.4 Implementation, Feature Selection and Dimensionality Reduction

In our BMI implementation, we have three mental states to be recognized (*left hand*, *right hand* and *foot*), which means three classes ( $L$ ,  $R$  and  $F$ ). In order to build a classifier that determines the class of a single trial, we compute the spatial filters  $\omega$  and the temporal filters  $\mathbf{A}$  (and their corresponding spectral filters  $\alpha$ ), and then extract the feature vectors for every two pair of classes:  $L \leftrightarrow R$ ,  $L \leftrightarrow F$  and  $R \leftrightarrow F$ . The biggest eigenvalues, their corresponding eigenvectors/spatial filters and temporal filters  $\{\lambda_f; \omega_f; \mathbf{A}_f\}_{f < d/2}$  determine the discriminant features for the first class and the smallest eigenvalues, their corresponding eigenvectors/spatial filters and temporal filters  $\{\lambda_f; \omega_f; \mathbf{A}_f\}_{f > d/2}$  determine the discriminant features for the second class of each pair.

Feature vectors  $\Phi$ , calculated from Eq. 12 have 15 features for each pair of classes. Hence, the total number of features extracted from a single trial for its classification over three classes, is  $3 * d = 45$ . Based on the estimation that the amount of data required describing properly different classes, increases exponentially with the dimensionality of the feature vector (Jain, Duin, and Mao 2000; Friedman 1997), ‘45’ is a relatively high number of features. Furthermore, the offline training data per each class is generally small because the training process is time consuming and relatively uncomfortable for subjects. If the amount of training data (trials) is relatively small compared to the number of features, the classification algorithm built from this data is likely to give low classification accuracy. Moreover, small number of features offer reduced computational time for offline classifier training and online performance.

Previous research has shown that most of the discriminatory features are extracted by the eigenvectors corresponding to the three biggest and three smallest eigenvalues of  $\bar{\Gamma}$  (Lotte and Guan 2011). Table 4-2 summarizes the outcomes of the spatial filtering and feature extraction methods used in our BMI implementation. All the filters  $\{\omega; \mathbf{A}; \alpha\}$  for every pair of class are called the *filtering model*.

Table 4-2 Filtering Model

Class pair	Class	Eigenvalues <sup>1</sup>	Filters			Features
			Spatial	Temporal	Spectral	
$L \leftrightarrow R$	$L$	$\lambda_{f_{max}}^{(L,R)}$	$\omega_{f_{max}}^{(L,R)}$	$\mathbf{A}_{f_{max}}^{(L,R)}$	$\alpha_{(k),f_{max}}^{(L,R)}$	$\phi_{f_{max}}^{(L,R)}$
	$R$	$\lambda_{f_{min}}^{(L,R)}$	$\omega_{f_{min}}^{(L,R)}$	$\mathbf{A}_{f_{min}}^{(L,R)}$	$\alpha_{(k),f_{min}}^{(L,R)}$	$\phi_{f_{min}}^{(L,R)}$
$L \leftrightarrow F$	$L$	$\lambda_{f_{max}}^{(L,F)}$	$\omega_{f_{max}}^{(L,F)}$	$\mathbf{A}_{f_{max}}^{(L,F)}$	$\alpha_{(k),f_{max}}^{(L,F)}$	$\phi_{f_{max}}^{(L,F)}$
	$F$	$\lambda_{f_{min}}^{(L,F)}$	$\omega_{f_{min}}^{(L,F)}$	$\mathbf{A}_{f_{min}}^{(L,F)}$	$\alpha_{(k),f_{min}}^{(L,F)}$	$\phi_{f_{min}}^{(L,F)}$
$R \leftrightarrow F$	$R$	$\lambda_{f_{max}}^{(R,F)}$	$\omega_{f_{max}}^{(R,F)}$	$\mathbf{A}_{f_{max}}^{(R,F)}$	$\alpha_{(k),f_{max}}^{(R,F)}$	$\phi_{f_{max}}^{(R,F)}$
	$F$	$\lambda_{f_{min}}^{(R,F)}$	$\omega_{f_{min}}^{(R,F)}$	$\mathbf{A}_{f_{min}}^{(R,F)}$	$\alpha_{(k),f_{min}}^{(R,F)}$	$\phi_{f_{min}}^{(R,F)}$

#### 4.4 Classification

In order to classify the feature vectors obtained from the previous section, a classifier must be built based on the offline trials. There are two types of classifiers: linear and nonlinear. A review of the classifiers commonly used in BMI is shown in Appendix C.

A linear classifier is an algorithm that uses a linear functions' value to distinguish classes. Linear classifiers are quite popular in BMI applications, especially Linear Discriminant Analysis (LDA) and Support Vector Machine (SVM).

LDA has a very low computational requirement, is simple to implement and it provides good results which makes it suitable for online BMI systems. Consequently, LDA has been used with success in a great number of BMI systems such as MI based BMI, P300 based speller, multiclass or asynchronous BMI applications (Perez and Cruz 2007; Scherer et al. 2004; Guger et al. 2009; Lotte et al. 2007).

Next section explains in detail the classic LDA algorithm. In our implementation we will use a regularized form of the LDA which reduces computational load and achieves better classification performance.

---

<sup>1</sup> The eigenvalue indexes for the first class of the pair are  $f_{max} \in \{1,2,3\}$  and for the second class of the pair are  $f_{min} \in \{d-2, d-1, d\}$

#### 4.4.1 Linear Discriminant Analysis

The aim of LDA (also known as Fisher's LDA) is to use hyperplanes to separate the data representing different classes (Fisher 1936; Marquand et al. 2011). Similar to Section 4.3.2, we first investigate the case of two classes ( $c \in C = \{L, R\}$ ) and then we generalize the method for multi class problem ( $|C| > 2$ ). The goal is to build a classifier that is able to determine the class of a feature vector  $\Phi_i$  extracted from the EEG signals trial  $Y_i$ . Let  $N = |\{\Phi_1, \Phi_2, \dots, \Phi_N\}|$  be the total number of feature vectors extracted from all the offline trials  $\{\Phi_1, \Phi_2, \dots, \Phi_N\}$ , where  $N_{c \in C}$  is the number of trials belonging to each class ( $N_L + N_R = N$ ). Mathematically, we need to find a projection vector  $w$  that projects all the feature vectors into a line by assigning them a scalar:

$$z = w^* \Phi \quad 13$$

This reduces the data dimensionality, but in order to achieve good discriminability, a good projector vector is needed as well. Fisher suggested finding a projection which maximizes the variance between the classes, normalized by a measure of the within class scatter Eq. 14 (the definitions of some of the class statistical properties are summarized in Table 4-3).

$$J(w) = \frac{|\tilde{\mu}_L - \tilde{\mu}_R|^2}{S_w} \quad 14$$

The LDA algorithm is looking for a projection where examples from the same class are projected as close as possible to each-other, while their projected means are as far as possible from each-other (Figure 4-7). What we need to do is to transform Eq. 14 in order to express  $J$  as a function of  $w$ , and then find the value of  $w$  that maximizes the value of  $J$ .

First, we express the class means and between class variances of the projected classes as a function of  $w$ , and their respective peers in the feature domain:

$$\begin{cases} \tilde{\mu}_c = \frac{1}{N_c} \sum_{i=1}^{N_c} z_i = \frac{1}{N_c} \sum_{i=1}^{N_c} w^* \Phi_i = w^* \mu_c \\ (\tilde{\mu}_L - \tilde{\mu}_R)^2 = (w^* \mu_L - w^* \mu_R)^2 = w^* (\mu_L - \mu_R) (\mu_L - \mu_R)^* w = w^* S_B w \end{cases} \quad 15$$

Next, we express the projected class scatter and the within class scatter:

$$\begin{aligned}\tilde{S}_c &= \sum_{i \in C} (z_i - \tilde{\mu}_c)(z_i - \tilde{\mu}_c)^* = \sum_{i \in C} (w^* \Phi_i - w^* \mu_c)(w^* \Phi_i - w^* \mu_c)^* = \\ &= \sum_{i \in C} w^* (\Phi_i - \mu_c)(\Phi_i - \mu_c)^* w = w^* S_c w\end{aligned}\quad 16$$

$$\tilde{S}_W = \tilde{S}_L + \tilde{S}_R = w^* S_L w + w^* S_R w = w^* S_W w \quad 17$$

We substitute the outcome of Eq. 15, 16 & 17 in Eq. 14 and the solution to the maximization problem is the projection vector  $w^{opt}$  found as follows:

$$J(W) = \frac{w^* S_B w}{w^* S_W w} \Rightarrow \left( w^{opt} = \arg \max \left[ \frac{w^* S_B w}{w^* S_W w} \right] \right) \quad 18$$

This is a generalized eigenvalue problem ( $|S_W^{-1} S_B - \lambda I| = 0$ ), and the solution is the eigenvector of the matrix  $S_W^{-1} S_B$ , with value  $w^{opt} = S_W^{-1} (\mu_L - \mu_R)$ .

**Table 4-3 Statistical definitions**

Mean	$\mu = \frac{1}{N} \sum_{i \in C} \Phi_i$ ; $\mu_c = \frac{1}{N_c} \sum_{i=1}^{N_c} \Phi_i$ ; $\tilde{\mu}_c = \frac{1}{N_c} \sum_{i=1}^{N_c} z_i$
Scatter	$S_c = \sum_{i=1}^{N_c} (\Phi_i - \mu_c)(\Phi_i - \mu_c)^*$ ; $\tilde{S}_c = \sum_{i=1}^{N_c} (z_i - \tilde{\mu}_c)(z_i - \tilde{\mu}_c)^*$
Within Class Scatter	$S_W = \sum_{c \in C} S_c = S_L + S_R$ ; $\tilde{S}_W = \sum_{c \in C} \tilde{S}_c = \tilde{S}_L + \tilde{S}_R$
Between Class Scatter	$S_B = (\mu_L - \mu_R)(\mu_L - \mu_R)^*$ ; $\tilde{S}_B = (\tilde{\mu}_L - \tilde{\mu}_R)(\tilde{\mu}_L - \tilde{\mu}_R)^*$

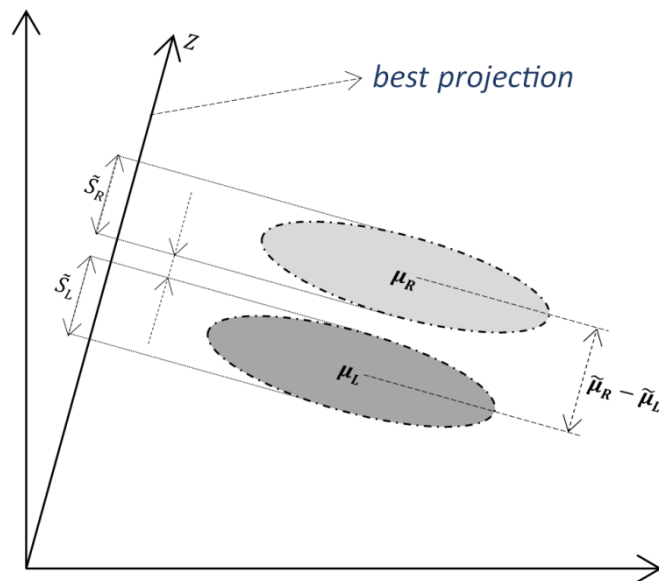


**Figure 4-7 Best class projection**

#### 4.4.2 Regularized and Multi-Class LDA

The main weaknesses of the standard LDA are, the per-class covariance matrix calculation procedure is very data hungry and it is outlier sensitive. In order to deal with this problems a RLDA is used instead (Blankertz, Curio, and Müller 2002; Müller et al. 2004; Friedman 1989). This method introduces the shrinkage covariance calculation instead of covariance (Schäfer and Strimmer 2005; Blankertz et al. 2011). This variant automatically computes the degree of regularization, and is therefore both fast and optimal (Ledoit and Wolf 2004). When enough trials are available, full covariance matrices are learned, but with fewer trials the covariance estimates heads to well-formed spherical shapes (Delorme and Makeig 2004). As outliers are common in EEG, the RLDA usually gives better results for BMI compared to the non-regularized version.

In the case of  $|C| > 2$  classes, the problem is to find a projection matrix  $W$  with columns the vectors  $w_{(i,j)}$  where  $i, j \in \{L, F, R | i \neq j\}$ . It can be easily shown that the optimal projection matrix  $W^{opt}$  is the matrix with columns the eigenvectors corresponding to the biggest eigenvalues of  $S_{W(i,j)}^{-1} S_{B(i,j)}$ , with value  $w_{(i,j)}^{opt} = S_{W(i,j)}^{-1} (\mu_i - \mu_j)$ .

After the optimal projectors  $W^{opt}$  are found from above, we calculate the projected value  $z^{(i,j)}$  of the features  $\Phi^{(i,j)}$ , for every pair of classes  $(i, j)$  using the projectors  $w_{(i,j)}^*$ :

$$z^{(i,j)} = w_{(i,j)}^* \Phi^{(i,j)} - b^{(i,j)} \quad 19$$

The value  $b^{(i,j)} = (\mu_i + \mu_j) w_{(i,j)}^*$  is the bias value of the linear classifier and it is used to move the projected value near the origin. Next, we restrict the projected value within the interval  $[-1, 1]$  and calculate the probability of each class in the current pair  $(i, j)$ , assuming equal distribution (Eq. 20 & 21).

$$\bar{z}^{(i,j)} = \begin{cases} -1 & z^{(i,j)} < -1 \\ z^{(i,j)} & -1 \leq z^{(i,j)} \leq 1 \\ 1 & z^{(i,j)} > 1 \end{cases} \quad 20$$

$$\begin{cases} p_i^{(i,j)} = \frac{1 - \bar{z}^{(i,j)}}{2} \\ p_j^{(j,i)} = 1 - \frac{1 - \bar{z}^{(i,j)}}{2} \end{cases} \quad 21$$

Last, we calculate the probability of each class by adding their probability values in each pair of classes from Eq. 21; this method is also known as *voting* (Appendix C.2).

$$P_k = \frac{1}{|C| - 1} \sum_{k=1; \forall(i,j)}^3 ((k = i) \cup (k = j)) \cdot p_k^{(i,j)} \quad 22$$

In our implementation, we have only three BMI classes noted  $L$ ,  $R$  and  $F$ . Thus, based on Eq. 21 & 22, the probability of each class is calculated using the formulas shown in Table 4-4.

#### 4.5 Online Predictive Module

By using the filtering model (Table 4-2) and the classification model (Table 4-4) created based on the offline EEG signals, an online predictive module (OPM) is build. During real time robot navigation, the OPM is used to collect, filter, extract features and classify the EEG signals acquired through an online data stream. The electrode placement, the EEG signal sampling rate and the data acquisition system is not changed during real time robot navigation.

Based on Table 4-4, the linear classifier output is given in the form of probability distribution over the three classes (mental tasks)  $c \in \{L, R, F\}$ . In order to reduce misclassifications, we have experimentally established a class probability threshold  $P_{th} = 0.45$  that is used to define the final OPM output  $C_{out}$  as follows:

$$C_{out} = c \Leftrightarrow \begin{cases} P_c = \max_{\forall k \in \{L,R,F\}} P_k \\ P_c > P_{th} \end{cases} \quad 23$$

**Table 4-4 Classification Model**

Class	Class Probability Calculation
$L$	$P_L = \frac{1}{2} (p_L^{(L,R)} + p_L^{(L,F)}) = 0.5 - 0.25(\bar{z}^{(L,R)} + \bar{z}^{(L,F)})$
$R$	$P_R = \frac{1}{2} (p_R^{(L,R)} + p_R^{(R,F)}) = 0.5 - 0.25(\bar{z}^{(R,F)} - \bar{z}^{(L,R)})$
$F$	$P_F = \frac{1}{2} (p_F^{(L,F)} + p_F^{(R,F)}) = 0.5 + 0.25(\bar{z}^{(L,F)} + \bar{z}^{(R,F)})$

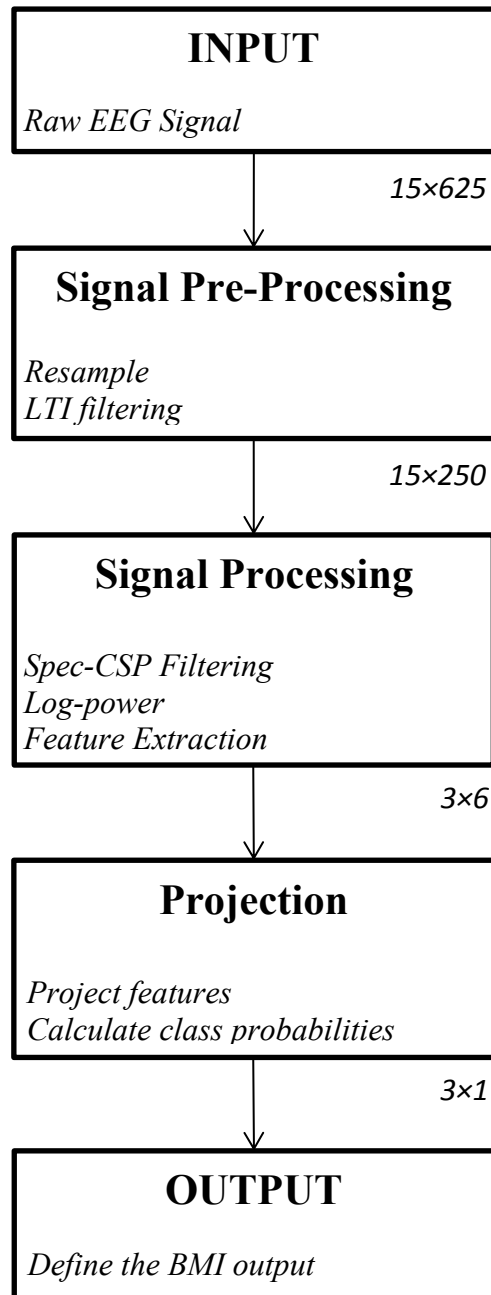


**Figure 4-8 Online Predictive Module flow chart**

The online EEG signal processing flow of the OPM is shown in Figure 4-8. Each signal processing is basically a matrix multiplication, and since the OPM is implemented in Matlab, this makes the online operation very fast.

At each step the processed signal dimensionality reduction is shown on the right side. In the pre-processing step, signal resampling and LTI filtering reduce the number of data values by 60%. During the signal processing step, the Spec-CSP filtering and the feature extraction method reduce the data dimensionality by more than 99%. This whole

transformation is done in few mathematical steps and very fast in Matlab, which allows the OPM to maintain a low computational time for the real time robot navigation. In the last step, the projections and the class probability distribution are calculated.

The output of the OPM ( $C_{out}$ ) is used for robot navigation (Section 5.3).

## 5 Robotic Wheelchair and Navigation Modules

This chapter describes in detail the robotic wheelchair system, all the modules that we have developed to assist the robot navigation and their functionality. Then, it introduces the environment where the experiments are conducted and the experimental setup. The developed robotic wheelchair system is explained in Section 5.1. Next, in Section 5.2 are explained the direct control, collision detection and autonomous navigation modules that we developed for robot navigation. Then, in Section 5.3 is explained the ANP and its functionality. Last, in section 4.5 the experimental environment is shown and the experimental tasks for the subject are explained.

### 5.1 Robotic Wheelchair

In our system, we developed a robotic wheelchair based on the commercial wheelchair form Kanayama Machinery Co., Ltd. (Figure 5-1). The wheelchair is equipped with two 16" wheels, actuated by two low noise AC servo motors. It is powered by a 24V, 6.7Ahr, rechargeable Ni-MH battery, with up to 5 hours battery life, and it can be controlled by a joystick. The AC servo motors and all the components shown in Figure 5-2 are part of the set "JOY UNIT X" from Yamaha Motor Co., Ltd.

In our experiments, we do not use the joystick to control the wheelchair, instead we use a USB-to-UART (i.e. Universal Asynchronous Receiver/Transmitter) bridge to interface it with the computer and control it from Matlab. We have mounted a LRF sensor and a camera in the front part of the wheelchair (Figure 5-1), while the Mitsar-EEG 201 electrode box can be placed in the back of the wheelchair during BMI navigation. In the next section we will explain the technical capabilities of the LRF sensor.

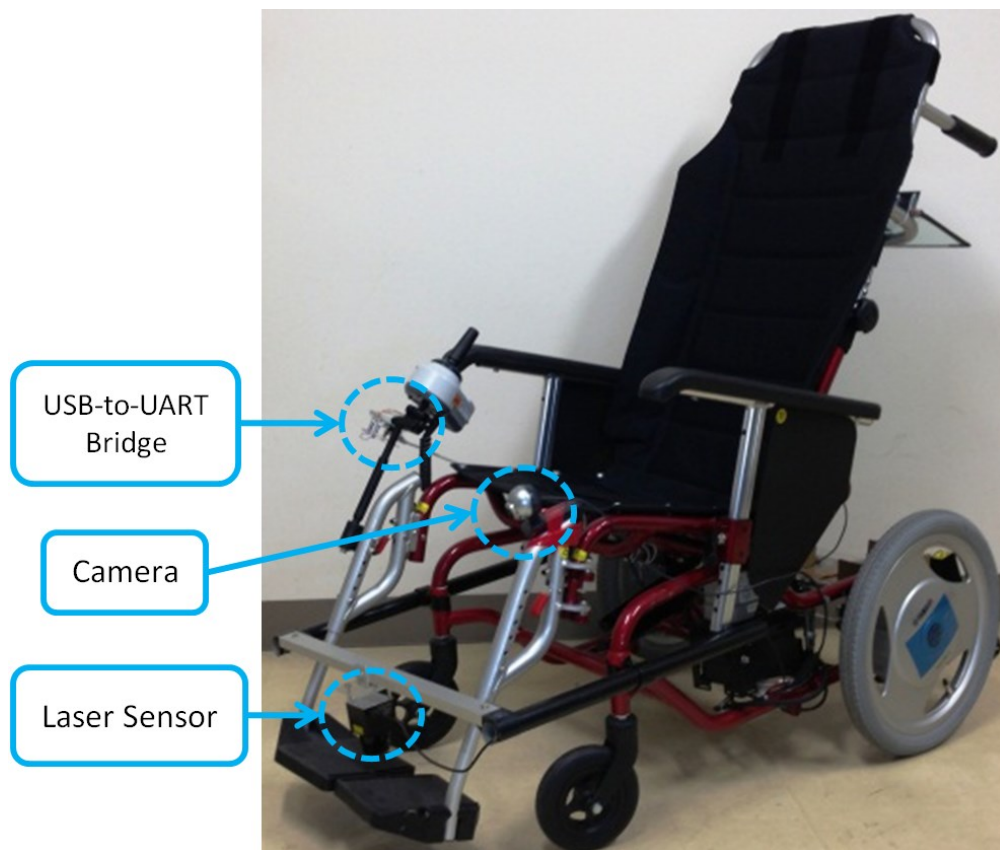


Figure 5-1 Robotic Wheelchair

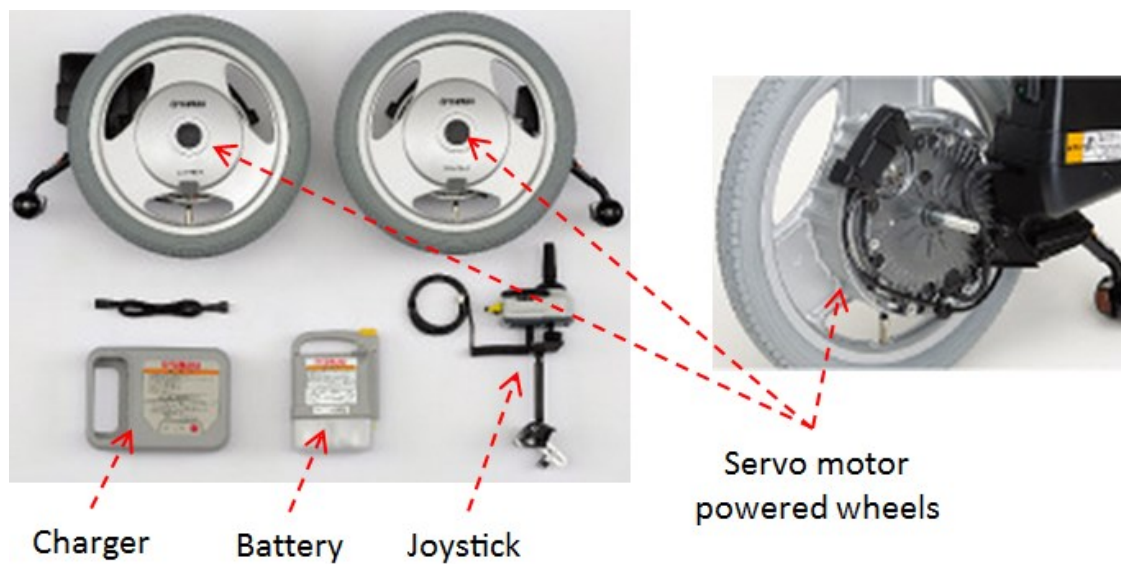


Figure 5-2 Servo motor wheel system components (adopted from Yamaha Motor [website](#))

### 5.1.1 Laser Range Finder Sensor

In our robotic system, we used a small and light LRF sensor, the model “URG-04LX-UG01” made by HOKUYO AUTOMATIC. This LRF sensor is ideal for our

application; it has low power consumption (2.5W) and it is powered over USB. Furthermore, its high accuracy, high resolution and wide range provide a good 2D scanning solution. The sensor is shown on Figure 5-3 and its technical specifications in Table 5-1.

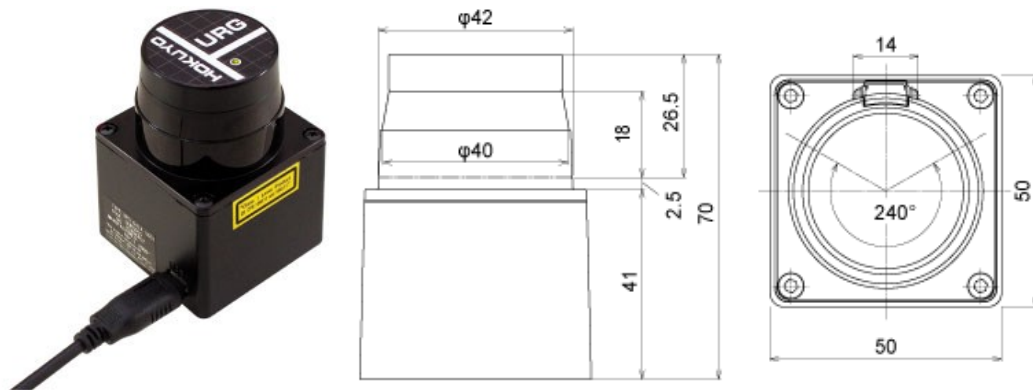


Figure 5-3 The “URG-04LX-UG01” model LRF sensor; all the values in the drawings are in mm  
(adopted from Hokuyo Automatic [website](#))

Table 5-1 The “URG-04LX-UG01” model LRF sensor technical specifications (adopted from Hokuyo Automatic [website](#))

Model No.	URG-04LX-UG01
Power source	5VDC $\pm$ 5%(USB Bus power)
Light source	Semiconductor laser diode ( $\lambda=785\text{nm}$ ), Laser safety class 1
Measuring area	20 to 5600mm (white paper with 70mm $\times$ 70mm), 240 $^\circ$
Accuracy	60 to 1,000mm : $\pm$ 30mm, 1,000 to 4,095mm : $\pm$ 3% of measurement
Angular resolution	Step angle : approx. 0.36 $^\circ$ (360 $^\circ$ /1,024 steps)
Scanning time	100ms/scan
Noise	25dB or less
Interface	USB2.0/1.1 [Mini B] (Full Speed)
Command System	SCIP Ver.2.0
Ambient luminance <sup>1</sup>	Halogen/mercury lamp: 10,000Lux or less, Florescent: 6000Lux (Max)
Ambient temperature/humidity	-10 to +50 degrees C, 85% or less (Not condensing, not icing)
Vibration resistance	10 to 55Hz, double amplitude 1.5mm each 2 hour in X, Y and Z directions

<sup>1</sup>these products are only for indoor applications. Strong sunlight may cause error output.

## 5.2 Navigation Assistive Modules

In order to control the robot and facilitate the BMI based wheelchair navigation, we have created three assistive modules. These modules are:

1. The DCM – to navigate the robot in a turn-by-turn style.
2. The CDM – to detect possible collisions and avoid them.
3. The ANM – to autonomously navigate the robot by following assistive information captured by the camera in real time.

In the following subsections we will explain in detail the functionality and the purpose of each module.

### 5.2.1 Direct Control Module

The DCM is used to navigate the robot in a basic turn-by-turn style navigation; it can turn the robot left, right or follow straight ahead. By using the USB-to-UART interface, we can simultaneously control the AC servo motors speeds and navigate the robot directly from Matlab. Both the robot's translational speed  $v$  and rotational speed  $\theta$  are kept constant during navigation, with values  $v = 0.5m/s$  and  $\theta = (\pi/4)rad/s$ . When using only the DCM for BMI based navigation, the robot navigates with constant speed  $v$  and slows down to minimal speed while the subject performs the mental task for the next turn direction.

A detailed description of the DCM interaction with other modules during robot navigation is presented in Section 5.3.

### 5.2.2 Collision Detection Module

The CDM uses the LRF sensor data to detect obstacles (objects) in front of the robot and avoids them during navigation. As shown in Table 5-1, the LRF sensor has a small measuring error ( $\pm 3\%$ ) in the range  $R \in [60, 4095] mm$ , and an angular resolution measuring step  $\alpha \cong 0.36^\circ (360^\circ/1,024)$ .

In our experiments, we need to find the objects in front of the robot; hence we have restricted the angular measuring area from  $240^\circ$  into  $A = 180^\circ$  (Figure 5-4). All the sensor readings  $s_i$ , corresponding to the area  $A$ , are collected in real time and stored in the

vector  $S = \{s_i\}_1^I$ , where  $I = A/\alpha = 510$ . The sensor readings have normalized values  $s_i \in [0, 1]$ , where  $R^{min} = 60 \Rightarrow s_i^{min} = 0$  and  $R^{max} = 4095 \Rightarrow s_i^{max} = 1$ .

In our implementation, the target distance range is set to  $R^t = 0.5m$ , which in normalized value is  $s^t = 0.45$ . This is the minimal distance for an object to be considered a navigation obstacle. By applying the target distance  $s^t$  threshold to the sensor readings values  $s_i$ , we gain a new vector of binary sensor indicators:

$$\check{s}_i = \begin{cases} 1, & s_i > s^t \\ 0, & s_i \leq s^t \end{cases} \quad \forall i \in I \quad 24$$

We have virtually divided the area in front of the robot in three equal angular subareas: left ( $S_L$ ), forward ( $S_F$ ) and right ( $S_R$ ) subarea. In Figure 5-5 these areas are viewed from above the robot. Each subarea covers one third of the sensor's angular measuring range ( $60^\circ$ ), which is translated into 170 binary indicators  $\check{s}_i$  per each subarea:

$$\begin{cases} S_L = \{\check{s}_i\}_1^{\frac{I}{3}} = \{\check{s}_i\}_1^{170} \\ S_F = \{\check{s}_i\}_{\frac{I}{3}+1}^{\frac{2I}{3}} = \{\check{s}_i\}_{171}^{340} \\ S_R = \{\check{s}_i\}_{\frac{2I}{3}+1}^I = \{\check{s}_i\}_{341}^{510} \end{cases} \quad 25$$

Based on Eq. 24, the presence of an obstacle in a subarea can be defined by evaluating the sum of its corresponding measurements ( $\sum \check{s}_i \geq 1$ ), or the "1-norm" of the measurement vector for each subarea ( $\|S_c\|_1 \geq 1; \forall c \in \{L, R, F\}$ ). During sensor evaluation we noticed sensor reading imperfections. In order to avoid false object detection we set a minimum value '17', which is 10% of the total measurements per subarea (170), and calculate the subarea obstacle indicators as follows:

$$O_c = \begin{cases} 1, & \|S_c\|_1 \geq 17 \\ 0, & \|S_c\|_1 < 17 \end{cases} \quad \forall c \in \{L, R, F\} \quad 26$$

In order to avoid the obstacles (if any), the CDM uses the above obstacle indicators to define the next robot direction change (turn)  $\varphi$  as:

$$\varphi = k \frac{\pi}{4} = \frac{\pi}{4} [(O_L + O_R)O_L O_R - O_L + O_R + O_F(O_R - O_L) + 2(\neg O_L)(\neg O_R)O_F] \quad 27$$

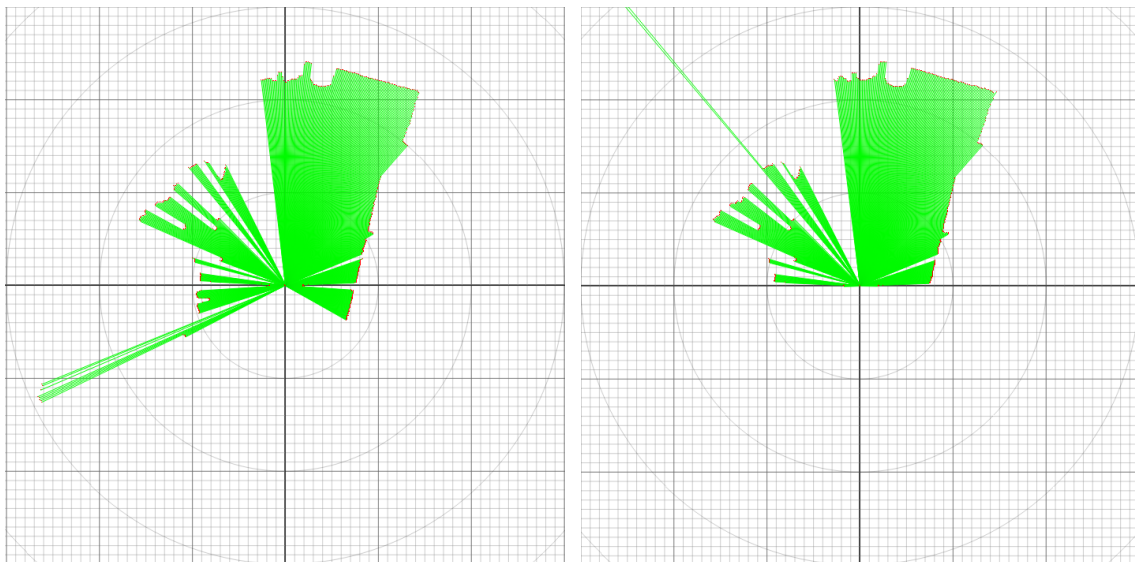


Figure 5-4 Sensor reading snapshots (a) before and (b) after area restriction to  $0^\circ - 180^\circ$

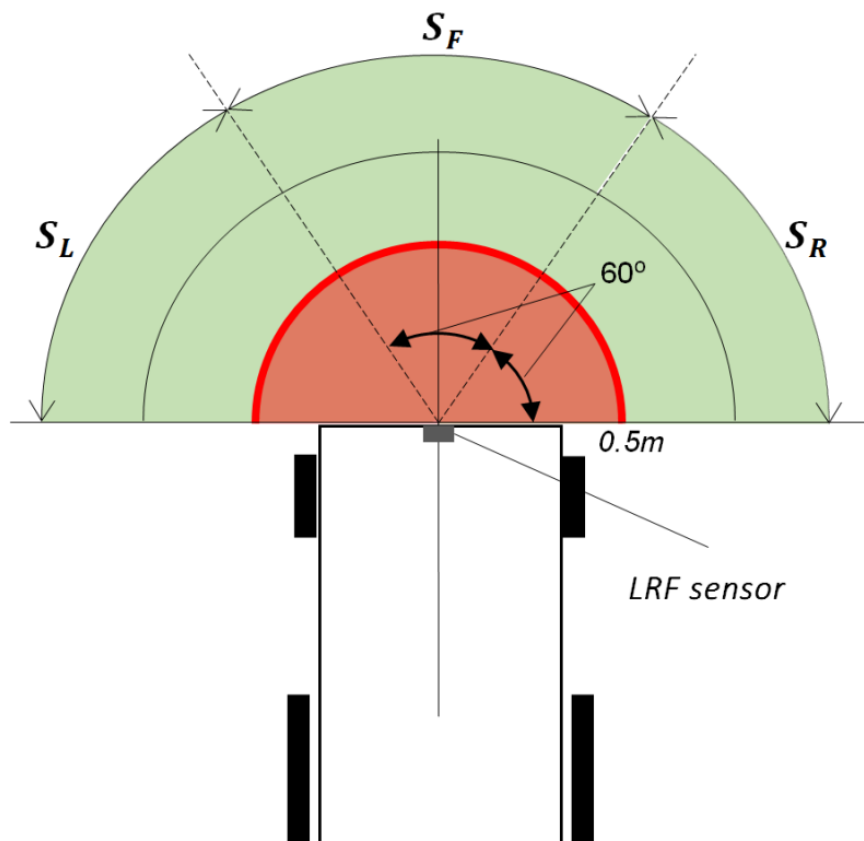


Figure 5-5 Sensor measuring subareas: left ( $S_L$ ), forward ( $S_F$ ) and right ( $S_R$ ) subarea

The expression in Eq. 27 is chosen such that  $k \in \{-2; -1; 0; 1; 2\}$ . Based on the location(s) of the object(s), the sign of  $k$  indicates the opposite direction with respect to the object(s) location(s). Next, the robot direction change value  $\varphi$  is sent to the robot controller.

The CDM algorithm (Algorithm 1) is shown below. Routines *ReadSensor()*, *RobotController()*, *StopNavigation()* are used to collect current sensor readings, change robot direction, and stop the robot and finish navigation (i.e. finish the current experimental trial).

In our experiments, we have configured the CDM to be an integral part of the system that is always running during robot navigation and cannot be switched off by the subject. Every  $\sim 0.2$  seconds, the CDM collects vector  $S$  and calculates  $O_c$ . If at a certain time, an obstacle is detected in the robot's path and any of the obstacle indicators  $O_c = 1$ , then the robot direction changes by  $\varphi$ . For example, if an object is located on the left subarea, indicators become  $\{O_L = 1; O_F = 0; O_R = 0\}$ , which means  $(O_L + O_F + O_R) = 1 > 0$ . From Eq. 27 we yield  $\varphi = -\pi/4$ , where “-” means that direction is clockwise or right. Then the robot is turned by  $\pi/4$  on the right direction.

In case the robot gets ‘stuck’ in an area where it cannot avoid the obstacle(s) after several attempts ( $n \geq 3\pi$ ), then the robot navigation is early terminated and the experiment is finished by the CDM. When collision detection is active, the translational speed of the robot is  $v = 0$ . The rotation during collision avoidance (Eq. 27) will be denoted as  $\varphi_{CDM}$ , in order to be distinguished from the rotation during normal navigation. The rotation speed  $\theta = (\pi/4)rad/s$  is constant in both cases, only rotation time is variable.

**Input:** *sensor*: laser sensor pointer

**Output:**

```

1  begin
2       $n = 0$ ;
3       $s = ReadSensor(sensor)$ ;
4      compute  $O_L, O_F, O_R$ ;          // Eq. 26
5      while  $(O_L + O_F + O_R) > 0$  do
6          compute  $\varphi$ ;                // Eq. 27
7          RobotController( $\varphi$ );
8           $d = ReadSensor(sensor)$ ;
9          compute  $O_L, O_F, O_R$ ;      // Eq. 26
10          $n = n + |\varphi|$ ;
11         if  $n \geq 3\pi$  then
12             StopNavigation;
13 end

```

**Algorithm 1** Robot direction change by CDM

### 5.2.3 Autonomous Navigation Module

As mentioned earlier, the robot is equipped with a web camera (Figure 5-6) that is used for autonomous navigation. In our experiment, we'll use the assistive information found on the floor of an office building, to autonomously navigate the robot. The assistive information consists of tactile paving for visually impaired people. The narrow tactile lines (or assistive lines) along the hallways (Figure 5-7 (a)) show the movement directions, and the cross sections (Figure 5-7 (b & c)) will be called decision points.

The ANM is able to navigate the robot following the assistive lines captured by the camera in real time. When the camera captures a decision point, the robot is stopped to allow the subject to send navigation control commands through BMI (Section 5.3.1).



Figure 5-6 Web camera used on our system

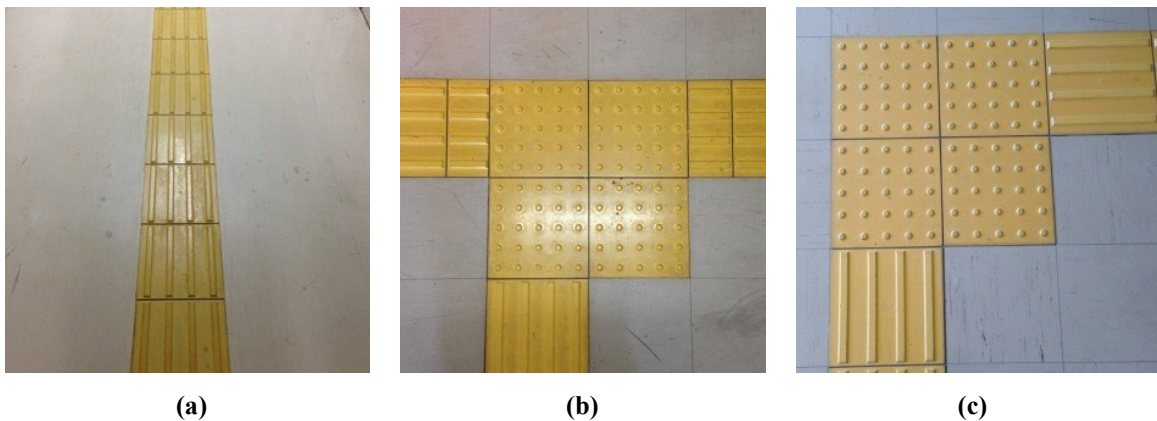


Figure 5-7 Assistive information: (a) line (b) decision point with 3 lines (c) decision point with 2 lines

The decision points and the assistive lines have different geometrical properties, and the camera position is fixed in the robotic wheelchair at a predefined distance from the floor; hence, we have tuned the image processing algorithm to recognize decision points based on their geometrical properties. The camera sensor matrix has  $V$ -vertical and  $H$ -horizontal pixels and captures RGB image frames with size  $V \times H \times 3$ .

After extracting the assistive information by using real time image processing, to every image frame we assign a binary matrix  $M_{V \times H}$ , which has the same size of the original image frame and its elements  $m_{i,j} \in \{0,1\}$  indicate the presence (1) or absence (0) of the assistive information on image pixel location  $(i,j)$ . Then, we use the binary information from  $M_{V \times H}$ , to calculate the robot translational and rotational speeds  $(v, \theta)$ , required to follow the assistive line.

In a typical processed frame (Figure 5-8), the assistive information ( $m_{i,j} = 1$ ) is represented in gray color while the background is represented in white color. For the  $(v, \varphi)$  calculation, we take into consideration only the top 10% image rows that contain assistive information. In Figure 5-8 the assistive information starts from the top, thus the top 10% rows that contain assistive information are also the top 10% rows of the selected image frame ( $V' = 0.9 * V$ ). Next, we calculate the horizontal center ( $h_{cen}$ ) of the selected part of the assistive line.

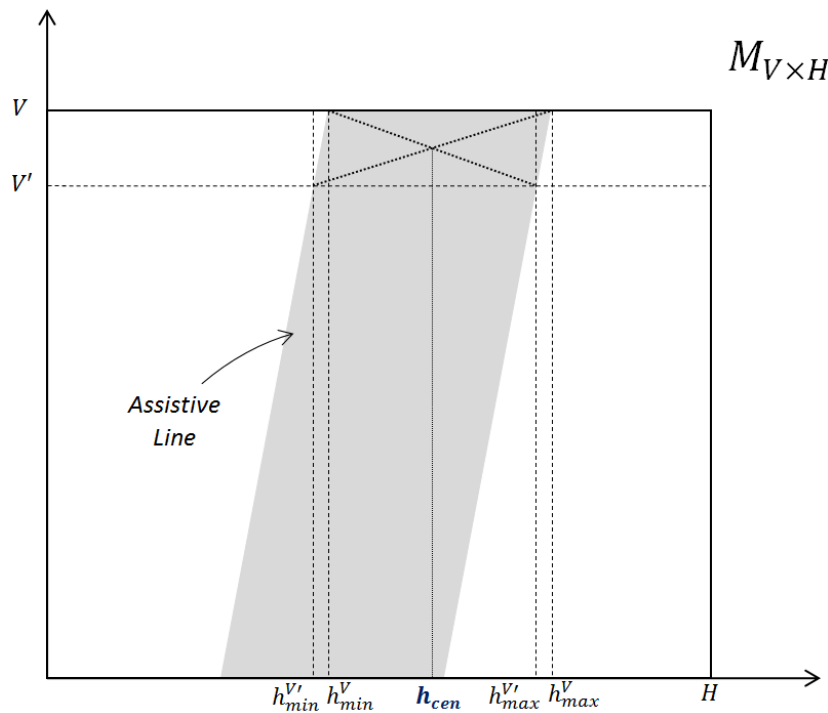


Figure 5-8 Processed image frame representation

$$h_{cen} = \frac{V}{20} \sum_{k=V'}^V (h_{max}^k - h_{min}^k) \quad 28$$

Where,  $h_{min}^k = \min_{(m_{kxj}=1)} j$  and  $h_{max}^k = \max_{(m_{kxj}=1)} j$  are the horizontal boundaries of each row of the selected area of the line. Using  $h_{cen}$  from Eq. 28 we define:

$$\begin{aligned} \theta &= \frac{\pi}{4} \left( \frac{2h_{cen} - H}{H} \right) \\ v &= 0.5 \left( 1 - \left| \frac{2h_{cen} - H}{H} \right| \right) \end{aligned} \quad 29$$

The whole procedure, from image processing to robot speed  $(v, \theta)$  extraction, is repeated every  $\sim 0.2$  seconds. This is done to avoid losing the line during real time navigation while still keeping a low computational load.

During autonomous navigation the robot moves with variable speeds  $(v, \theta)$ . In contrast with previous sections, here we use rotational speed  $\theta$  instead of direction change; this is because here we use a variable rotational speed. Anyway, the direction change for every 0.2 seconds is calculated as follows:

$$\varphi = 0.2 * \theta = \frac{\pi}{20} \left( \frac{2h_{cen} - H}{H} \right) \quad 30$$

In the next section, we are going to explain in detail the functionality of the ANP. There, we will explain how the ANM is integrated and interacts with the other modules during real time robot navigation.

### 5.3 Adaptive Navigation Platform

The role of the ANP is to provide assistance based on the environment context, in order to reduce the subject's mental workload, eliminate collisions and facilitate robot navigation experience.

The ANP integrates the subject's mental task predictions ( $C_{out}$ ) with the robot sensing information ( $s_i$  and  $M$ ) and controls the robot navigation  $(v, \varphi)$  in real time. The block diagram of the ANP is shown in Figure 5-9.

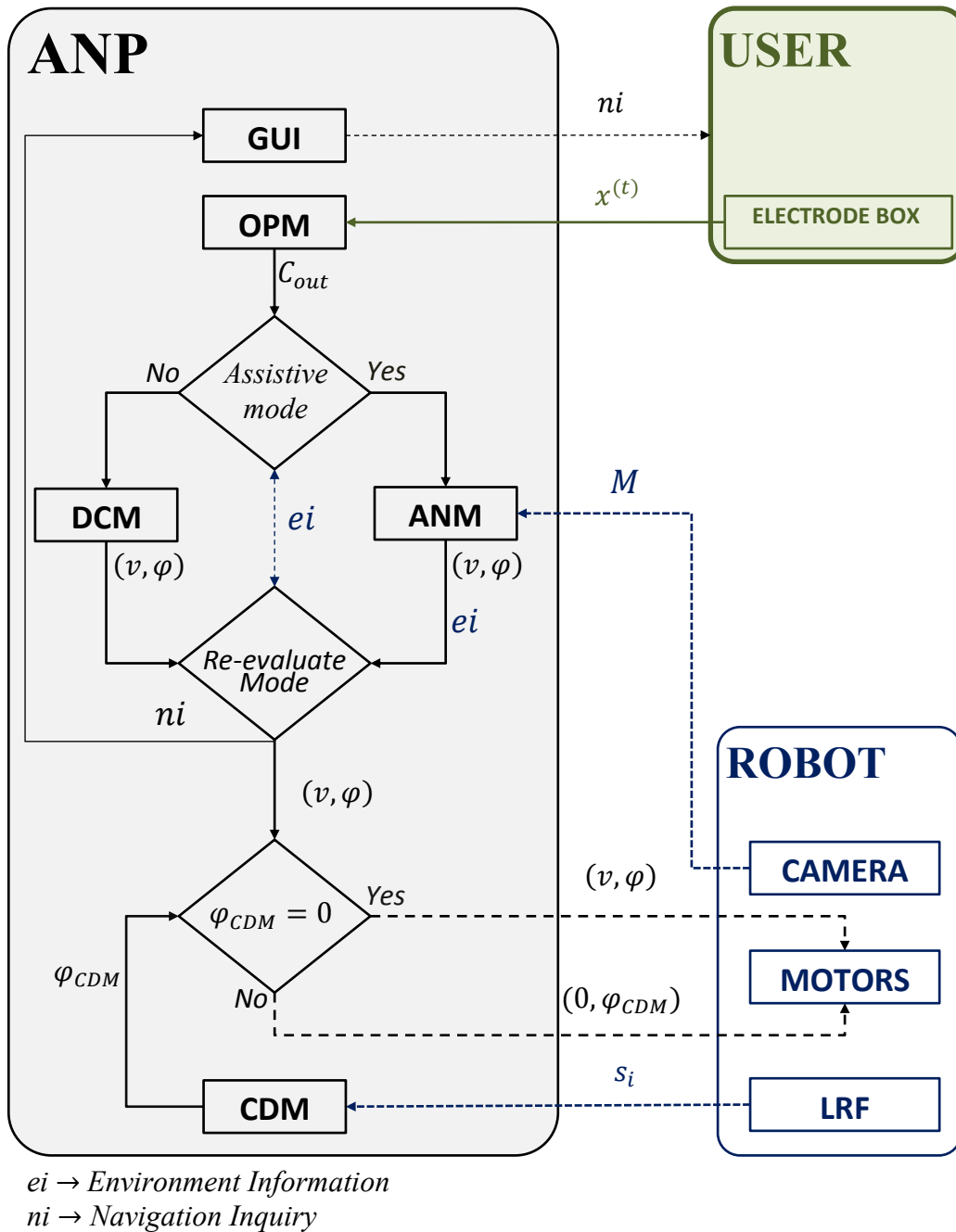


Figure 5-9 Block diagram of the BMI-based robotic wheelchair control system using ANP

In our experiments, the BMI based robot navigation trials are conducted in two different control modes: 1) unassisted control (direct control) mode, where the ANM is unavailable and the subject navigates the robot turn-by-turn, 2) assisted control mode, where the ANP assists the navigation by using the ANM and assistive information.

**Unassisted Control** – In this mode, the subject controls the robot using only the DCM, while the ANM is not available throughout all navigation duration. The ANP assists navigation only with the CDM. In this mode, every OPM output ( $C_{out}$ ) translates into a

robot moving direction change following Table 5-2. After each mental task the robot moves for 3 seconds, and then slows down to minimal speed while the subject performs the consecutive mental task. This is done to improve subject's concentration while performing the mental task.

**Assisted Control** – In this mode, the subject controls the robot using full assistance from ANP and with all three navigation modules. If the assistive information is available, the ANM can navigate the robot by following the assistive lines. When a decision point is detected during autonomous navigation, the mental task prediction translates into a robot direction change following Table 5-2, and after that, the robot continues autonomous navigation again. In case the assistive information is missing the subject is still able to navigate the robot turn-by-turn. Mode change during navigation will be explained in the next section. During autonomous navigation the direction and speed are calculated by using Eq. 29.

The ANP is equipped with a Graphical User Interface (GUI) that is responsible for the subject interaction during navigation. The GUI displays different information to the subject; it has a live video feed and a live processed video feed from the camera, it gives online BMI classification feedback in the form of probability distribution over three tasks ('*info*' box) and shows the current action in the "*Action*" box (Figure 5-10. (c))

By using the GUI (Figure 5-10), the ANP asks the subject to:

- 1) Activate the ANM at the beginning of the robot navigation
- 2) Switch between the two different modes during robot navigation
- 3) Select the next robot movement direction ("*Action*" box).

Furthermore, audible information is played simultaneously in order to notify the subject that its attention (mental activity) is required for the next control command.

**Table 5-2 OPM output translations into real time robot direction change in assisted and unassisted control modes**

OPM output	Direction ( $\varphi$ ) change	
	Unassisted Control	Assisted Control
$C_{out} = L$	$\pi/4$	$\pi/2$
$C_{out} = R$	$-\pi/4$	$-\pi/2$
$C_{out} = F$	0	0
$C_{out} = U$	0	0

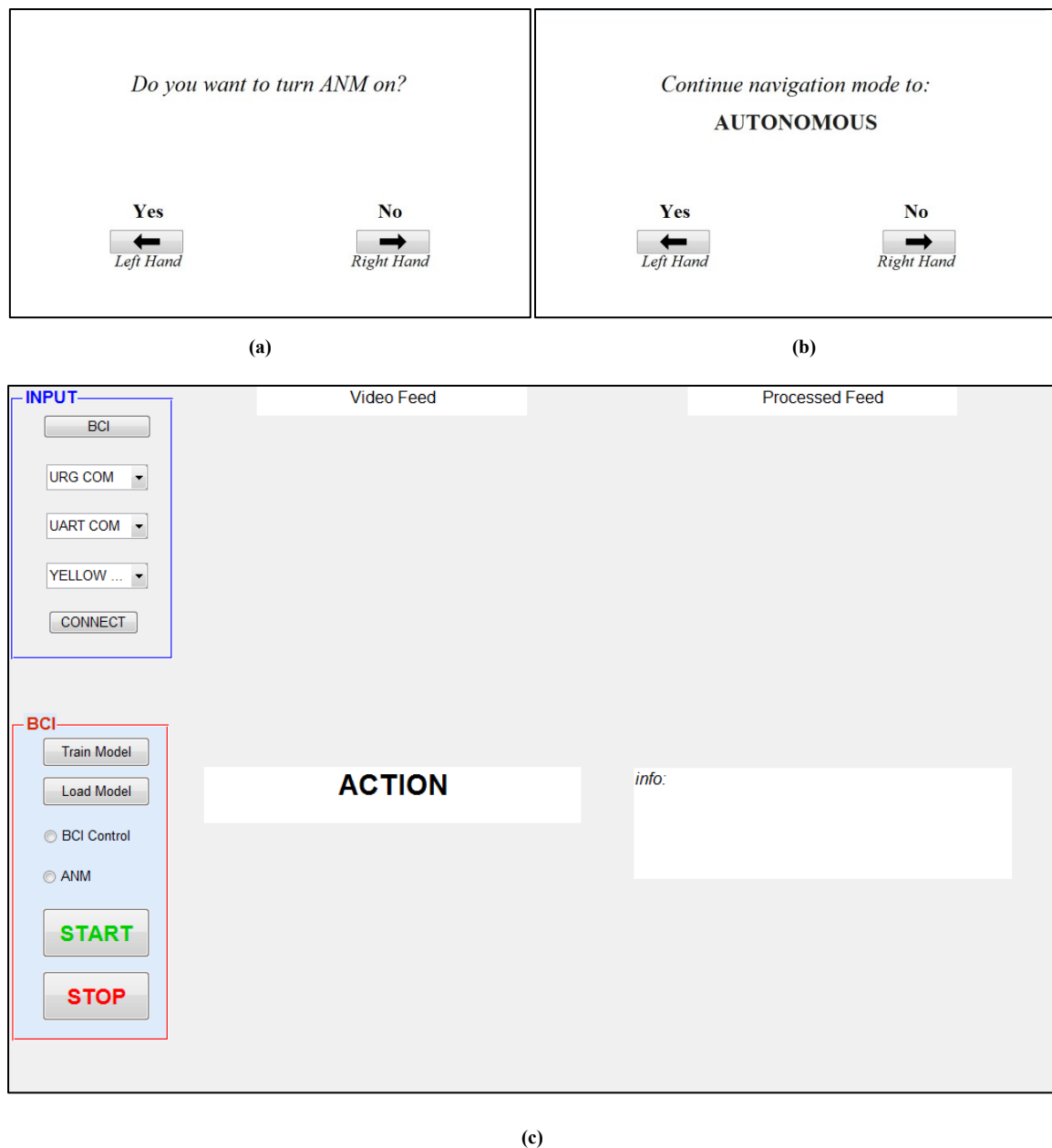


Figure 5-10 (a) Activate ANM popup GUI, (b) Change Navigation Mode popup GUI, and (c) Main GUI of the system

### 5.3.1 Control Mode Transitions and Finite State Machine

Changing from unassisted to assisted mode can be done only when assistive information is captured by the camera. While in unassisted mode, if a tactile line is detected, the subject is offered by the GUI to switch control mode. If the ANP offer is declined from the subject, the navigation will continue in unassisted mode. Otherwise, the navigation will switch to assisted mode, and the robot will then autonomously navigate by following the assistive information.

To prevent asking the subject repeatedly to switch modes, when a line is detected and the subject refuses to change mode, a predefined penalty counter is triggered and for the next three unassisted robot movements the subject is not asked to change mode, even when the assistive information is captured by the camera.

Changing from assisted to unassisted control mode can be done when a decision point is detected; the subject is offered to switch between modes by the GUI. When the line is lost (i.e. line is covered or is not available anymore) or an obstacle is detected during autonomous navigation, the navigation will immediately switch to direct control mode without asking the subject.

Switching modes is done only by using the mental task predictions ( $C_{out}$ ). In our implementation, the OPM outputs  $\{L, F\}$  are used to change mode and the OPM outputs  $\{R, U\}$  are used to reselect the existing mode. Nevertheless, they can be changed according to the subject's choice (i.e. it is possible to select the easiest mental tasks that the subject can perform, and assign them to specific navigation tasks accordingly).

#### ❖ Finite State Machine

The entire robot control system can be considered a finite state machine (FSM) with 6 states: TURN LEFT, TURN RIGHT, FORWARD, STOP, TL (robot following a tactile line) and STOP DP (robot over decision point). The diagram of the FSM is shown on Figure 5-11. The transitions between the FSM states are: **a)** five OPM outputs translated by ANP: left (L/L(T), right (R/R(T)), forward (F/F(T)), uncertain (U) and change mode (C), and **b)** five additional robot sensory readings based outputs: object detected (O), object avoided (A), line detected (T), decision point detected (D) and empty (E) (i.e. assistive information is lost or is not available anymore).

In different modes the OPM output transitions are translated differently (Table 5-2); e.g. in assisted control mode, transition left means turn left and follow line (with respect to the available lines). Furthermore, in case the current decision point is connected with only two lines (e.g. only forward and right line), the transition left means turn left and since there is no available line, transition empty occurs automatically. Robot state will change to STOP and navigation will automatically switch to unassisted control mode.

The OPM output “mode not changed” is not a transition since it does not change the state of the robot. Hence it is not shown in the FSM diagram. Also the robot movement during collision avoidance is not shown, since the state of the robot is not changed until

the object is avoided. When the ANM module is rejected at the beginning of the experimental trial, the FSM is simplified as shown in Figure 5-12, and the robot navigation does not benefit from the autonomous navigation since only DCM is used.

The implicit terminal state, the GOAL, can be reached from any other state when the goal is achieved.

There is not any specific transition to make a U-turn. However, this can be achieved by turning left or right for four consecutive steps in unassisted mode. Also, the subject could be prompted to make a U-turn when on decision point or when an object is detected, but given the physical size of the robot, the environment construction and the scope of our experiment (Section 5.4), this feature was not included as a navigation option.

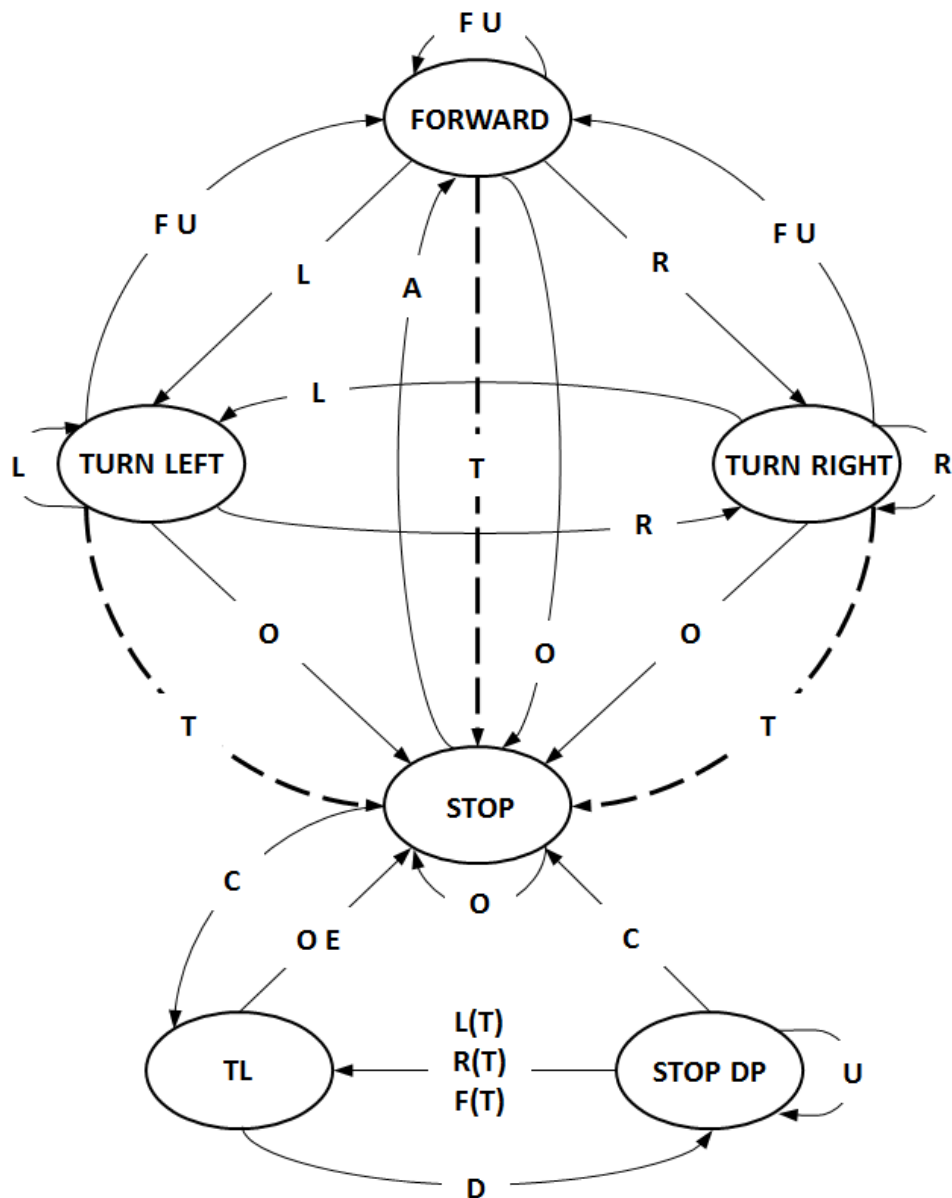


Figure 5-11 FSM diagram

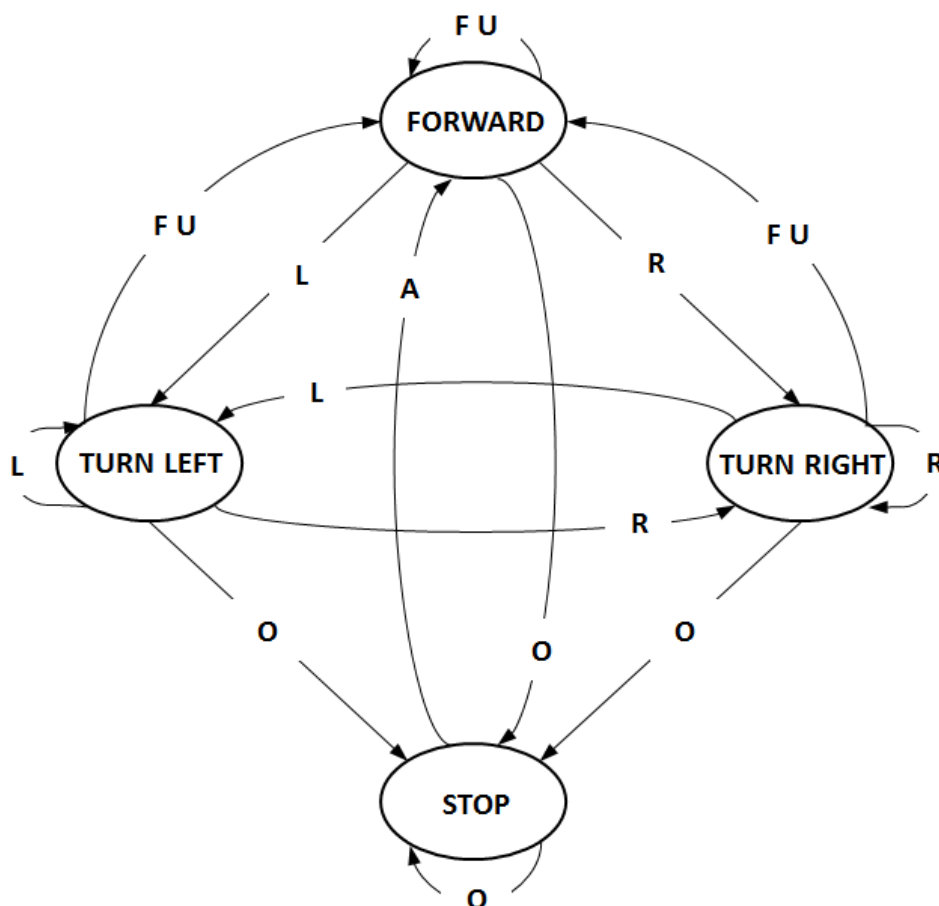


Figure 5-12 FSM diagram during unassisted control mode

## 5.4 Environment and Experimental Setup

The layout of the environment where the wheelchair navigation experiments were conducted is shown in Figure 5-13. It's a typical hallway of an office building floor, with several offices, cross sections, etc., and it is equipped with tactile paving for visually impaired people. The decision points are placed on cross-sections or in front of areas where there is a place of interest (e.g. an office). The goal is to navigate the robot using BMI, from the start to the finish line in front of the second office on the right. If the robot encounters a human during the experiment, the CDM treats it as a routine collision detection scenario.

In total, three experimental sessions with six navigation trial each, were conducted. Only one BMI model was build prior to navigation. Then the OPM based on the same BMI model was used in all sessions. Before the first session, the subject was familiarized with the experimental tasks and the navigation capabilities of the robotic wheelchair.

In order to familiarize with the navigation task, prior to the first experimental session, the subject used a pushbutton interface (instead of BMI) to navigate the robot for 10 minutes. Furthermore, at the beginning of each session, there were two BMI calibration trials, during which the subject was able to navigate the robot without any specific goal by using only BMI. After finishing the calibration trials, the subject started to navigate the robot to the goal (finish line in Figure 5-13). If the robot enters in a wrong office room or the subject asks to stop, the trial is considered failed.

In order to achieve good electrode impedance the electrode cap must be tightened to the skull. Experimental sessions longer than two hours may cause headache due to the scalp pressure caused from disk electrode plastic enclosures. Furthermore, the BMI subjects may fatigue and face focus decline when the session are longer than two hours. In our experiments, we set the entire session duration to approximately two hours, including cap installation, electrode impedance correction and all robot navigation trials in both assisted and unassisted modes.

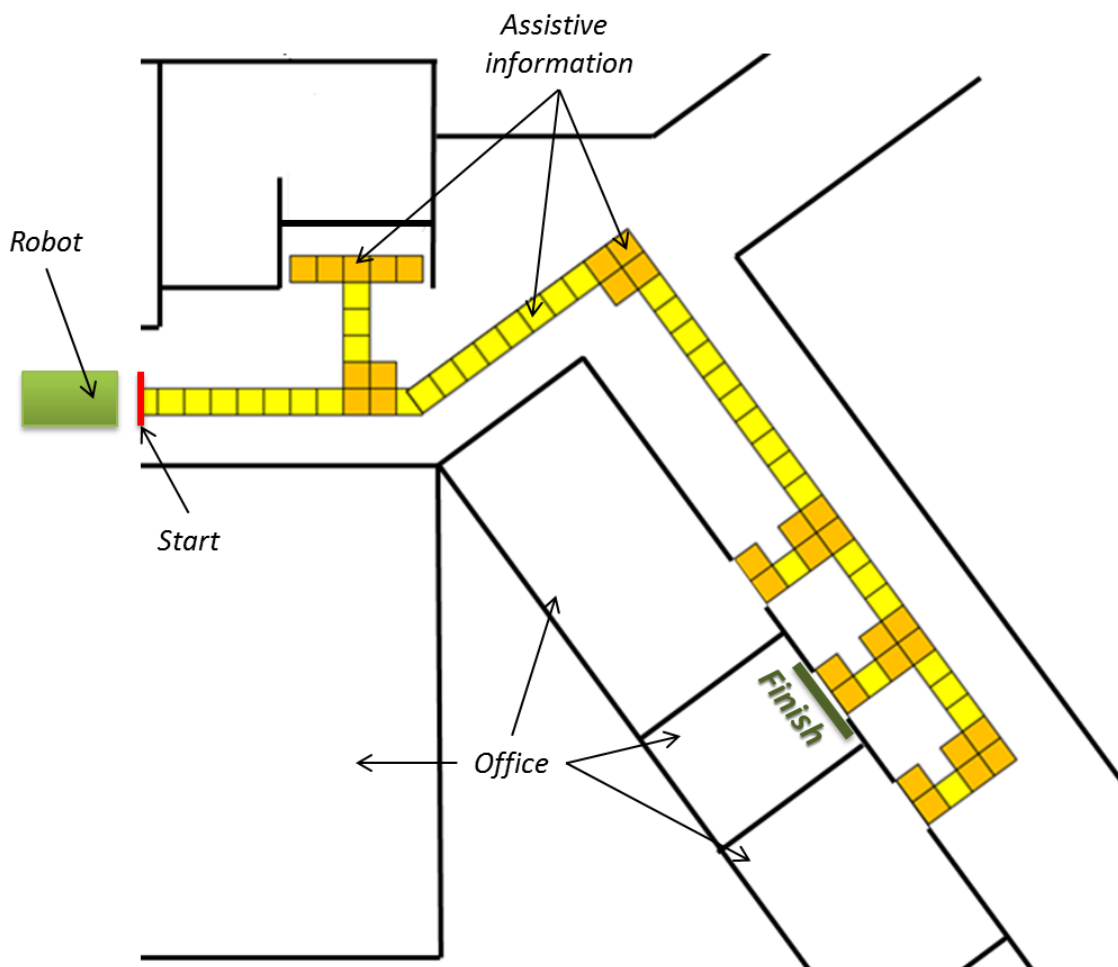


Figure 5-13 Experimental environment

The purpose of our experiments is to evaluate the benefits of using ANP with all its modules and the assistive information, when navigating a robotic wheelchair by using BMI. For these purpose we compared the robot navigation performances with and without the assistance from ANP. At the beginning of each trial, the subject was asked for the ANM assistance and it could choose by using BMI. The experimental trials were equally split into assisted and unassisted trials.

## 6 Results

This chapter shows the results of our experiments and it is divided it three sections. In Section 6.1 are shown the results of the BMI system, including signal processing and offline BMI training results. In Section 6.2 are shown the online BMI system performance results during robot navigation. In Section 6.3 are shown the results of the robot navigation including the performances of different ANP modules during assisted and unassisted control modes as well as the results of the robot navigation metrics.

### 6.1 Offline BMI Results

In order to build the OPM, at first we collected an offline recording EEG dataset with 120 trials: 40 per each mental task (Section 4). The raw 15 channel EEG signals acquired at 250 Hz during a single trial (RH – *right hand*) are shown in Figure 6-1, in the time domain. Its mean log power spectrum, which was calculated by using Welch's averaged periodogram method, is shown in Figure 6-2.

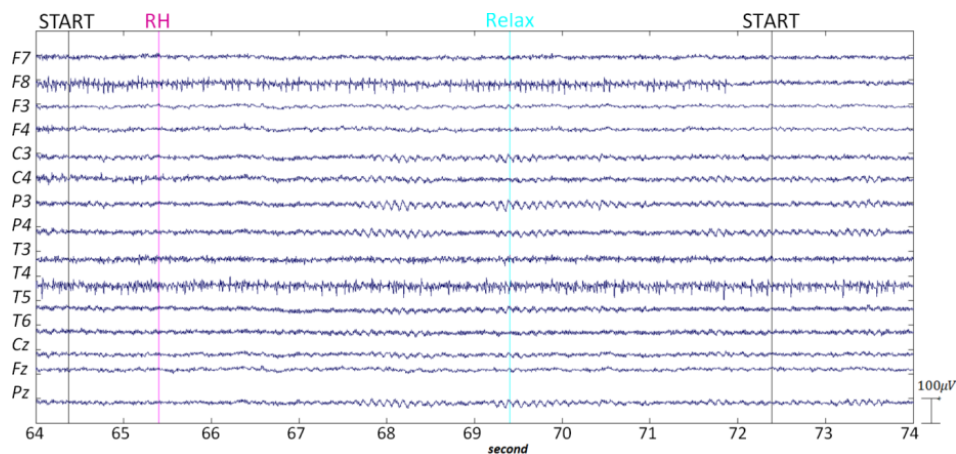


Figure 6-1 Raw 15 channel EEG signal recordings during an offline trial

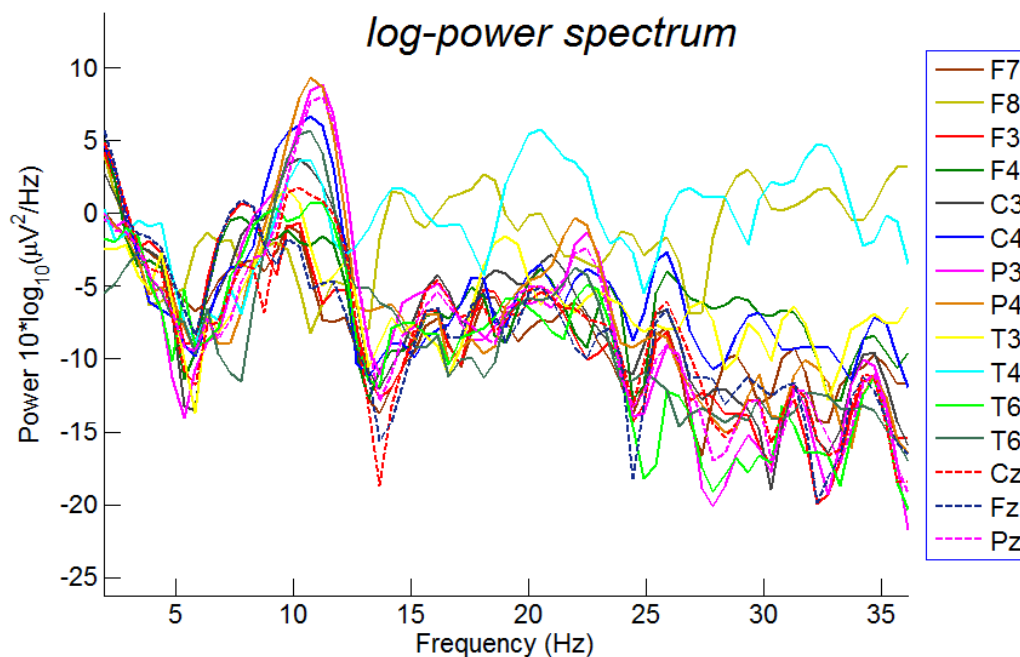


Figure 6-2 Single trial power spectrum

### 6.1.1 Preprocessing

Following Section 4.3, the signal is resampled at 100 Hz, LTI filtered, band-pass filtered in the frequency band [8, 30], and then data epochs were extracted in the time interval [0.5, 3] seconds after each event.

#### ❖ LTI filtering results

The mean log-power spectrum of the offline dataset shows an increased activity (i.e. power spike) in the  $\mu$  brain rhythms frequency range [8, 12] Hz and in the  $\beta$  brain rhythms frequency range [18, 22] Hz. The mean log-power spectrum of the continuous 15 channel EEG dataset resampled at 100 Hz, before and after  $f^{1,-1}$  filtering is shown in Figure 6-3.

In Figure 6-3 (b), the overall spectral power has decreased but the spike in the  $\mu$  brain rhythms frequency band [8, 12] Hz is enhanced compared to Figure 6-3 (a). The activity in this rhythm ( $\mu$ ) is associated with the motor cortex (central scalp), and changes with limb movement or an intent to move (Sanei and Chambers 2007). On the other hand the  $\beta$  frequency range is not suppressed and the high rhythm spike on the frequency band [19, 22] Hz is enhanced as well. The result of  $f^{1,-1}$  LTI filtering is a noise reduction preprocessing operation which enhances the difference between the spectral power of the

target and the background brain activity, which in our case is considered noise. Thus, the LTI filtered signal has a higher SNR.

In Appendix D, the performance of the  $f^{1,-1}$  filtering on the CSP and Spec-CSP methods is evaluated with 17 offline datasets recorded in our lab and 19 publicly available datasets.

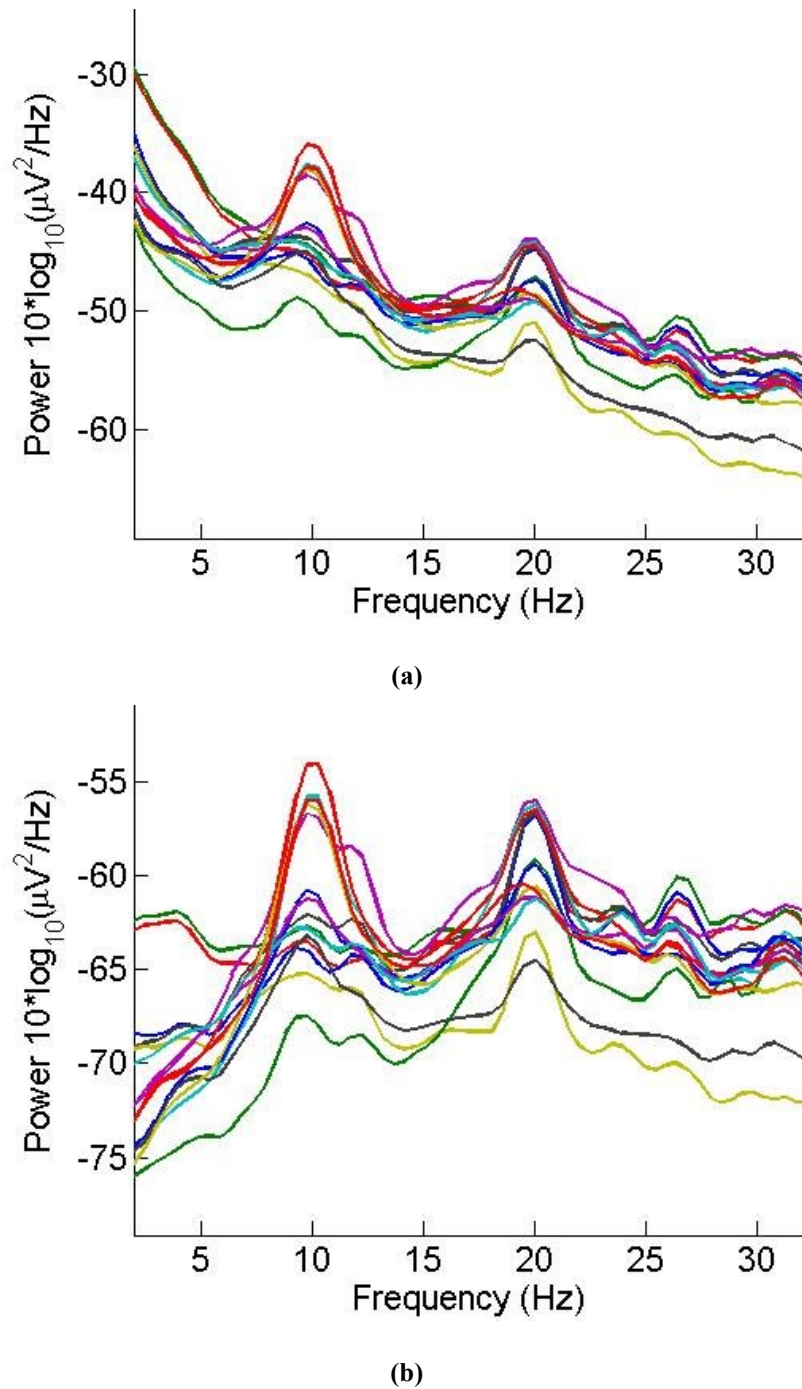


Figure 6-3 Mean log power spectrum of a continuous 15 channel EEG dataset: (a) without LTI filtering, and (b) with LTI filtering

### 6.1.2 Filtering Model

With the epochs extracted from the filtered signals (Figure 6-4), we optimized spatio-temporal filters for every pair of mental tasks ( $L \leftrightarrow R$ ,  $L \leftrightarrow F$  and  $R \leftrightarrow F$ ). The spatial filter matrix  $\mathbf{\Omega} = \{\omega_i\}_1^d$ , with filters  $\omega_i$  as columns from Table 4-2, is a square matrix ( $\mathbf{\Omega} \in \mathbb{R}^{d \times d}$ ). A spatial pattern  $\varpi_i$  is the  $i^{th}$  column of the inverse spatial filter matrix  $\mathbf{\Omega}^{-1}$ , such that  $\varpi_i^* \omega_i = 1, \forall i \in \{1, \dots, d\}$ . These patterns represent the mental task specific normalized brain activity, which maximizes the corresponding filter output.

The spatial patterns  $\varpi$  and the filters  $\alpha$  corresponding to the three biggest and smallest eigenvalues  $\lambda$  (Table 4-2) are shown on Figure 6-5 and Figure 6-6, respectively.

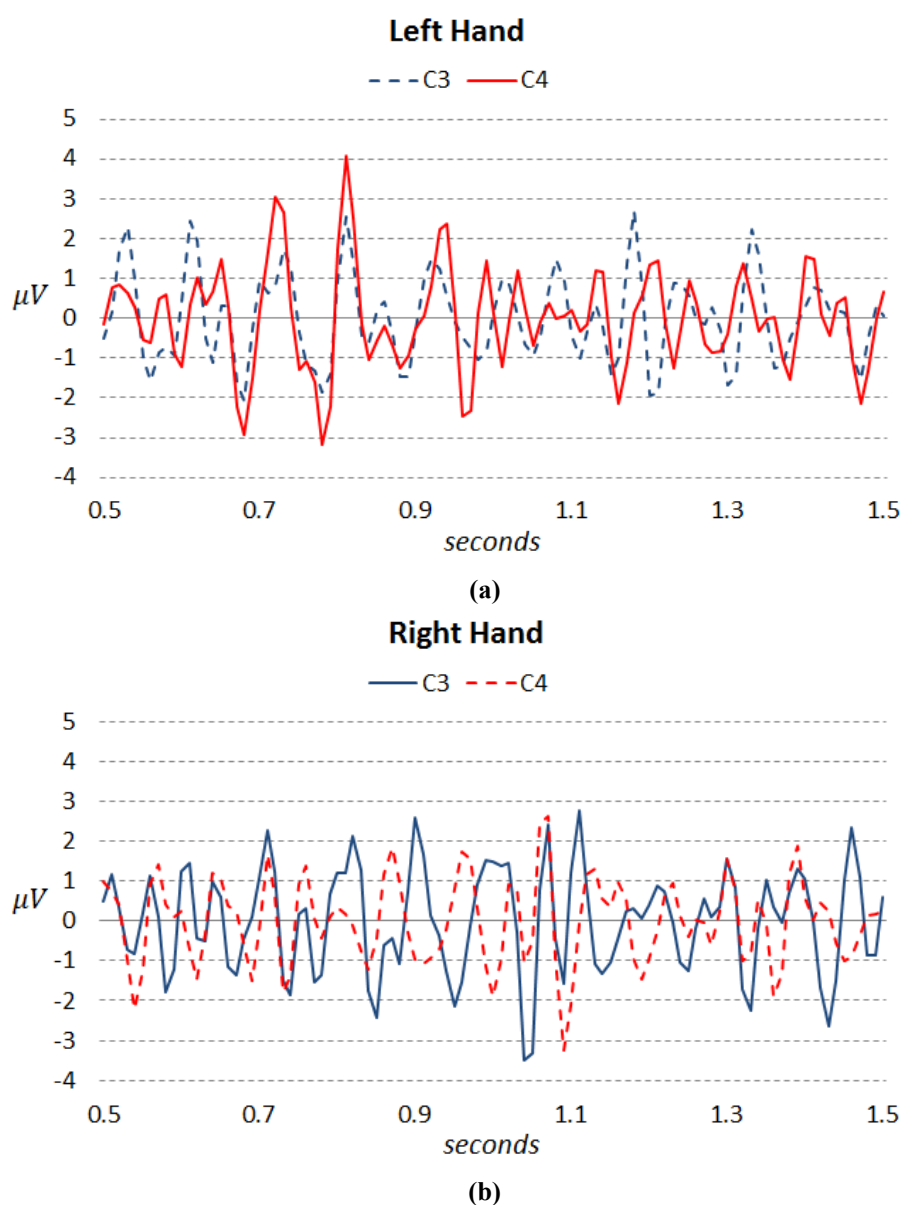
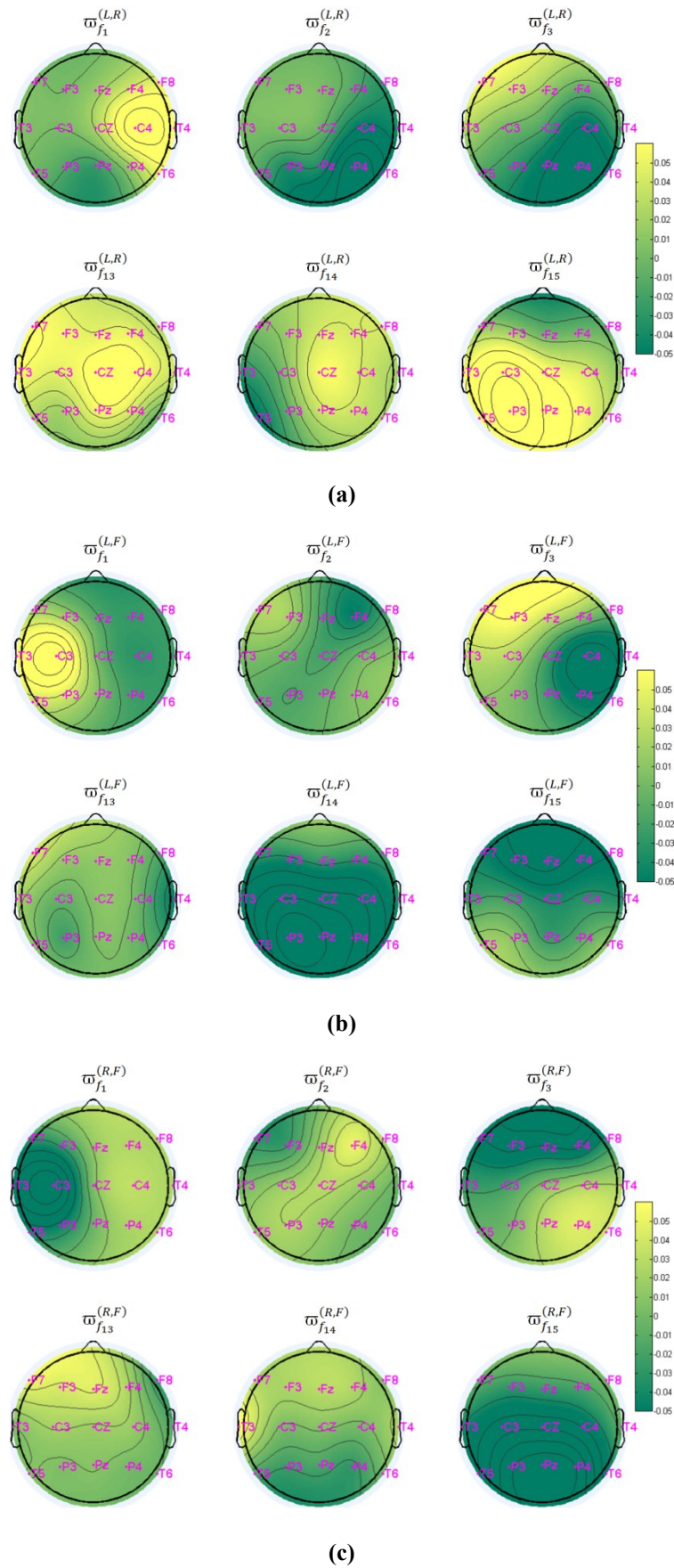


Figure 6-4 The C3 and C4 Electrode (channel) signal averaged over trials, after preprocessing in the time interval [0.5, 1.5] seconds after the cue during: (a) Left Hand tasks and (b) Right Hand tasks



**Figure 6-5 Scalp topographic maps of the spatial patterns for the three biggest & smallest eigenvalues of the MI pair: (a) Left Hand v. Right Hand, (b) Left Hand v. Foot and (c) Right Hand v. Foot**

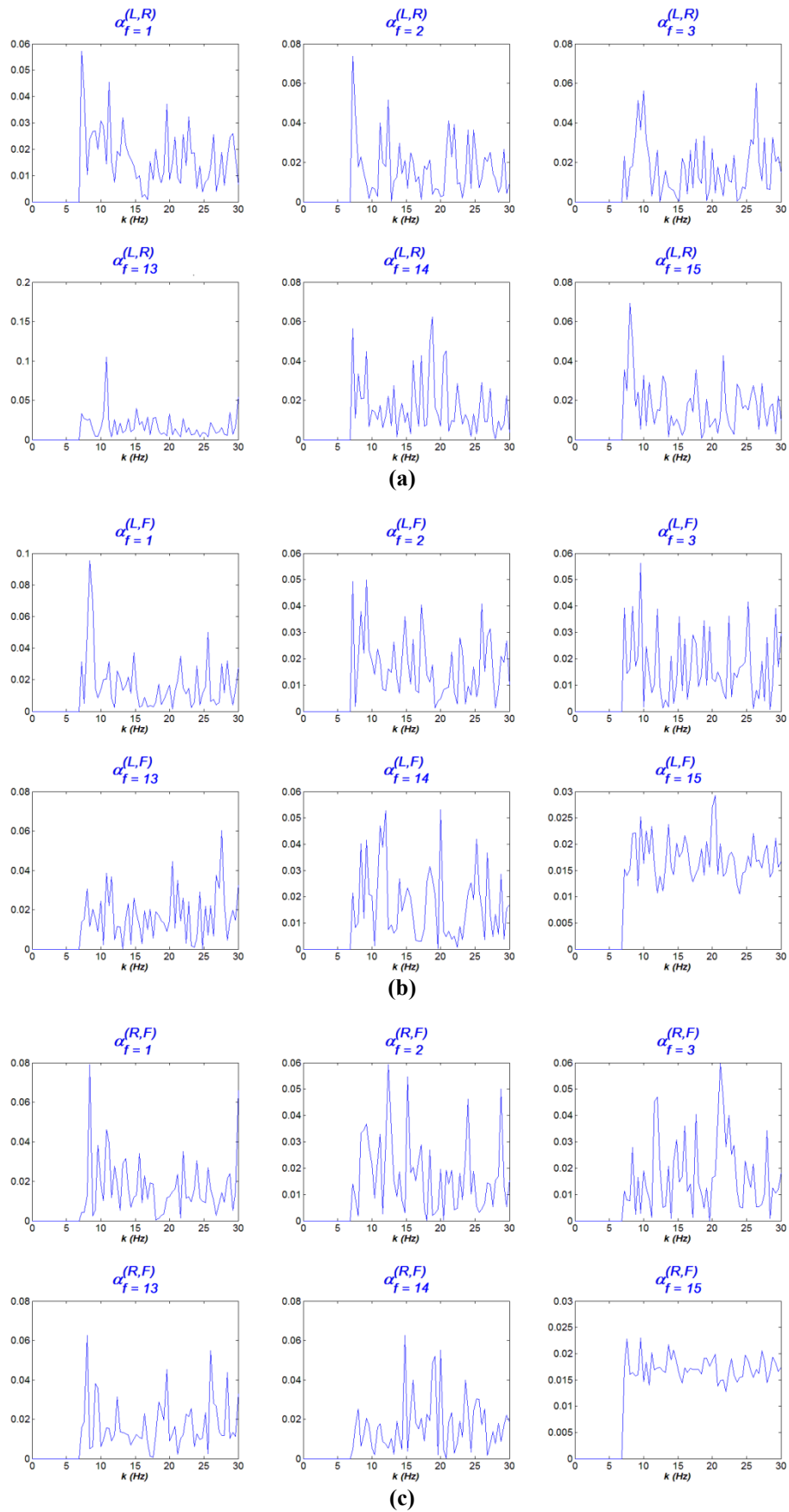


Figure 6-6 Frequency filters  $\alpha$  corresponding to the three biggest & smallest eigenvalues of the MI pair: (a) Left Hand v. Right Hand, (b) Left Hand v. Foot and (c) Right Hand v. Foot

## 6.2 Online BMI results

The OPM performance results during online robotic wheelchair navigation sessions are summarized in Table 6-1. The average number of misclassifications per trial is reduced approximately three times during the assisted navigation mode. The increased number of misclassifications in unassisted mode resulted into navigation mistakes which lead to additional mental tasks required to recover the desired trajectory and to proceed towards the goal. Furthermore, BMI accuracy during assisted navigation mode was approximately 30% higher compared to unassisted navigation mode. Although there is no direct correlation between BMI classification algorithm and ANP, the results show improved classification during assisted navigation. The total number of mental tasks required in assisted mode was lower compared to unassisted mode. This reduced the mental workload, which indirectly improved BMI classification.

**Table 6-1** The mean and the standard deviation of the BMI misclassifications and the BMI accuracy during each experimental session

BMI Metrics	Session	Assisted		Unassisted	
		mean	std	mean	std
Misclassifications (counts/trial)	I	7.0	1.7	15.0	6.0
	II	3.7	1.5	11.7	3.1
	III	1.0	1.0	4.0	1.0
	<b>Total</b>	<b>3.9</b>	<b>2.9</b>	<b>10.2</b>	<b>6.0</b>
Classification Accuracy (%)	I	69.1%	9.8%	52.1%	9.4%
	II	79.2%	6.8%	62.0%	7.8%
	III	91.2%	8.3%	76.9%	5.4%
	<b>Total</b>	<b>77.4%</b>	<b>12.3%</b>	<b>61.3%</b>	<b>12.2%</b>

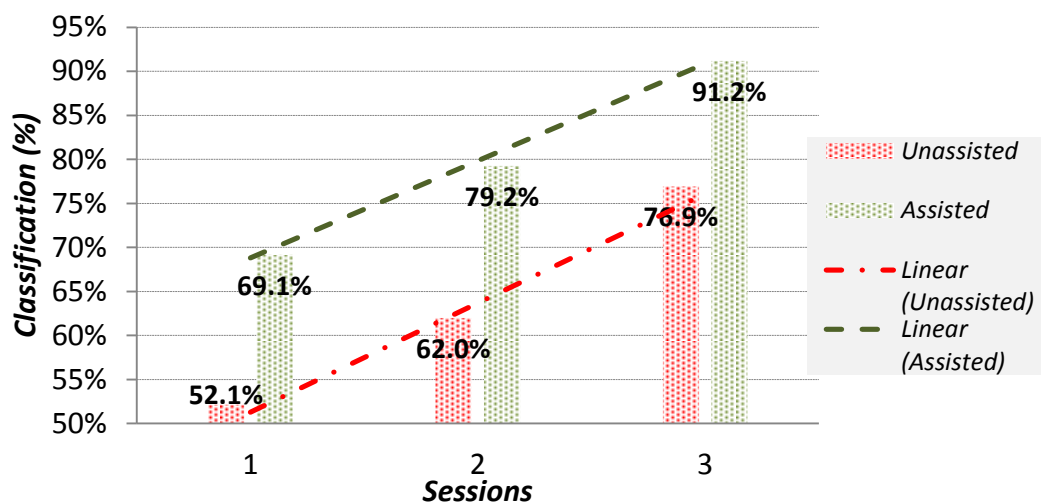


**Figure 6-7** BMI classification accuracy distribution over experimental sessions

Figure 6-7 shows the BMI classification accuracy distribution over three experimental sessions. Generally, there is an improvement in BMI accuracy in later sessions. This is no surprise since it is well known within BMI community that the BMI classification improves as the BMI subject gain experience.

### 6.3 Robot Navigation Results

The performance of the robot navigation in assisted and unassisted mode is measured by the number of collisions detected and avoided, the number of mental task required to achieve the goal, and the time to achieve the goal.

#### 6.3.1 Collision Detection and Avoidance Performance

The CDM was able to detect and avoid all the obstacles during all sessions in both navigation modes, without causing any false object detection. The numbers of collision detected ( $cd$ ) during each trial were recorded and the results of all experimental sessions are shown on Table 6-2. In some collision detection scenarios (i.e. when the robot was in a corner) the CDM changed the robot direction more than one time in order to avoid a collision. The accumulated absolute value of the robot turn during collision avoidance ( $ca$ ), is gained by adding all values of  $n$  from Algorithm 1 that occur during a full experimental trial ( $ca = \sum n = \sum \sum |\varphi|$ ). The value of ( $ca$ ) directly reflects the total CDM activity during each trial to avoid the object. The results of ( $ca$ ) during all experimental sessions are shown on Table 6-2. Figure 6-8 and Figure 6-9 show that the results of collision detection and avoidance also improved when the subject gained experience.

**Table 6-2 CDM Performance**

<i>CDM Metrics</i>	<i>Session</i>	<i>Assisted</i>		<i>Unassisted</i>	
		<i>mean</i>	<i>std</i>	<i>mean</i>	<i>std</i>
<i>Collision Detection (cd)</i> <i>(count/trial)</i>	<i>I</i>	5.0	0.0	16.0	5.3
	<i>II</i>	1.7	0.6	9.7	3.1
	<i>III</i>	0.7	0.6	5.3	3.8
	<b>Total</b>	<b>2.4</b>	<b>2.0</b>	<b>10.3</b>	<b>5.9</b>
<i>Collision Avoidance (ca)</i> <i>(<math>\pi</math>/trial)</i>	<i>I</i>	3.7	1.8	4.9	2.5
	<i>II</i>	0.7	0.1	3.1	0.5
	<i>III</i>	0.3	0.3	1.6	0.9
	<b>Total</b>	<b>1.5</b>	<b>1.8</b>	<b>3.2</b>	<b>2.0</b>

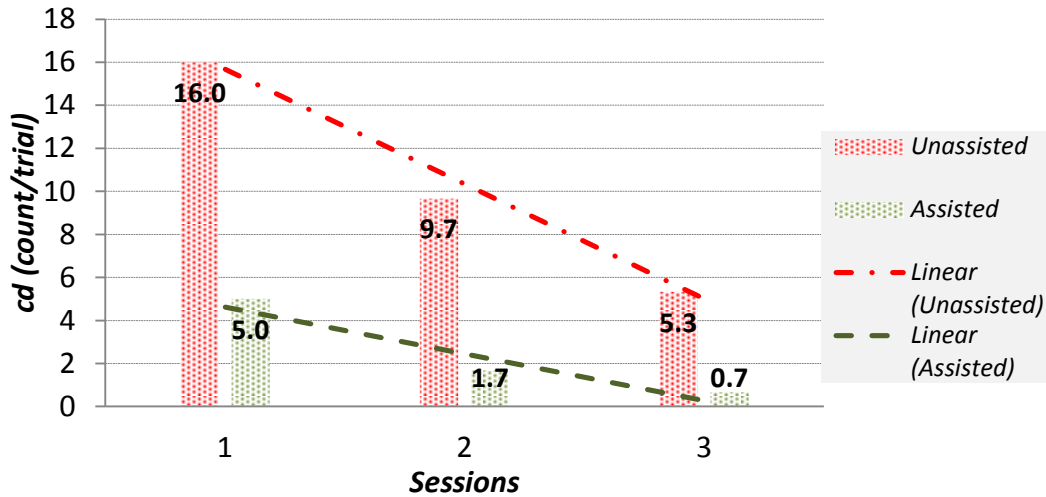


Figure 6-8 Collision detection results over experimental sessions

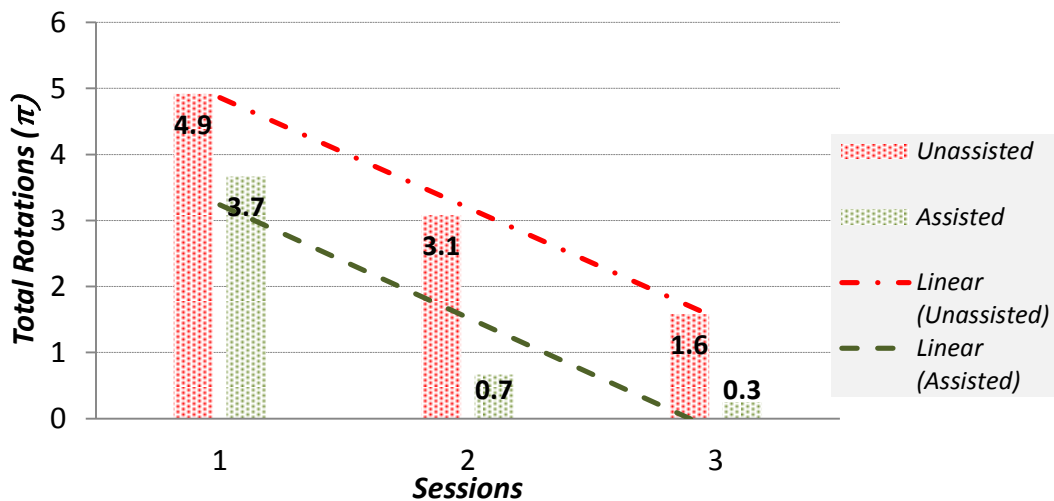
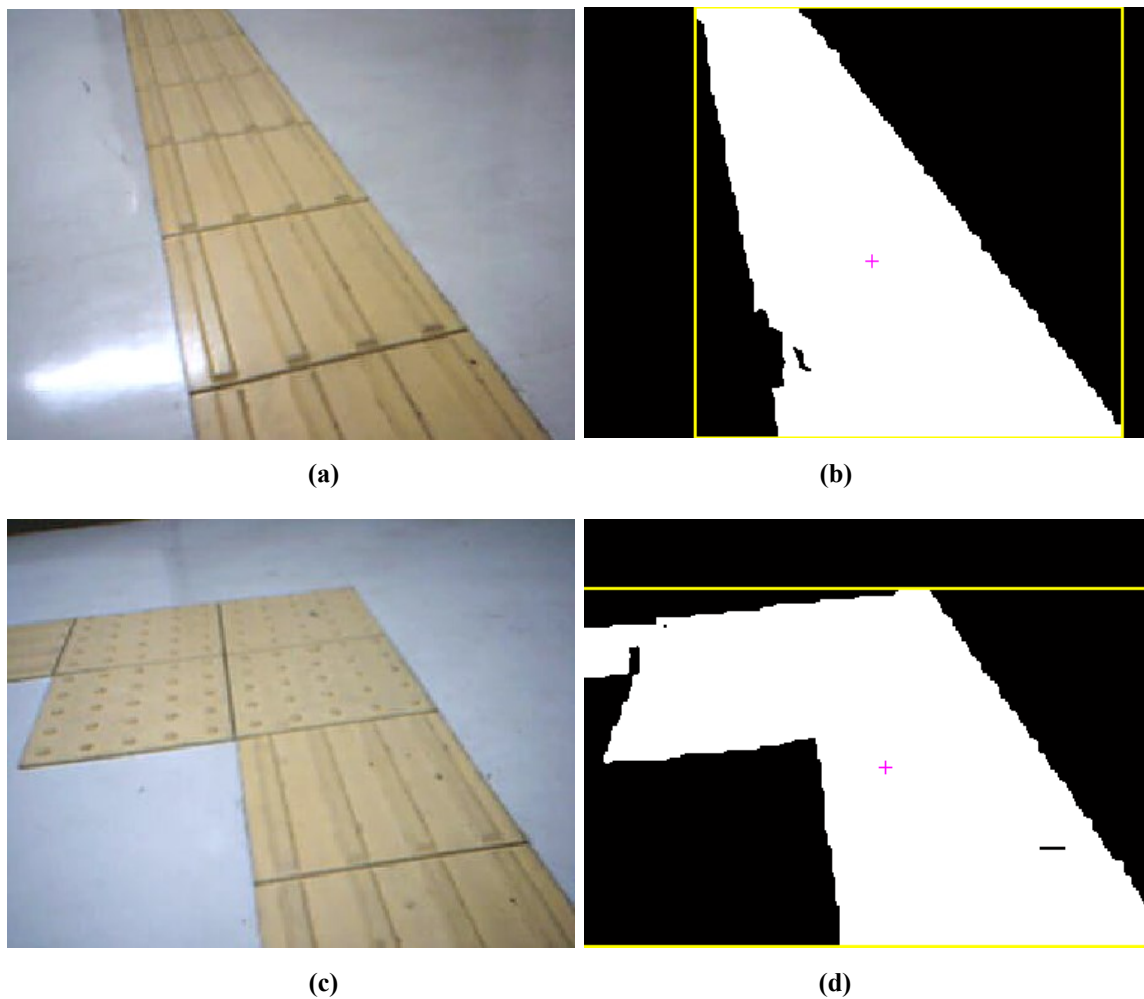


Figure 6-9 Collision avoidance results over experimental sessions

### 6.3.2 Autonomous Navigation Performance

The camera feed was processed online to extract assistive information (Figure 6-10), and the results were sent to the ANM. The ANM was very accurate and the robot followed the assistive information accordingly as described in Section 5.2.3.

During all experimental trials conducted in assisted navigation mode, in all sessions, the ANM failed to detect and follow the assistive line only twice during the first session. After the first session the image processing algorithm was tuned to perform in different light intensity and as a result the assistive information was not lost anymore.



**Figure 6-10 Assistive information extraction from the real-time image processing algorithm of a line (captured image in (a) and its result in (b)) and a decision point (captured image in (c) and its result in (d))**

However, in some trials the assistive information was lost due to a wrong BMI output while on decision point. In those cases, there was no available line in the direction indicated by the BMI output, and the navigation followed immediately in direct control mode until the next assistive line was detected by the ANM.

### 6.3.3 Adaptive Robotic Navigation Results

Besides the collision detection (*cd*) and avoidance (*ca*) results introduced above, here we will introduce the results of two very important navigation task metrics. In Table 6-3 are shown the results of mental tasks or BMI mental predictions (*mp*) required during a full trial and the total trial time (*t*). In assisted mode the subject was able to navigate the robot from starting position to the goal faster and with fewer mental tasks.

Table 6-3 Navigation Metrics

Navigation Metrics	Session	Assisted		Unassisted	
		mean	std	mean	std
Mental Predictions (mp) (counts/trial)	I	31.3	7.1	22.7	4.0
	II	30.7	3.2	17.7	2.1
	III	17.3	3.5	11.3	0.6
	<b>Total</b>	<b>26.4</b>	<b>8.0</b>	<b>17.2</b>	<b>5.4</b>
Trial Time (t) (seconds)	I	298.2	61.9	256.7	56.9
	II	262.6	29.3	212.6	23.9
	III	157.8	24.9	148.2	18.6
	<b>Total</b>	<b>239.5</b>	<b>72.9</b>	<b>205.8</b>	<b>57.2</b>

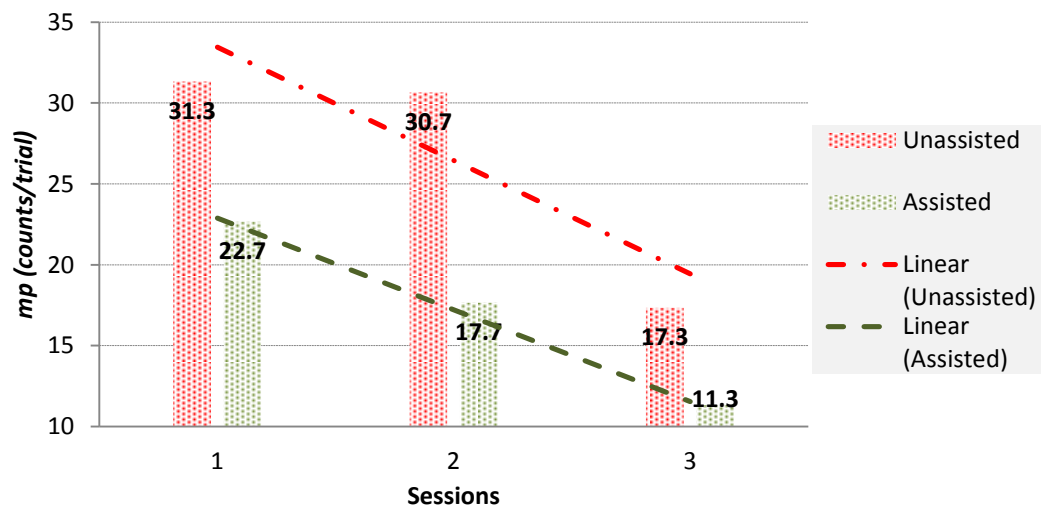


Figure 6-11 Mental task results over experimental sessions

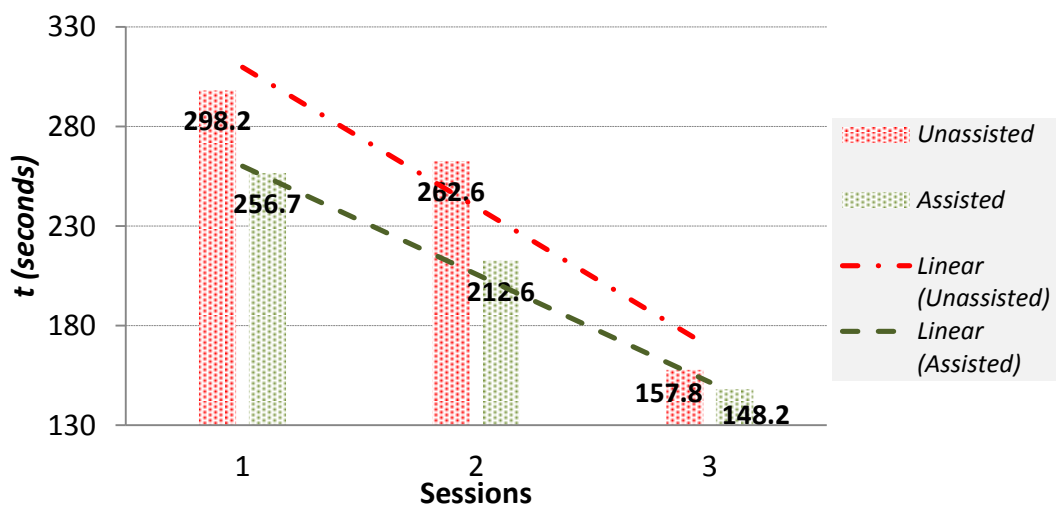


Figure 6-12 Trial time results over experimental sessions

All robot navigation performance metrics during assisted mode show improvement compared to unassisted mode navigation (Figure 6-13). The average number of mental tasks ( $mp$ ) was reduced by more than 34%, the navigation time ( $t$ ) was reduced by more than 14% and the number of collisions was reduced by more than 77%. This shows that the assistance provided by the ANP improves the navigation quality significantly by choosing a better robot motion trajectory following the assistive information and by reducing the number of encountered collisions, improving thus the total navigation time.

Figure 6-14 (a) shows the robot navigation in assisted mode. The navigation started in unassisted mode and after the first mental task the camera detected the tactile paving. The subject switched to assisted mode at point 'S'. In total there are two mental tasks (double) at the same place. At the first decision point (A), the robot stopped and the subject was asked again to switch control mode. Assisted mode was selected again. Next, the robot movement direction was asked and forward direction was selected (double MI task again). Following navigation according to the dotted line, the robot arrived at the goal location 'G'.

Figure 6-14 (b) shows the robot navigation route in a trial conducted entirely in unassisted mode. In this trial, we have only one mental task (single) at each location since the subject was never asked to switch mode. During this trial a collision was detected at 'C1' and avoided utilizing the CDM.

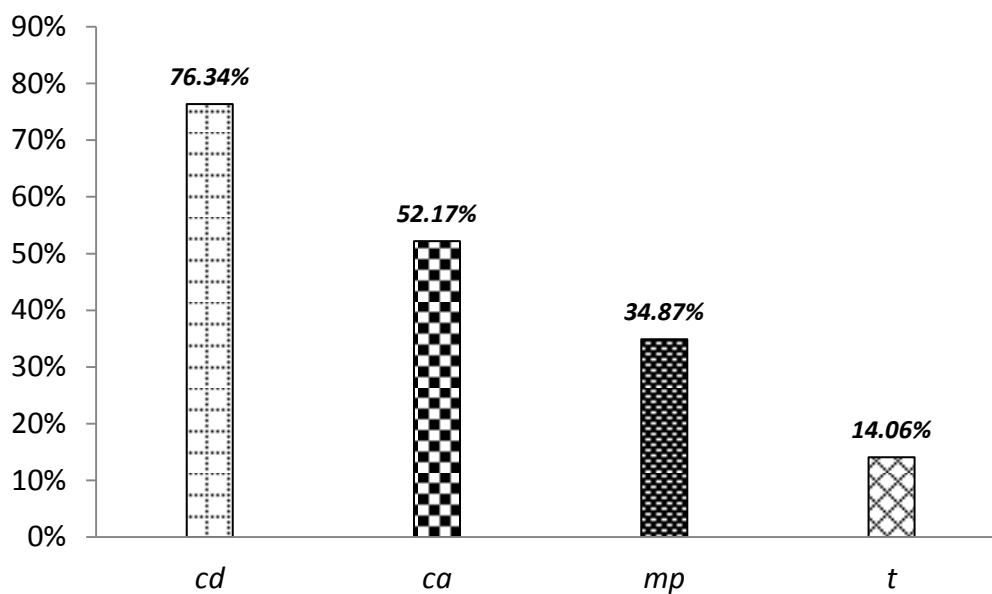
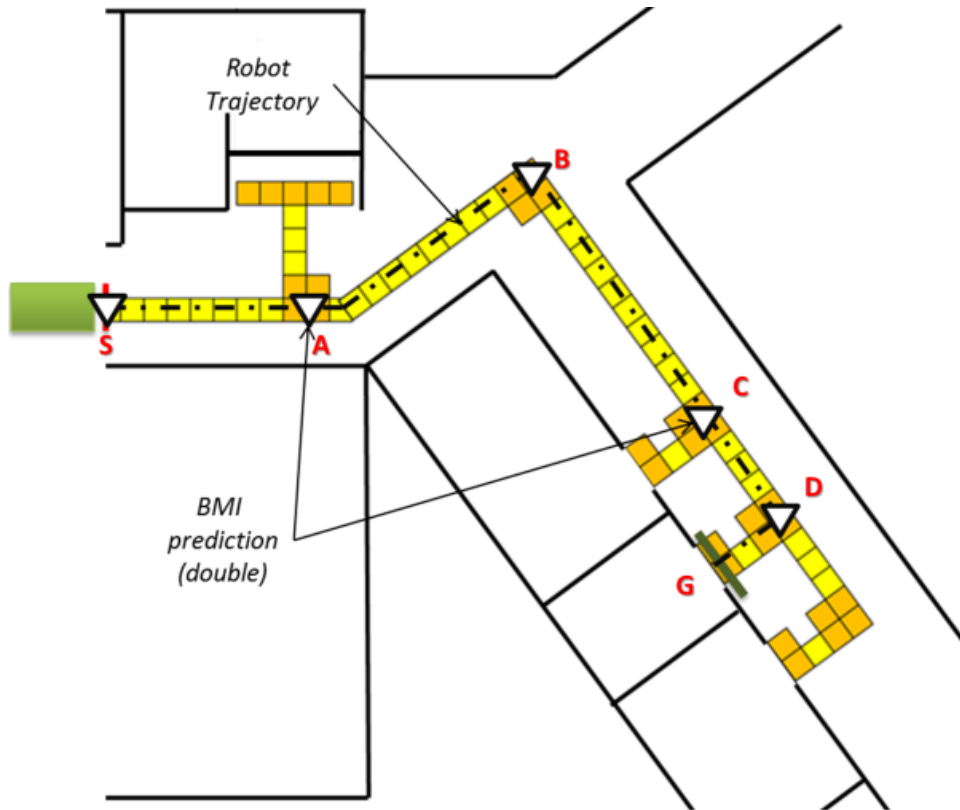
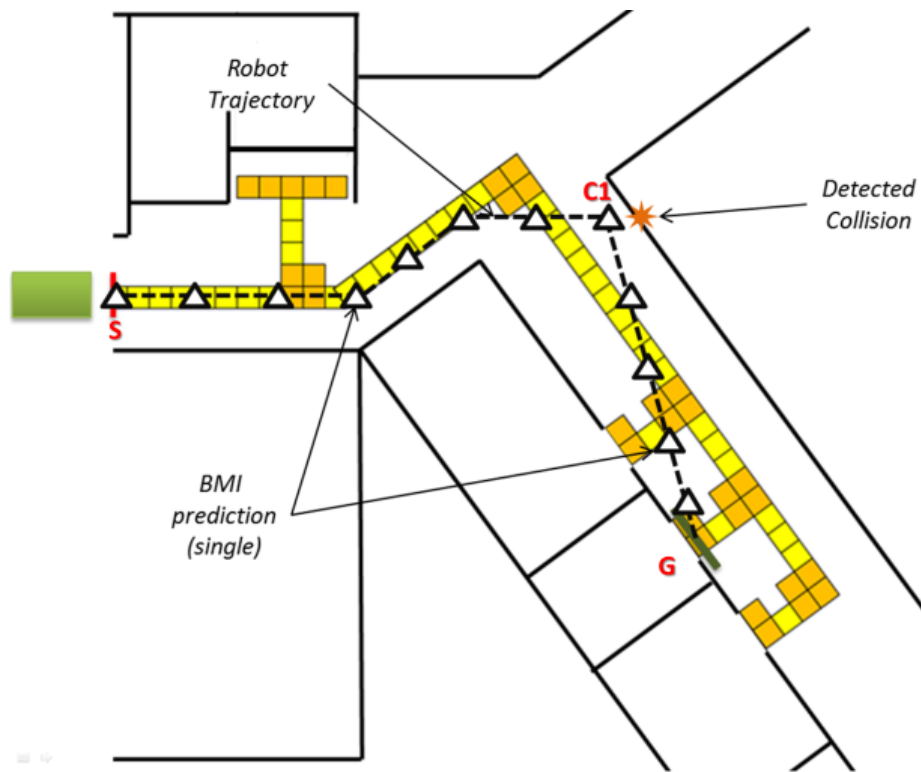


Figure 6-13 Robot navigation metric improvement during assisted navigation



(a)



(b)

Figure 6-14 A navigation trial conducted in (a) assisted mode (b) unassisted mode



## 7 Conclusions

In this thesis, we proposed an adaptive navigation method for the robotic wheelchair using brain signals. We introduced a de-noising filtering to improve the BMI performance, and proposed an adaptive method to assist and improve the navigation of the wheelchair.

The advantages of the proposed method were proved by its experimental application with a robotic wheelchair, developed in our lab, in an indoor environment. We found that by using the ANP, the number of mental tasks, the number of collisions and the navigation time improved significantly. Furthermore, the BMI classification accuracy was improved during assisted navigation. Moreover, all navigation performance indicators improved considerably when the subject gained experience.

The main advantages of the proposed method are as follows:

- In our method, we used only EEG signal based BMI to control the robotic wheelchair, compared to other methods (Gneo et al. 2011) that use residual motor functions. In the case of severely paralyzed people other motor functions do not exist or even when they do, it is very hard for the subjects to control them.
- In contrast with other BMI based navigation methods (Gneo et al. 2011; Lopes, Pires, and Nunes 2013), in our method, we did not use EPs. This means the BMI system was not synchronized to any stimuli device, and the subject was not required to continuously stare at the screen in order to produce mental activity.
- The majority of the existing work in BMI controlled wheelchairs is done in simulated or virtual environments (Gentiletti et al. 2009; Philips et al. 2007; Tsui, Gan, and Hu 2011; Cho, Winod, and Cheng 2009; Montesano et al. 2010; Leeb,

---

Friedman, Müller-Putz, et al. 2007; Leeb, Friedman, Slater, et al. 2007). In our method, all the experiments were taken with a real robotic wheelchair in a real indoor environment.

- Our navigation method did not require any prior environment training for the robot. Furthermore, there was no map and/or goal location provided to the robot, as used in other BMI wheelchair applications (Perrin et al. 2010; Lopes et al. 2011; Carlson and del R. Millan 2013; Lopes, Pires, and Nunes 2013). This made the navigation environment independent.
- Our method reduced the subject's mental workload. Since the subject was asked to perform a mental task only on a decision point, while the robot navigated autonomously, the subject was able to relax and prepare for the next task.
- The subject was always in control of navigation by deciding to accept or reject the assistance, and not the robot as shown in other methods (Perrin et al. 2010; Lopes et al. 2011). The navigation assistance used in our method was not restrictive because the subject was able to reject it and directly control the robot.

In our method, we employed computer vision coupled with assistive information to provide autonomous navigation capabilities to the robotic wheelchair. The advantages of this method are the following:

- The tactile paving assistive information already exists in many hospitals and most of the public buildings.
- They are built with safety as a priority, and designated for disable people. This somehow, helps avoiding congestions (non-disable people try to avoid blocking the path) and may reduce the number of potential collisions.
- Computer vision can be adapted to different sceneries and different kind of assistive information. For instance, some hospitals in Japan have already implemented similar color coded lines to guide existing robotic equipment. Our computer vision algorithm can be easily tuned to autonomously navigate using the existing guide lines instead of tactile paving or both.
- The combination of computer vision with tactile paving offers a global solution that provides good and reliable navigation capabilities without requiring prior robot training. This makes the robot navigation environment independent.

# Appendices

## A Brain Activity Measurement Techniques

Most brain activity measurement techniques (Table A-1) are based in two main principles.

The **first** principle (and the most popular in BMI field) is based on the measurement of the electromagnetic activity generated by the action potentials of targeted neural populations. This includes non-invasive measurement made by electrodes placed on the scalp (EEG and MEG) and invasive measurements made by electrodes inside the skull (ECoG) or even implanted in cortex (Local Field Potentials (LFP) and Single/Multi-Unit Action Potentials (SUA/MUA)).

The **second** principle is based on the measurement of metabolic processes of the brain (fMRI, PET and NIRS). The idea behind this principle is that brain activity in a specific area is always associated with metabolic activity, thus measuring metabolic activity enables the detection of areas with current brain activity.

**Table A-1 Brain Activity measuring methods and their main distinctive features**

Method	Type	Electrode Position	Measurement	Signal	Description
MEG	Non-invasive	Scalp	Electromagnetic	Magnetic Field	<i>Magnetic field generated by neural activity on scalp</i>
EEG	Non-invasive	Scalp	Electromagnetic	Electric Potential	<i>Electrical field generated by neural activity on scalp</i>
ECoG	Invasive	Cortex Surface	Electromagnetic	Electric Potential	<i>Electrical activity generated by neural activity on cortex surface</i>
LFP	Invasive	Inside Cortex	Electromagnetic	Electric Potential	<i>Electrical activity generated by neural activity inside cortex</i>
fMRI	Non-invasive	N/A	Metabolic	Blood oxygen level	<i>Blood oxygenation magnetic penetration properties</i>
NIRS	Non-invasive	N/A	Metabolic	Blood oxygen level	<i>Blood oxygenation light penetration properties</i>
PET/ CT-PET	Non-invasive	N/A	Metabolic	Positron Emitting Substance radioactivity level	<i>Gamma rays emitted by the positron emitting substance</i>

---

## **B Other Electrophysiological Signals Used in BMI**

Besides the signals shown in Section 2.3, in this appendix, we will introduce some additional electrophysiological signals captured by EEG and used for BMI applications. First, we will introduce the SCP as a part of spontaneous signals, and then the most common types of EPs.

### **B.1 Slow Cortical Potentials**

SCPs are gradual variations of the cortical activity, which can last from hundreds of milliseconds to several seconds. They have the lowest frequency range of all EEG electrophysiological signals suitable for BMI systems.

Positive deflections of SCP are associated with reduced cortical activity ([Rockstroh et al. 1984](#)), while a negative deflection usually indicates increased cortical activity as it appears during movements or other activity involving cortical structures. It is possible to learn to make these variations positive or negative using operant conditioning (Section 2.3.3). SCP can be used in a BCI to generate binary commands, according to the positivity or negativity of the potential ([Hinterberger, Schmidt, et al. 2004](#); [Birbaumer et al. 2000](#); [Kleber and Birbaumer 2005](#)).

### **B.2 Common Evoked Potentials Used in BMI Systems**

In this section, we are going to give some details about the visually evoked potentials (VEP) especially the steady-state visually evoked potentials (SSVEP), which are the most common EP used in BMI applications. Furthermore, different components of the ERP, with the main focus on P300 component, are introduced.

#### **B.2.1 Visual Evoked Potentials**

VEP are generated from the brain activity in response to external visual stimuli and can be measured above the visual cortex area. Several types of visual stimuli can elicit VEPs; the most common are flash (luminance) and pattern stimulation (see ([Odom et al. 2004](#))). The average amplitude of the measured signals on scalp is up to 10 microvolts. There are different types of VEP including, sweep, binocular, chromatic, hemi-field,

flash, LED, motion, multifocal, multi-channel, multi-frequency, stereo-elicited and SSVEP.

The SSVEP are brain originated electrical signals that occur in response to a visual stimulation, with frequency in the range [3.5, 75] Hz. The frequency range of the SSVEP is the same (or multiple) as the stimuli frequency (Ding, Sperling, and Srinivasan 2006). They appear to have almost constant (steady) amplitude and phase discrete frequency components during the stimuli application period. SSVEP is the most used VEP in BMI applications (Vialatte et al. 2010).

### B.2.2 Event Related Potentials

An ERP is the voltage change measured on the scalp due to an electrophysiological activity in response to a specific sensory, cognitive, or motor event. The ERP components are labeled according to their potential polarity (P or N) and approximate occurrence latency (in *ms*). For example, a component peak occurring at 300*ms* with positive potential is labeled P300 whereas a component peak at 200*ms* latency with a negative potential is labeled N200 (Figure A-1). Another commonly used annotation refers to the occurring sequence, where N1 is the first occurring negative potential and P3 is the third occurring positive potential (Figure A-2). The labels N1 and N100, P1 and P100, etc., refer to the same component.

There exist a variety of ERP components. Furthermore, the components can be divided into subcomponents according to their usage in neurophysiology (Patel and Azzam 2005; Rugg and Coles 1996; Folstein and Van Petten 2008), but this is beyond the scope of this thesis.

Common ERP components include *N100*, *N200*, *P300* and *N400*. Table A-2 summarizes the distinguishing features of these components. The most popular ERP component used in BMI is the P300. P300 response is correlated to the brain reaction to an unpredictable stimuli, this experiment is also known as the *oddball paradigm* (Squires, Squires, and Hillyard 1975). In this paradigm, frequent *background* stimuli (or no stimuli at all) are shown in rapid succession and at a random position, in that sequence, a less frequent *target stimulus* is interspersed. Due to this target stimulus, a 'strong' positive peak at around 300*ms* can be observed in the EEG signals.

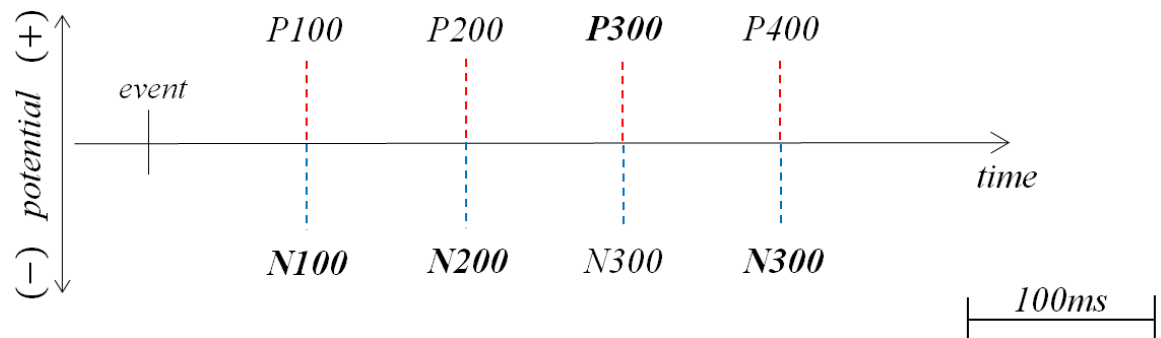


Figure A-1 ERP component’s approximate positions relative to the event or stimulus

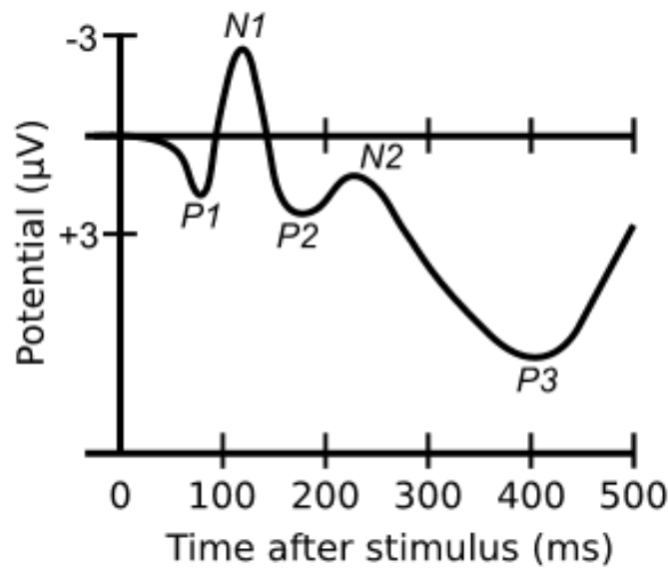


Figure A-2 An EEG waveform showing typical ERP components (adopted from [Wikipedia](#))

Table A-2 ERP component properties

ERP Component	Latency (ms)		Recording Place (over scalp)	Generated in Response to
	Window	Peak		
<b>N100</b>	80-120	100	Frontal Central lobes	<i>unpredictable auditory, visual, olfactory or somatosensory stimuli</i>
<b>N200</b>	200-350	230	Anterior lobes	<i>odd stimulus in a sequence of similar stimuli</i>
<b>P300</b>	250-500	300	Parietal lobe	<i>unpredictable stimuli</i>
<b>N400</b>	250-500	400	Central Parietal lobes	<i>meaningful audio or visual stimuli (words, sign language, pictures, faces, environmental sounds, and smells)</i>

---

## C BMI Classifiers

Apart the linearity/nonlinearity and regularization explained in Section 4.4, here we will introduce some other characteristics that are used to define the classifier's functionality and usage (Lotte et al. 2007).

**Dynamic** classifiers are able to determine the class of a feature sequence which allows them to catch temporal dynamics. **Static** classifiers are able to classify only a single feature vector and not a sequence.

**Informative** classifiers compute the likelihood of each class of the feature vector, and then choose the most likely class. **Discriminative** classifiers learn the way of discriminating the classes or the class membership in order to classify a feature vector directly.

**Stable** classifiers are not complex and have stable performance toward small variations in the training set. **Unstable** classifiers have a high complexity and even small variations in the training set may lead to significant performance changes.

In the next section, we will show some of the most commonly used classifiers in BMI applications.

### C.1 Classifiers Used in BMI

Besides the LDA and RLDA (Section 4.4), other popular types of linear classifiers used to classify feature vectors in BMI applications are the linear support vector machine (LIN-SVM) and the radial basis function kernel support vector machine (RBF-SVM) (Furdea et al. 2012).

After linear classifiers, **Artificial Neural Networks** (ANN) is the category of classifiers mostly used in BMI. The Multi-Layer Perceptron (MLP) (Haykin Simon 1999) is the most widely used ANN architecture in BMI, and has been applied to a wide range of BMI applications (Hiraiwa, Shimohara, and Tokunaga 1990; C. W. Anderson and Sijercic 1996; Haselsteiner and Pfurtscheller 2000; Silvia Chiappa et al. 2004; Palaniappan 2005; Rodrak and Wongsawat 2012; Elghrabawy and Wahed 2012; Nawroj et al. 2012). MLP performance is very sensitive to noisy and non-stationary EEG signals, therefore their architecture must be carefully chosen. Besides MLP, different types of ANN architectures are used in the field of BMI. These architectures include the Radial

Basis Function Neural Network (RBFNN) (Mano et al. 2013; Khare et al. 2011; Bassani and Nievola 2008), the local neural classifier (Local-NN) (Millan et al. 2000; Millan et al. 2004), Adaptive Probabilistic Neural Network (Hazrati and Erfanian 2008), Learning Vector Quantization (LVQ) Neural Network (Kohonen 1990; Trung et al. 2012; Mizuno et al. 2010), Fuzzy Adaptive Resonance Theory Neural Networks (ARTMAP) (Cano-Izquierdo, Ibarrola, and Almonacid 2012; Palaniappan et al. 2002; Lledo et al. 2012), the Bayesian Logistic Regression Neural Network (BLRNN) (Penny et al. 2000), the Probability estimating Guarded Neural Classifier (PeGNC) (Felzer and Freisleben 2003) and other dynamic Neural Networks such as the Finite Impulse Response Neural Network (FIRNN) (Haselsteiner and Pfurtscheller 2000), or Time-Delay Neural Network (TDNN) (Cecotti and Gräser 2008; H. Zhang et al. 2012)

Other nonlinear classifiers used in BMI include Bayes quadratic (Lemm, Schäfer, and Curio 2004; Solhjoo and Moradi 2004; Keirn and Aunon 1990; Barreto, Frota, and de Medeiros 2004), Hidden Markov Model (HMM) (Helmy et al. 2008; Zimmermann et al. 2013; Obermaier et al. 2001; Cincotti et al. 2003; McCormick, Ma, and Coleman 2010; Nazarpour, Stastny, and Miall 2009) the Input-Output HMM (IOHMM) (Silvia Chiappa et al. 2004) and Bayesian Network (BN) (Ko, Yang, and Sim 2009; Tavakolian and Rezaei 2004).

The last type of nonlinear classifiers introduced here, are the nearest neighbor classifiers. The classifiers from this type that are used in BMI include, k-Nearest Neighbors (k-NN) (Bhattacharyya et al. 2011; Loo, Samraj, and Lee 2011; Blankertz, Curio, and Müller 2002; Bhattacharyya et al. 2010) and Mahalanobis Distance (MD) (Babiloni et al. 2001; Cincotti et al. 2003).

The main properties of the classifiers introduced in this section are summarized in Classification accuracies (mean, standard deviation and train loss) of the online feedback experiments. There are also other classifiers less frequently used in BMI, like the Adaptive Logic Network (ALN) (Kostov and Polak 2000), that are not shown here.

## C.2 Classifier Combination

To improve BMI classification accuracy sometimes classifier combination strategies are used. Combining classifiers is known to reduce the classification error. The advantage lies in the assumption that a combination of similar classifiers is very likely to outperform any of the classifiers on its own.

**Table A-3 Properties of classifiers used in BMI research (adopted from (Lotte et al. 2007))**

	Linear	Non Linear	Generative	Discriminant	Dynamic	Static	Regularized	Stable	Unstable	High dimension robust
LDA	○			○		○		○		
RFLDA	○			○		○	○	○		
linear-SVM	○			○		○	○	○		○
RBF-SVM		○		○		○	○	○		○
MLP		○		○		○			○	
BLR NN		○		○		○			○	
TDNN		○		○	○				○	
FIRNN		○		○	○				○	
Local NN		○	○			○			○	
LVQ NN		○		○		○			○	
Perceptron	○			○		○		○		
RBF-NN		○	○			○			○	
PeGNC		○		○		○	○		○	
fuzzy ARTMAP NN		○		○			○		○	
HMM		○	○		○				○	
IOHMM		○		○	○				○	
Bayes quadratic		○	○			○			○	
Bayes graphical network		○	○			○			○	
k-NN		○		○		○			○	
Mahalanobis distance		○	○			○			○	

The most common classifier combination strategies are *voting*, *boosting*, *stacking* and *random subspaces* (Lotte et al. 2007).

In **voting**, several classifiers are being used to find the class of the feature vector and the final class is determined by the majority (Section 4.4.2). Voting is a very popular way of combining classifiers in BMI research, probably because it is simple and efficient.

In **boosting**, several different classifiers are used in cascade where each classifier is focused only on the errors committed by the previous ones. It can build up a powerful classifier out of several weak ones, and it is unlikely to over train.

In **stacking**, several classifiers are used in different levels. The output of the feature vector classifier(s) (level-0) is the input of the next classifier(s) (level-1 or meta-classifier). The output of the meta-classifier is the final classification result.

The **random subspace** technique consists in generating new training set based on random subsets of the original training set, and train a different classifier for each one of these new training sets.

The combinations of the classifiers can be linear/nonlinear, regularized, etc. The results of the combined classifications are generally good, but sometimes associated with high computational load and not very effective for online applications. Regularized classifiers or classifiers able to accommodate outliers in the training data tend to give the best results in terms of correct classification rates (Lotte et al. 2007).

## D Offline BMI Method Evaluation

In this appendix, are shown the results of  $f^{1,-1}$  LTI filtering on two BMI paradigms during training and offline classification, with datasets acquired offline from 36 subjects. The first paradigm uses CSP and the second uses Spec-CSP for EEG signal filtering.

### D.1 Datasets

In order to assess the performance of the BMI paradigm used for single-trial classification, EEG datasets recorded in our lab from 17 subjects together with publicly available EEG datasets from 19 subjects, were used. All datasets used for evaluation of the classification of single EEG trials method are explained in following of this section.

#### D.1.1 BCI Competition iii & iv Datasets

These datasets are available to download from BCI competitions [website](#). Datasets contain EEG signals recorded while subjects imagine limb movements (e.g., hand or foot movements). All subjects' datasets are dividend in two subsets i.e. training and testing subset (Pfurtscheller and Neuper 2001).

From [BCI competition iii](#) (Blankertz, Müller, Krusienski, Schalk, et al. 2006), two datasets were selected: **a)** Dataset IVa (Dornhege et al. 2004b) contains 5 sets of continuous 118 channel EEG signals from 5 subjects, performing right hand and foot MI tasks. Each original set had 280 trials available for each subject, among which 168, 224, 84, 56 and 28 form the training subset for subject *aa*, *al*, *av*, *aw* and *ay* respectively (here A1–A5), and the remaining trials form their test subsets. **b)** Dataset IIIa (Schlögl et al. 2005) contains 3 sets (B1–B3) of continuous 60 channel EEG signals from 3 subjects, performing left hand, right hand, foot and tongue MI tasks. Each training/testing subset contains 45 trials per class for subject B1, and 30 trials per class for subjects B2 and B3.

From [BCI competition IV](#), Dataset IIa (Naeem et al. 2006) is selected. This dataset contains continuous 22 channel EEG signals from 9 subjects (C1–C9) who performed left hand, right hand, foot and tongue MI tasks. Each training/testing subset contains 72 trials for each class.

### D.1.2 BCILAB Datasets

These datasets can be downloaded together with BCILAB [toolbox](#), which is an open source Matlab Toolbox for BMI research ([Delorme et al. 2011](#)).

The first dataset (BA1) contains a sequence of trials in which a subject was instructed to imagine moving either the left hand or the right hand. Markers in the data set indicate the timing and type of these instructions ([Grandchamp and Delorme 2009](#)).

The second dataset (BA2) contains a sequence of trials in which a subject was instructed to imagine moving the left hand, the right hand, or a foot ([Wang et al. 2007](#)).

Both datasets have four sessions; the first two sessions were used for training and the remaining two for testing.

### D.1.3 Intelligent Robotics Laboratory Datasets

All the subjects involved in this study were volunteer undergraduate and graduate students, all males and from 20 to 35 years old. Two of them were experienced with BMI recordings and the others had little or no experience during the time of the experiments.

The major part of the datasets recorded in our laboratory was processed offline using a method very similar to the one described in Section 4.2. Only two datasets had online feedback. The EEG signals were recorded on scalp using 9 and then later 15 channels at signal sampling rate of 0.5 kHz or 1 kHz and then resampled at 100 Hz.

The datasets OF1–OF8 contain recordings with 9 EEG channels. The data was acquired using nine separated [GRASS](#) (FEB10) gold contact electrodes, individually pasted on subject's scalp by using conductive paste (Figure A-3). Then, electrodes were connected to the electrode box and NEC Synafit 5800 EEG device. Next, by using G.tec's g.16sys, the signal was amplified and sent to the PC. A NIDAQCard-6036E was used to convert the data from analog to digital and finally the data was collected in MATLAB. Each set contains EEG signals recorded while subjects were performing MI tasks (i.e. right and left hand MI). Each set has an equal training and testing subset composition of 50 trials per each task.

The datasets OFC1–OFC7 contain recordings with 15 EEG channels. The data was acquired using 15 electrodes mounted in an electrode cap (Figure 4-1 (a)) and posi-

tioned as shown in Figure 4-1 (b). Apart from the number of electrodes, the rest of the data acquisition method is similar to above. With the exception of OFC4 and OFC5 which have respectively 60 trials and 30 trials per task, all other datasets have 50 trials per each task. Each set has an equal training and testing subset composition.

The datasets OLC1–OLC2 are acquired in the same manner with the OFC1–7 datasets. The offline calibration sets have the same structure with the OFC7 set. They have two MI tasks (left hand and right hand) with 50 trials each. In contrast with OFC7 set, their testing sets were acquired while the subjects had visual feedback of their mental activity. During the online feedback 80 and 90 trials respectively were taken. The training procedure is the same as the one used above in the datasets without feedback. After the training session was over, the BMI model acquired from it was used for single trial classification. After every trial the subject was shown on screen the result of its mental state prediction.

## D.2 Results of LTI Filtering

In this subsection, we will show the results of using the  $f^{1,-1}$  on EEG signals and the spatial filters (patterns) obtained by using Spec–CSP on the filtered EEG channels. Figure A-4 shows the effect of the  $f^{1,-1}$  filtering on single EEG channels (epochs for each class are extracted first). In both right hand and left hand trials, the activity power spectrum changes and in all channels the activity in the band [8, 30] Hz is emphasized when  $f^{1,-1}$  filtering is applied.

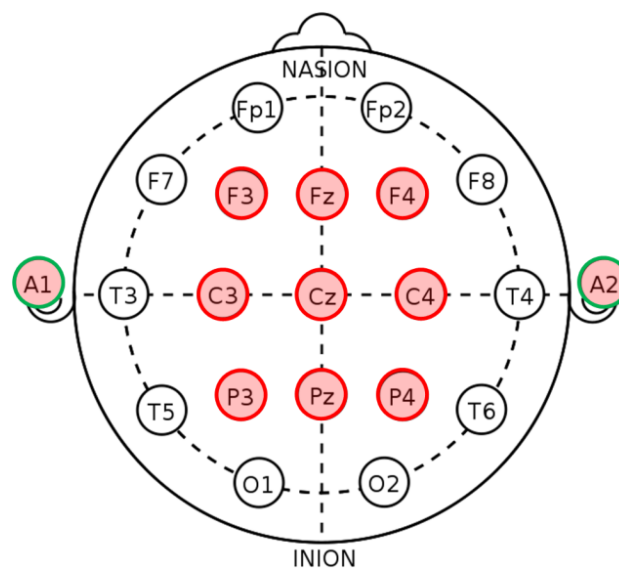


Figure A-3 Electrode placement labels/positions

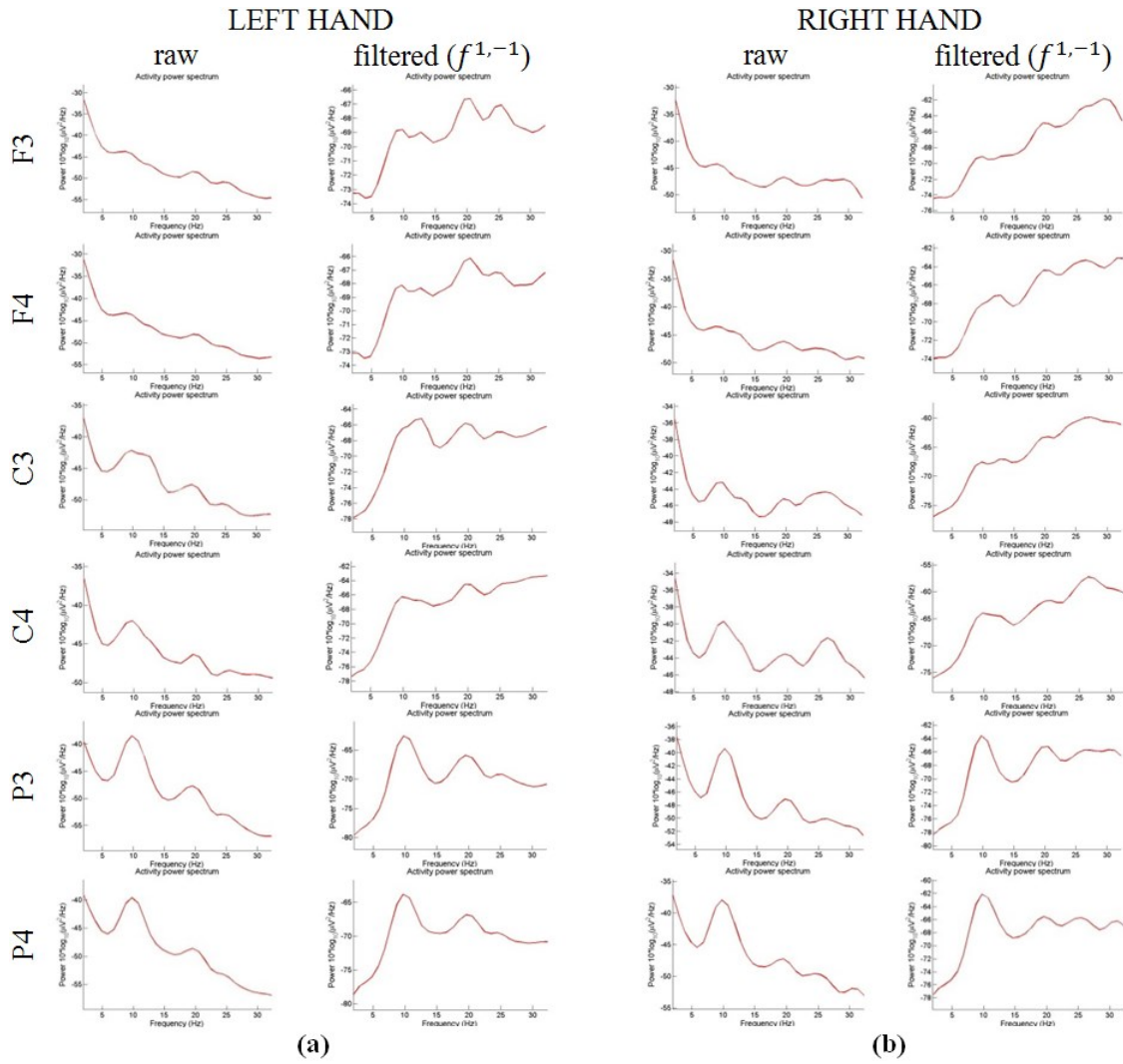


Figure A-4 Single channel mean activity log power spectrum of subset OFC4: a) left hand MI trials, and b) right hand MI trials

### D.3 Classification Results

The BMI classification results of the 19 public datasets (A1–A5, B1–B3, C1–C9, and BA1–BA2) from the BCI competitions III, IV and BCILAB, are summarized on Table A-4. The mean classification results show improvement in both CSP and Spec-CSP based methods, when applying the  $f^{1,-1}$  filter. The highest classification rate is obtained when applying Spec-CSP method to optimize the spatial filters of the  $f^{1,-1}$  filtered EEG signals. Sets A2 & B1 achieve 100% recognition when  $f^{1,-1}$  is applied. In our evaluation, only left and right hand MI tasks were taken into consideration.

The sets that benefit the most from  $f^{1,-1}$  and Spec-CSP filtering are C4, C7, A3, A5 and BA2 where the classification rates increases from 6% to 11%. These sets show an

increased classification rate on the CSP filtering method (with  $f^{1,-\bar{1}}$ ) as well. Sets C5, C9, A1, A2, B1, B3 and BA1 have a classification increase from 0 to 2% when using  $f^{1,-\bar{1}}$  with Spec-CSP but they have fluctuations on classification rate when using CSP.

In some sets, the CSP with  $f^{1,-\bar{1}}$  performance increases (C5 has 11.2% increase) and in some other sets decreases. Sets C1, C2, C3, C6, C8 and B2 have a decrease in performance from 0.6% to 2.1% in the Spec-CSP method when is applied, but they have fluctuating results on the CSP method. The highest decrease in classification obtained from applying  $f^{1,-\bar{1}}$ , is in the case of set A4. The classification performance decreased 9.6% with Spec-CSP and 21.7% with CSP filtering.

Overall the mean performance of the 19 selected sets is increased by 1.7% and 1.1% on Spec-CSP and CSP respectively when  $f^{1,-\bar{1}}$  is applied. The standard deviation is also decreased with 1.1% and 1.2% for CSP and Spec-CSP respectively.

**Table A-4 Classification accuracies (mean and standard deviation) obtained for each dataset for the standard CSP and Spec-CSP, with and without  $f^{1,-\bar{1}}$  filtering**

METHOD		CSP		Spec-CSP		
$f^{1,-\bar{1}}$ filtering		<i>no</i>	<i>yes</i>	<i>no</i>	<i>yes</i>	
BCI competition IV	(IIA)	<i>C1</i>	87.5%	<b>90.3%</b> <sup>1</sup>	<b>93.1%</b>	91.7%
		<i>C2</i>	53.5%	<b>54.2%</b>	<b>56.9%</b>	56.3%
		<i>C3</i>	<b>94.4%</b>	93.1%	<b>96.5%</b>	95.1%
		<i>C4</i>	59.7%	<b>72.2%</b>	59.7%	<b>66.7%</b>
		<i>C5</i>	56.9%	<b>68.1%</b>	<b>67.4%</b>	<b>67.4%</b>
		<i>C6</i>	<b>68.8%</b>	68.1%	<b>66.7%</b>	64.6%
		<i>C7</i>	81.3%	<b>86.1%</b>	75.7%	<b>85.4%</b>
		<i>C8</i>	95.1%	<b>96.5%</b>	<b>96.5%</b>	94.4%
		<i>C9</i>	91.0%	<b>91.7%</b>	89.6%	<b>91.0%</b>
BCI competition III	(IVA)	<i>A1</i>	<b>70.5%</b>	69.6%	71.4%	<b>73.2%</b>
		<i>A2</i>	98.2%	<b>100.0%</b>	98.2%	<b>100.0%</b>
		<i>A3</i>	64.3%	<b>72.5%</b>	63.3%	<b>74.5%</b>
		<i>A4</i>	<b>87.5%</b>	63.8%	<b>92.4%</b>	84.8%
		<i>A5</i>	49.2%	<b>52.0%</b>	50.0%	<b>58.3%</b>
	(IIIA)	<i>B1</i>	<b>97.8%</b>	<b>97.8%</b>	98.9%	<b>100.0%</b>
		<i>B2</i>	<b>66.7%</b>	65.0%	<b>51.7%</b>	50.0%
		<i>B3</i>	<b>96.7%</b>	95.0%	<b>96.7%</b>	<b>96.7%</b>
BCILAB DATASETS	<i>BA1</i>	<b>89.1%</b>	88.3%	<b>93.0%</b>	<b>93.0%</b>	
	<i>BA2</i>	87.6%	<b>92.8%</b>	89.7%	<b>95.9%</b>	
<b>TOTAL</b>	<i>mean</i>	78.7%	<b>79.8%</b>	79.3%	<b>81.0%</b>	
	<i>std</i>	16.6%	15.5%	17.5%	16.3%	

<sup>1</sup>For each set, the highest classification result is in bold text.

The classification results of the datasets taken in our lab are shown in Table A-5 (the datasets with only 9 EEG channels (without cap): OF1–OF8; the datasets with 15 EEG channels (with cap): OFC1–OFC7).

The results of  $f^{1,-\bar{1}}$  with Spec–CSP filtering on sets OF2, OF3, OF6, OFC1, OFC2 and OFC6 show a classification performance increase from 5% to 12%. The performance of these sets is increased in the case of CSP as well (except OF6). Sets OF4, OF8, OFC3, OFC4, and OFC5 show an increase up to 3% in classification accuracy when  $f^{1,-\bar{1}}$  filtering is applied with Spec–CSP, but they have mixed results with CSP.

Sets OF1 and OF7 show only 1% decrease with Spec–CSP but they show an increase with CSP. Only set OFC7 has a decrease higher than 1% (i.e. 4%) in classification performance when  $f^{1,-\bar{1}}$  is used with Spec–CSP.

In total, the mean classification performance of the all sets was increased by 3.8% and 3.2% on Spec–CSP and CSP respectively after  $f^{1,-\bar{1}}$  is applied. The standard deviation decreased by 2.1% and 1.3% for Spec–CSP and CSP respectively.

**Table A-5 Classification accuracies (mean and standard deviation) obtained for each dataset collected in the intelligent robotics lab, for the standard CSP and Spec–CSP, with and without  $f^{1,-\bar{1}}$  filtering**

METHOD		CSP		Spec–CSP	
$f^{1,-\bar{1}}$ filtering		<i>no</i>	<i>yes</i>	<i>no</i>	<i>yes</i>
9 Channel Datasets	OF1	83.0%	<b>84.0%</b> <sup>1</sup>	<b>90.0%</b>	89.0%
	OF2	77.0%	<b>83.0%</b>	68.0%	<b>80.0%</b>
	OF3	58.0%	<b>64.0%</b>	59.0%	<b>65.0%</b>
	OF4	66.0%	<b>57.0%</b>	81.0%	<b>83.0%</b>
	OF5	64.0%	<b>71.0%</b>	69.0%	<b>76.0%</b>
	OF6	<b>58.0%</b>	52.0%	54.0%	<b>59.0%</b>
	OF7	68.0%	<b>79.0%</b>	<b>78.0%</b>	77.0%
	OF8	63.0%	<b>75.0%</b>	68.0%	<b>71.0%</b>
15 Channel Datasets	OFC1	61.0%	<b>67.0%</b>	68.0%	<b>76.0%</b>
	OFC2	52.0%	<b>68.0%</b>	66.0%	<b>72.0%</b>
	OFC3	<b>86.0%</b>	82.0%	87.0%	<b>89.0%</b>
	OFC4	<b>87.5%</b>	80.0%	88.3%	<b>90.0%</b>
	OFC5	91.7%	<b>93.3%</b>	<b>96.7%</b>	<b>96.7%</b>
	OFC6	68.0%	<b>75.0%</b>	67.0%	<b>77.0%</b>
	OFC7	<b>73.0%</b>	<b>73.0%</b>	<b>75.0%</b>	71.0%
<b>TOTAL</b>	<i>mean</i>	70.4%	<b>73.6%</b>	74.3%	<b>78.1%</b>
	<i>std</i>	12.1%	10.8%	12.2%	10.1%

<sup>1</sup>For each set, the highest classification result is in bold text.

The results in Table A-4 and Table A-5 show that the mean classification performance of the Spec-CSP method after  $f^{1,-\bar{1}}$  is higher than the Spec-CSP without  $f^{1,-\bar{1}}$  and both variants of CSP. Therefore the former method was chosen for online feedback experiments and for BMI robot control simulation experiments.

The results of classification accuracy of the experiments with online feedback are summarized in Table A-6. The classification rate is slightly higher compared to the offline datasets. This may be due to the engagement of the subject to improve its mental task dynamic based on the online feedback.

**Table A-6 Classification accuracies (mean, standard deviation and train loss) of the online feedback experiments**

ONLINE FEEDBACK DATASETS	Spec-CSP (with $f^{1,-1}$ )
	<i>classification (train loss)</i>
<i>OF1</i>	86.3% (14.0%)
<i>OF2</i>	80.0% (17.0%)
<b><i>TOTAL</i></b>	<b>83.1% (14.0%)</b>
<i>STD</i>	4.4% (N/A)

## Bibliography

- Allison, Brendan Z., Bernhard Graimann, and Axel Gräser. 2007. "Why Use A BCI If You Are Healthy?" *Brain*: 7–11.
- Allison, Brendan Z., Elizabeth W. Wolpaw, and Jonathan R. Wolpaw. 2007. "Brain-computer Interface Systems: Progress and Prospects." *Expert Review of Medical Devices* 4 (4) (July): 463–74. doi:10.1586/17434440.4.4.463.
- Anderson, Charles W., and Zlatko Sijercic. 1996. "Classification of EEG Signals from Four Subjects During Five Mental Tasks." In *Proceedings of the Conference on Engineering Applications in Neural Networks*, 407–414. Turkey.
- Anderson, Kim D. 2004. "Targeting Recovery: Priorities of the Spinal Cord-injured Population." *Journal of Neurotrauma* 21 (10) (October): 1371–83.
- Babiloni, Fabio, Luigi Bianchi, Francesco Semeraro, Jose del R. Millan, Josep Mourino, Angela Cattini, Serenella Salinari, Maria Grazia Marciani, and Febo Cincotti. 2001. "Mahalanobis Distance-based Classifiers Are Able to Recognize EEG Patterns by Using Few EEG Electrodes." In *2001 Conference Proceedings of the 23rd Annual International Conference of the IEEE Engineering in Medicine and Biology Society*, 1:651–654. IEEE. doi:10.1109/IEMBS.2001.1019019.
- Babiloni, Fabio, Febo Cincotti, Maria Grazia Marciani, Serenella Salinari, Laura Astolfi, Andrea Tocci, Fabio Aloise, Fabrizio De Vico Fallani, Simona Bufalari, and Donatella Mattia. 2007. "The Estimation of Cortical Activity for Brain-computer Interface: Applications in a Domotic Context." *Computational Intelligence and Neuroscience* 2007 (January): 91651. doi:10.1155/2007/91651.
- Baillet, Sylvain, John C. Mosher, and Richard M. Leahy. 2001. "Electromagnetic Brain Mapping." *IEEE Signal Processing Magazine* 18 (6): 14–30. doi:10.1109/79.962275.
- Barreto, Guilherme A., Reubenio A. Frota, and Fatima. N. S. de Medeiros. 2004. "On the Classification of Mental Tasks: a Performance Comparison of Neural and Statistical Approaches." In *Proceedings of the 2004 14th IEEE Signal Processing Society Workshop Machine Learning for Signal Processing, 2004.*, 529–538. IEEE. doi:10.1109/MLSP.2004.1423016.

- Bashashati, Ali. 2007. "Towards Development of a 3-state Self-paced Brain-computer Interface." *Computational Intelligence and Neuroscience*. University of British Columbia. doi:10.1155/2007/84386.
- Bashashati, Ali, Mehrdad Fatourech, Rabab K. Ward, and Gary E. Birch. 2007. "A Survey of Signal Processing Algorithms in Brain-computer Interfaces Based on Electrical Brain Signals." *Journal of Neural Engineering* 4 (2) (June): R32–57. doi:10.1088/1741-2560/4/2/R03.
- Bassani, Thiago, and Julio Cesar Nievola. 2008. "Pattern Recognition for Brain-computer Interface on Disabled Subjects Using a Wavelet Transformation." In *2008 IEEE Symposium on Computational Intelligence in Bioinformatics and Computational Biology*, 180–186. IEEE. doi:10.1109/CIBCB.2008.4675776.
- Bayliss, Jessica D., and Dana H. Ballard. 2000. "A Virtual Reality Testbed for Brain-computer Interface Research." *IEEE Transactions on Rehabilitation Engineering* 8 (2) (June): 188–190. doi:10.1109/86.847811.
- Belouchrani, Adel, Karim Abed-Meraim, Jean-Francois Cardoso, and Eric Moulines. 1997. "A Blind Source Separation Technique Using Second-order Statistics." *IEEE Transactions on Signal Processing* 45 (2): 434–444. doi:10.1109/78.554307.
- Bensch, Michael, Ahmed A. Karim, Jürgen Mellinger, Thilo Hinterberger, Michael Tangermann, Martin Bogdan, Wolfgang Rosenstiel, and Niels Birbaumer. 2007. "Nessi: An EEG-controlled Web Browser for Severely Paralyzed Patients." *Computational Intelligence and Neuroscience* (January): 71863. doi:10.1155/2007/71863.
- Berger, Hans. 1929. "Über Das Elektrenkephalogramm Des Menschen." *Archiv Für Psychiatrie Und Nervenkrankheiten* 87 (1) (December): 527–570. doi:10.1007/BF01797193.
- Bernhard Graimann, Gert Pfurtscheller, and Brendan Z. Allison. 2010. *Brain-Computer Interfaces*. Berlin, Heidelberg: Springer Berlin Heidelberg. doi:10.1007/978-3-642-02091-9.
- Besserve, Michel, Line Garnero, and Jacques Martinerie. 2007. "Cross-Spectral Discriminant Analysis (CSDA) for the Classification of Brain Computer Interfaces." In *2007 3rd International IEEE/EMBS Conference on Neural Engineering*, 1:375–378. IEEE. doi:10.1109/CNE.2007.369688.
- Besserve, Michel, Karim Jerbi, Francois Laurent, Sylvain Baillet, Jacques Martinerie, and Line Garnero. 2007. "Classification Methods for Ongoing EEG and MEG Signals." *Biological Research* 40 (4) (January): 415–37. doi:/S0716-97602007000500005.
- Bhattacharyya, Saugat, Anwasha Khasnobish, Somsirsa Chatterjee, Amit Konar, and D.N. Tibarewala. 2010. "Performance Analysis of LDA, QDA and KNN Algorithms in Left-right Limb Movement Classification from EEG Data." In *2010 International Conference on Systems in Medicine and Biology*, 126–131. IEEE. doi:10.1109/ICSMB.2010.5735358.

- Bhattacharyya, Saugat, Anwesha Khasnobish, Amit Konar, D. N. Tibarewala, and Atulya K. Nagar. 2011. "Performance Analysis of Left/right Hand Movement Classification from EEG Signal by Intelligent Algorithms." In *2011 IEEE Symposium on Computational Intelligence, Cognitive Algorithms, Mind, and Brain (CCMB)*, 1–8. IEEE. doi:10.1109/CCMB.2011.5952111.
- Bianchi, Luigi, Saber Sami, Arjan Hillebrand, Ian P. Fawcett, Lucia Rita Quitadamo, and Stefano Seri. 2010. "Which Physiological Components Are More Suitable for Visual ERP Based Brain-computer Interface? A Preliminary MEG/EEG Study." *Brain Topography* 23 (2) (June): 180–5. doi:10.1007/s10548-010-0143-0.
- Birbaumer, Niels. 2006. "Breaking the Silence: Brain-computer Interfaces (BCI) for Communication and Motor Control." *Psychophysiology* 43 (6) (November): 517–32. doi:10.1111/j.1469-8986.2006.00456.x.
- Birbaumer, Niels, Andrea Kubler, Nimr Ghanayim, Thilo Hinterberger, Jouri Perelmouter, Jochen Kaiser, Iver Iversen, Boris Kotchoubey, Nicola Neumann, and Herta Flor. 2000. "The Thought Translation Device (TTD) for Completely Paralyzed Patients." *IEEE Transactions on Rehabilitation Engineering* 8 (2) (June): 190–193. doi:10.1109/86.847812.
- Birbaumer, Niels, Ander Ramos Murguialday, and Leonardo Cohen. 2008. "Brain-computer Interface in Paralysis." *Current Opinion in Neurology* 21 (6) (December): 634–8. doi:10.1097/WCO.0b013e328315ee2d.
- Blankertz, Benjamin, Gabriel Curio, and Klaus-Robert Müller. 2002. "Classifying Single Trial EEG: Towards Brain Computer Interfacing." Edited by T G Dietterich, S Becker, and Z Ghahramani. *Advances in Neural Information Processing Systems* 1 (c): 157–164.
- Blankertz, Benjamin, Guido Dornhege, Matthias Krauledat, Klaus-Robert Müller, and Gabriel Curio. 2007. "The Non-invasive Berlin Brain-Computer Interface: Fast Acquisition of Effective Performance in Untrained Subjects." *NeuroImage* 37 (2) (August 15): 539–50. doi:10.1016/j.neuroimage.2007.01.051.
- Blankertz, Benjamin, Guido Dornhege, Matthias Krauledat, Klaus-Robert Müller, Volker Kunzmann, Florian Losch, and Gabriel Curio. 2006. "The Berlin Brain-Computer Interface: EEG-based Communication Without Subject Training." *IEEE Transactions on Neural Systems and Rehabilitation Engineering: a Publication of the IEEE Engineering in Medicine and Biology Society* 14 (2) (June): 147–52. doi:10.1109/TNSRE.2006.875557.
- Blankertz, Benjamin, Guido Dornhege, Matthias Krauledat, Michael Schroder, John Williamson, Roderick Murray-Smith, and Klaus-Robert Müller. 2006. "The Berlin Brain-Computer Interface Presents the Novel Mental Typewriter Hex-o-Spell." In *Proceedings of the 3rd International Brain-Computer Interface Workshop and Training Course*, 1–2.
- Blankertz, Benjamin, Motoaki Kawanabe, Ryota Tomioka, Friederike Hohlefeld, Vadim Nikulin, and Klaus-Robert Müller. 2008. "Invariant Common Spatial Patterns:

Alleviating Nonstationarities in Brain-computer Interfacing.” *Advances in Neural Information Processing Systems* 20: 1–8.

Blankertz, Benjamin, Steven Lemm, Matthias Treder, Stefan Haufe, and Klaus-Robert Müller. 2011. “Single-trial Analysis and Classification of ERP Components--a Tutorial.” *NeuroImage* 56 (2) (May 15): 814–25. doi:10.1016/j.neuroimage.2010.06.048.

Blankertz, Benjamin, Klaus-Robert Müller, Gabriel Curio, Theresa M. Vaughan, Gerwin Schalk, Jonathan R. Wolpaw, Alois Schlögl, et al. 2004. “The BCI Competition 2003: Progress and Perspectives in Detection and Discrimination of EEG Single Trials.” *IEEE Transactions on Bio-medical Engineering* 51 (6) (June): 1044–51. doi:10.1109/TBME.2004.826692.

Blankertz, Benjamin, Klaus-Robert Müller, Dean J. Krusienski, Gerwin Schalk, Jonathan R. Wolpaw, Alois Schlögl, Gert Pfurtscheller, Jose del R. Millan, Michael Schröder, and Niels Birbaumer. 2006. “The BCI Competition. III: Validating Alternative Approaches to Actual BCI Problems.” *IEEE Transactions on Neural Systems and Rehabilitation Engineering : a Publication of the IEEE Engineering in Medicine and Biology Society* 14 (2) (June): 153–9. doi:10.1109/TNSRE.2006.875642.

Blankertz, Benjamin, Michael Tangermann, Carmen Vidaurre, Siamac Fazli, Claudia Sannelli, Stefan Haufe, Cecilia Maeder, et al. 2010. “The Berlin Brain-Computer Interface: Non-Medical Uses of BCI Technology.” *Frontiers in Neuroscience* 4 (December) (January): 198. doi:10.3389/fnins.2010.00198.

Blankertz, Benjamin, Ryota Tomioka, Steven Lemm, Motoaki Kawanabe, and Klaus-robert Muller. 2008. “Optimizing Spatial Filters for Robust EEG Single-Trial Analysis.” *IEEE Signal Processing Magazine* 25 (1): 41–56. doi:10.1109/MSP.2008.4408441.

Bonnet, Laurent, Fabien Lotte, and Anatole Lecuyer. 2013. “Two Brains, One Game: Design and Evaluation of a Multiuser BCI Video Game Based on Motor Imagery.” *IEEE Transactions on Computational Intelligence and AI in Games* 5 (2) (June): 185–198. doi:10.1109/TCIAIG.2012.2237173.

Bourhis, G, and Y Agostini. 1998. “The VAHM Robotized Wheelchair: System Architecture and Human-machine Interaction.” *Journal of Intelligent and Robotic Systems* 22 (1): 39–50. doi:10.1023/A:1007934111358.

Brumberg, Jonathan S., Frank H. Guenther, and Philip R. Kennedy. 2013. “An Auditory Output Brain–Computer Interface for Speech Communication.” In *Brain-Computer Interface Research*, 7–15. Springer. doi:10.1007/978-3-642-36083-1\_2.

Brumberg, Jonathan S., Alfonso Nieto-Castanon, Philip R. Kennedy, and Frank H. Guenther. 2010. “Brain-Computer Interfaces for Speech Communication.” *Speech Communication* 52 (4) (April 1): 367–379. doi:10.1016/j.specom.2010.01.001.

Cabrera, Alvaro Fuentes, Dario Farina, and Kim Dremstrup. 2010. “Comparison of Feature Selection and Classification Methods for a Brain-computer Interface Driven

- by Non-motor Imagery.” *Medical & Biological Engineering & Computing* 48 (2) (February): 123–32. doi:10.1007/s11517-009-0569-2.
- Cano-Izquierdo, Jose-Manuel, Julio Ibarrola, and Miguel Almonacid. 2012. “Improving Motor Imagery Classification with a New BCI Design Using Neuro-fuzzy S-dFasArt.” *IEEE Transactions on Neural Systems and Rehabilitation Engineering : a Publication of the IEEE Engineering in Medicine and Biology Society* 20 (1) (January): 2–7. doi:10.1109/TNSRE.2011.2169991.
- Carlson, Tom E., and Jose del R. Millan. 2013. “Brain-Controlled Wheelchairs: A Robotic Architecture.” *IEEE Robotics & Automation Magazine* 20 (1) (March): 65–73. doi:10.1109/MRA.2012.2229936.
- Carlson, Tom E., Robert Leeb, Ricardo Chavarriaga, and Jose del R. Millan. 2012. “The Birth of the Brain-controlled Wheelchair.” In *2012 IEEE/RSJ International Conference on Intelligent Robots and Systems*, 5444–5445. IEEE. doi:10.1109/IROS.2012.6386299.
- Carlson, Tom E., Robert Leeb, Guillaume Monnard, Abdul Al-Khodairy, and Jose del R. Millan. 2012. “Driving a BCI Wheelchair: A Patient Case Study.” In *Proc. of TOBI Workshop III: Bringing BCIs to End-Users: Facing the Challenge*, 59–60.
- Cecotti, Hubert. 2011. “Spelling with Non-invasive Brain-Computer Interfaces--current and Future Trends.” *Journal of Physiology, Paris* 105 (1-3): 106–14. doi:10.1016/j.jphysparis.2011.08.003.
- Cecotti, Hubert, and A Gräser. 2008. “Time Delay Neural Network with Fourier Transform for Multiple Channel Detection of Steady-state Visual Evoked Potential for Brain-computer Interfaces.” In *16th European Signal Processing Conference (EUSIPCO 2008)*, 5p. Lausanne, Switzerland: EURASIP.
- Chai, Rifai, Sai Ho Ling, Gregory P. Hunter, and Hung T. Nguyen. 2012. “Toward Fewer EEG Channels and Better Feature Extractor of Non-motor Imagery Mental Tasks Classification for a Wheelchair Thought Controller.” *Conference Proceedings : 34th Annual International Conference of the IEEE Engineering in Medicine and Biology Society*. 2012 (January): 5266–9. doi:10.1109/EMBC.2012.6347182.
- Chapin, John K., Karen A. Moxon, Ronald S. Markowitz, and Miguel A. Nicolelis. 1999. “Real-time Control of a Robot Arm Using Simultaneously Recorded Neurons in the Motor Cortex.” *Nature Neuroscience* 2 (7) (July): 664–70. doi:10.1038/10223.
- Cho, S.-Y., A.P. Winod, and K.W.E Cheng. 2009. “Towards a Brain-Computer Interface Based Control for Next Generation Electric Wheelchairs.” In *Power Electronics Systems and Applications*, 1–5.
- Cincotti, F, A Scipione, A Timperi, D Mattia, M.G Marciani, J Millan, S Salinari, L Bianchi, and F Babiloni. 2003. “Comparison of Different Feature Classifiers for Brain Computer Interfaces.” In *First International IEEE EMBS Conference on Neural Engineering, 2003. Conference Proceedings.*, 645–647. IEEE. doi:10.1109/CNE.2003.1196911.

- Collinger, Jennifer L., Brian Wodlinger, John E. Downey, Wei Wang, Elizabeth C. Tyler-Kabara, Douglas J. Weber, Angus J. C. McMorland, Meel Velliste, Michael L. Boninger, and Andrew B. Schwartz. 2013. "High-performance Neuroprosthetic Control by an Individual with Tetraplegia." *Lancet* 381 (9866) (February 16): 557–64. doi:10.1016/S0140-6736(12)61816-9.
- Coyle, Damien, Jhonatan Garcia, Abdul R. Satti, and T. Martin McGinnity. 2011. "EEG-based Continuous Control of a Game Using a 3 Channel Motor Imagery BCI: BCI Game." In *2011 IEEE Symposium on Computational Intelligence, Cognitive Algorithms, Mind, and Brain (CCMB)*, 1–7. IEEE. doi:10.1109/CCMB.2011.5952128.
- Coyle, Shirley M., Tomás E. Ward, and Charles M. Markham. 2007. "Brain-computer Interface Using a Simplified Functional Near-infrared Spectroscopy System." *Journal of Neural Engineering* 4 (3) (September): 219–26. doi:10.1088/1741-2560/4/3/007.
- Curran, Eleanor A., and Maria J. Stokes. 2003. "Learning to Control Brain Activity: A Review of the Production and Control of EEG Components for Driving Brain-computer Interface (BCI) Systems." *Brain and Cognition* 51 (3) (April): 326–336. doi:10.1016/S0278-2626(03)00036-8.
- Daly, Janis J., and Jonathan R. Wolpaw. 2008. "Brain-computer Interfaces in Neurological Rehabilitation." *Lancet Neurology* 7 (11) (November): 1032–43. doi:10.1016/S1474-4422(08)70223-0.
- Delorme, Arnaud, and Scott Makeig. 2004. "EEGLAB: An Open Source Toolbox for Analysis of Single-trial EEG Dynamics Including Independent Component Analysis." *Journal of Neuroscience Methods* 134 (1) (March 15): 9–21. doi:10.1016/j.jneumeth.2003.10.009.
- Delorme, Arnaud, Tim Mullen, Christian Kothe, Zeynep Akalin Acar, Nima Bigdely-Shamlo, Andrey Vankov, and Scott Makeig. 2011. "EEGLAB, SIFT, NFT, BCILAB, and ERICA: New Tools for Advanced EEG Processing." *Computational Intelligence and Neuroscience* 2011 (January): 130714. doi:10.1155/2011/130714.
- Diez, Pablo F., Sandra M. Torres Müller, Vicente A. Mut, Eric Laciari, Enrique Avila, Teodiano Freire Bastos-Filho, and Mário Sarcinelli-Filho. 2013. "Commanding a Robotic Wheelchair with a High-frequency Steady-state Visual Evoked Potential Based Brain-computer Interface." *Medical Engineering & Physics* 35 (8) (January 19): 1155–1164. doi:10.1016/j.medengphy.2012.12.005.
- Ding, Jian, George Sperling, and Ramesh Srinivasan. 2006. "Attentional Modulation of SSVEP Power Depends on the Network Tagged by the Flicker Frequency." *Cerebral Cortex (New York, N.Y. : 1991)* 16 (7) (July): 1016–29. doi:10.1093/cercor/bhj044.
- Donchin, Emanuel, Kevin M. Spencer, and Ranjith Wijesinghe. 2000. "The Mental Prosthesis: Assessing the Speed of a P300-based Brain-computer Interface." *IEEE Transactions on Rehabilitation Engineering* 8 (2) (June): 174–179. doi:10.1109/86.847808.

- Dornhege, Guido, Benjamin Blankertz, Gabriel Curio, and Klaus-Robert Müller. 2004a. "Increase Information Transfer Rates in BCI by CSP Extension to Multi-class." *Advances in Neural Information Processing Systems*: 733–740.
- . 2004b. "Boosting Bit Rates in Noninvasive EEG Single-trial Classifications by Feature Combination and Multiclass Paradigms." *IEEE Transactions on Bio-medical Engineering* 51 (6) (June): 993–1002. doi:10.1109/TBME.2004.827088.
- Dornhege, Guido, Benjamin Blankertz, Matthias Krauledat, Florian Losch, Gabriel Curio, and Klaus-Robert Müller. 2006. "Combined Optimization of Spatial and Temporal Filters for Improving Brain-computer Interfacing." *IEEE Transactions on Bio-medical Engineering* 53 (11) (November): 2274–81. doi:10.1109/TBME.2006.883649.
- Elghrabawy, Ayman, and Manal A. Wahed. 2012. "Prediction of Five-class Finger Flexion Using ECoG Signals." In *2012 Cairo International Biomedical Engineering Conference (CIBEC)*, 1–5. IEEE. doi:10.1109/CIBEC.2012.6473300.
- Faller, Josef, Gernot Müller-Putz, Dieter Schmalstieg, and Gert Pfurtscheller. 2010. "An Application Framework for Controlling an Avatar in a Desktop-Based Virtual Environment via a Software SSVEP Brain–Computer Interface." *Presence: Teleoperators and Virtual Environments* 19 (1) (February): 25–34. doi:10.1162/pres.19.1.25.
- Farwell, Lawrence A., and Emanuel Donchin. 1988. "Talking Off the Top of Your Head: Toward a Mental Prosthesis Utilizing Event-related Brain Potentials." *Electroencephalography and Clinical Neurophysiology* 70 (6) (December): 510–23.
- Felzer, Torsten, and Bernd Freisleben. 2003. "Analyzing EEG Signals Using the Probability Estimating Guarded Neural Classifier." *IEEE Transactions on Neural Systems and Rehabilitation Engineering: a Publication of the IEEE Engineering in Medicine and Biology Society* 11 (4) (December): 361–71. doi:10.1109/TNSRE.2003.819785.
- Fisher, Ronald A. 1936. "The Use of Multiple Measurements in Taxonomic Problems." *Annals of Eugenics* 7 (2) (September 29): 179–188. doi:10.1111/j.1469-1809.1936.tb02137.x.
- Folstein, Jonathan R., and Cyma Van Petten. 2008. "Influence of Cognitive Control and Mismatch on the N2 Component of the ERP: a Review." *Psychophysiology* 45 (1) (January): 152–70. doi:10.1111/j.1469-8986.2007.00602.x.
- Friedman, Jerome H. 1989. "Regularized Discriminant Analysis." *Journal of the American Statistical Association* 84 (405) (March): 165. doi:10.2307/2289860.
- . 1997. "On Bias, Variance, 0/1—loss, and the Curse-of-dimensionality." *Data Mining and Knowledge Discovery* 77 (1): 55–77. doi:10.1023/A:1009778005914.
- Friebs, Gerhard M., Vasilios A. Zerris, Catherine L. Ojakangas, Mathew R. Fellows, and John P. Donoghue. 2004. "Brain-Machine and Brain-Computer Interfaces." *Stroke*

35 (11\_suppl\_1) (September 16): 2702–2705.  
doi:10.1161/01.STR.0000143235.93497.03.

Furdea, A., C.A. Ruf, S. Halder, D. De Massari, M. Bogdan, W. Rosenstiel, T. Matuz, and N. Birbaumer. 2012. “A New (semantic) Reflexive Brain-computer Interface: In Search for a Suitable Classifier.” *Journal of Neuroscience Methods* 203 (1) (January 15): 233–40. doi:10.1016/j.jneumeth.2011.09.013.

Galán, Ferran, Marnix Nuttin, Eileen Lew, Pierre W. Ferrez, Gerolf Vanacker, Johan Philips, and Jose del R. Millan. 2008. “A Brain-actuated Wheelchair: Asynchronous and Non-invasive Brain-computer Interfaces for Continuous Control of Robots.” *Clinical Neurophysiology : Official Journal of the International Federation of Clinical Neurophysiology* 119 (9) (September): 2159–69.  
doi:10.1016/j.clinph.2008.06.001.

Gentiletti, G.G., J.G. Gebhart, R.C. Acevedo, O. Yáñez-Suárez, and V. Medina-Bañuelos. 2009. “Command of a Simulated Wheelchair on a Virtual Environment Using a Brain-computer Interface.” *IRBM* 30 (5-6) (November): 218–225.  
doi:10.1016/j.irbm.2009.10.006.

Gerloff, Christian, Christoph Braun, Martin Staudt, Yiwen Li Hegner, Johannes Dichgans, and Ingeborg Krägeloh-Mann. 2006. “Coherent Corticomuscular Oscillations Originate from Primary Motor Cortex: Evidence from Patients with Early Brain Lesions.” *Human Brain Mapping* 27 (10) (October): 789–98.  
doi:10.1002/hbm.20220.

Gneo, Massimo, Giacomo Severini, Silvia Conforto, Maurizio Schmid, and Tommaso D’Alessio. 2011. “Towards a Brain-Activated and Eye-Controlled Wheelchair.” *International Journal of Bioelectromagnetism* 13 (1): 44–45.

Grandchamp, Romain, and Arnaud Delorme. 2009. “NeuroTRIP: A Framework for Bridging Between Open Source Software. Application to Training a Brain Machine Interface.” In *2009 Fifth International Conference on Signal Image Technology and Internet Based Systems*, 451–457. IEEE. doi:10.1109/SITIS.2009.76.

Grave de Peralta Menendez, Rolando, Sara Gonzalez Andino, Lucas Perez, Pierre W. Ferrez, and Jose del R. Millan. 2005. “Non-invasive Estimation of Local Field Potentials for Neuroprosthesis Control.” *Cognitive Processing* 6 (1) (January 18): 59–64. doi:10.1007/s10339-004-0043-x.

Green, Andrea M., and John F. Kalaska. 2011. “Learning to Move Machines with the Mind.” *Trends in Neurosciences* 34 (2) (February): 61–75.  
doi:10.1016/j.tins.2010.11.003.

Guger, Christoph, Shahab Daban, Eric Sellers, Clemens Holzner, Gunther Krausz, Roberta Carabona, Furio Gramatica, and Guenter Edlinger. 2009. “How Many People Are Able to Control a P300-based Brain-computer Interface (BCI)?” *Neuroscience Letters* 462 (1) (October 2): 94–8. doi:10.1016/j.neulet.2009.06.045.

- Hammon, Paul S., and Virginia R. de Sa. 2007. "Preprocessing and Meta-classification for Brain-computer Interfaces." *IEEE Transactions on Bio-medical Engineering* 54 (3) (March): 518–25. doi:10.1109/TBME.2006.888833.
- Hasan, Bashar Awwad Shiekh, and John Q. Gan. 2012. "Hangman BCI: An Unsupervised Adaptive Self-paced Brain-Computer Interface for Playing Games." *Computers in Biology and Medicine* 42 (5) (May): 598–606. doi:10.1016/j.combiomed.2012.02.004.
- Haselsteiner, Ernst, and Gert Pfurtscheller. 2000. "Using Time-dependent Neural Networks for EEG Classification." *IEEE Transactions on Rehabilitation Engineering* 8 (4) (December): 457–463. doi:10.1109/86.895948.
- Haykin Simon. 1999. *Neural Networks: a Comprehensive Foundation*. Edited by John Griffin. *The Knowledge Engineering Review*. 2nd ed. Vol. 13. New Jersey: Prentice Hall. doi:10.1017/S0269888998214044.
- Hazrati, Mehrnaz Kh., and Abbas Erfanian. 2008. "An On-line BCI for Control of Hand Grasp Sequence and Holding Using Adaptive Probabilistic Neural Network." *30th Annual International Conference of the IEEE Engineering in Medicine and Biology Society* 2008 (January): 1009–12. doi:10.1109/IEMBS.2008.4649326.
- Helmy, Salah, Tarik Al-ani, Yskandar Hamam, and Essam El-madbouly. 2008. "P300 Based Brain-computer Interface Using Hidden Markov Models." In *2008 International Conference on Intelligent Sensors, Sensor Networks and Information Processing*, 127–132. IEEE. doi:10.1109/ISSNIP.2008.4761974.
- Hinterberger, Thilo, Nicola Neumann, Mirko Pham, Andrea Kübler, Anke Grether, Nadine Hofmayer, Barbara Wilhelm, Herta Flor, and Niels Birbaumer. 2004. "A Multimodal Brain-based Feedback and Communication System." *Experimental Brain Research. Experimentelle Hirnforschung. Expérimentation Cérébrale* 154 (4) (February): 521–6. doi:10.1007/s00221-003-1690-3.
- Hinterberger, Thilo, Stefan Schmidt, Nicola Neumann, Jürgen Mellinger, Benjamin Blankertz, Gabriel Curio, and Niels Birbaumer. 2004. "Brain-computer Communication and Slow Cortical Potentials." *IEEE Transactions on Bio-medical Engineering* 51 (6) (June): 1011–8. doi:10.1109/TBME.2004.827067.
- Hiraiwa, Alkira, Katsunori Shimohara, and Yakio Tokunaga. 1990. "EEG Topography Recognition by Neural Networks." *IEEE Engineering in Medicine and Biology Magazine : the Quarterly Magazine of the Engineering in Medicine & Biology Society* 9 (3) (January): 39–42. doi:10.1109/51.59211.
- Hochberg, Leigh R., Mijail D. Serruya, Gerhard M. Friehs, Jon A. Mukand, Maryam Saleh, Abraham H. Caplan, Almut Branner, David Chen, Richard D. Penn, and John P. Donoghue. 2006. "Neuronal Ensemble Control of Prosthetic Devices by a Human with Tetraplegia." *Nature* 442 (7099) (July 13): 164–71. doi:10.1038/nature04970.
- Hoffmann, Ulrich, Jean-Marc Vesin, Touradj Ebrahimi, and Karin Diserens. 2008. "An Efficient P300-based Brain-computer Interface for Disabled Subjects." *Journal of*

*Neuroscience Methods* 167 (1) (January 15): 115–25.  
doi:10.1016/j.jneumeth.2007.03.005.

Hoya, Tetsuya, Gen Hori, Hovagim Bakardjian, Tomoaki Nishimura, Taiji Suzuki, Yoichi Miyawaki, Arao Funase, and Jianting Cao. 2003. “Classification of Single Trial EEG Signals by a Combined Principal+ Independent Component Analysis and Probabilistic Neural Network Approach.” In *In International Symposium on Independent Component Analysis and Blind Signal Separation ICA2003*, " In Inter:197–202.

Hyvärinen, Aapo, and Erkki Oja. 2000. “Independent Component Analysis: Algorithms and Applications.” *Neural Networks* 13 (4-5): 411–30.

Jain, Anil K., Robert P.W. Duin, and Jianchang Mao. 2000. “Statistical Pattern Recognition: a Review.” *IEEE Transactions on Pattern Analysis and Machine Intelligence* 22 (1): 4–37. doi:10.1109/34.824819.

Jutten, Christian, and Jeanny Herault. 1991. “Blind Separation of Sources, Part I: An Adaptive Algorithm Based on Neuromimetic Architecture.” *Signal Processing* 24 (1) (July): 1–10. doi:10.1016/0165-1684(91)90079-X.

Kachenoura, Amar, Laurent Albera, Lotfi Senhadji, and Pierre Comon. 2008. “Ica: a Potential Tool for Bci Systems.” *IEEE Signal Processing Magazine* 25 (1): 57–68. doi:10.1109/MSP.2008.4408442.

Kameyama, Junichi, Yasunobu Handa, Nozomu Hoshimiya, and Minoru Sakurai. 1999. “Restoration of Shoulder Movement in Quadriplegic and Hemiplegic Patients by Functional Electrical Stimulation Using Percutaneous Multiple Electrodes.” *The Tohoku Journal of Experimental Medicine* 187 (4) (April): 329–37.

Karim, Ahmed A., Thilo Hinterberger, Jürgen Richter, Jürgen Mellinger, Nicola Neumann, Herta Flor, Andrea Kübler, and Niels Birbaumer. 2006. “Neural Internet: Web Surfing with Brain Potentials for the Completely Paralyzed.” *Neurorehabilitation and Neural Repair* 20 (4) (December): 508–15. doi:10.1177/1545968306290661.

Katevas, Ni I., N.M. Sgouros, S.G. Tzafestas, G. Papakonstantinou, P. Beattie, J.M. Bishop, P. Tsanakas, and D. Koutsouris. 1997. “The Autonomous Mobile Robot SENARIO: a Sensor Aided Intelligent Navigation System for Powered Wheelchairs.” *IEEE Robotics & Automation Magazine* 4 (4): 60–70. doi:10.1109/100.637806.

Keirn, Zachary A., and Jorge I. Aunon. 1990. “A New Mode of Communication Between Man and His Surroundings.” *IEEE Transactions on Bio-medical Engineering* 37 (12) (December): 1209–14. doi:10.1109/10.64464.

Khare, Vijay, Jayashree Santhosh, Sneha Anand, and Manvir Bhatia. 2011. “Brain Computer Interface Based Real Time Control of Wheelchair Using Electroencephalogram.” *International Journal of Soft Computing* (5): 41–45.

- Kleber, Boris, and Niels Birbaumer. 2005. "Direct Brain Communication: Neuroelectric and Metabolic Approaches at Tübingen." *Cognitive Processing* 6 (1) (January 27): 65–74. doi:10.1007/s10339-004-0045-8.
- Klem, G H, H O Lüders, H H Jasper, and C Elger. 1999. "The Ten-twenty Electrode System of the International Federation. The International Federation of Clinical Neurophysiology." *Electroencephalography and Clinical Neurophysiology. Supplement* 52 (2) (January): 3–6.
- Ko, Kwang-Eun, Hyun-Chang Yang, and Kwee-Bo Sim. 2009. "Emotion Recognition Using EEG Signals with Relative Power Values and Bayesian Network." *International Journal of Control, Automation and Systems* 7 (5) (October 8): 865–870. doi:10.1007/s12555-009-0521-0.
- Kohonen, Teuvo. 1990. "The Self-organizing Map." *Proceedings of the IEEE* 78 (9): 1464–1480. doi:10.1109/5.58325.
- Kostov, Aleksander, and Mark Polak. 2000. "Parallel Man-machine Training in Development of EEG-based Cursor Control." *IEEE Transactions on Rehabilitation Engineering : a Publication of the IEEE Engineering in Medicine and Biology Society* 8 (2) (June): 203–5.
- Krauledat, Matthias, Michael Tangermann, Benjamin Blankertz, and Klaus-Robert Müller. 2008. "Towards Zero Training for Brain-computer Interfacing." *PloS One* 3 (8) (January): e2967. doi:10.1371/journal.pone.0002967.
- Krusienski, Dean J., and Jerry J. Shih. 2011. "Control of a Brain-computer Interface Using Stereotactic Depth Electrodes in and Adjacent to the Hippocampus." *Journal of Neural Engineering* 8 (2) (April): 025006. doi:10.1088/1741-2560/8/2/025006.
- Kübler, Andrea. 2006. "BCI Meeting 2005—Workshop on Clinical Issues and Applications." *IEEE Transactions on Neural Systems and Rehabilitation Engineering* 14 (2) (June): 131–134. doi:10.1109/TNSRE.2006.875585.
- Kübler, Andrea, Boris Kotchoubey, Jochen Kaiser, Jonathan R. Wolpaw, and Niels Birbaumer. 2001. "Brain-computer Communication: Unlocking the Locked In." *Psychological Bulletin* 127 (3) (May): 358–375. doi:10.1037/0033-2909.127.3.358.
- Lalor, Edmund C., Simon P. Kelly, Ciarán Finucane, Robert Burke, Ray Smith, Richard B. Reilly, and Gary Mcdarby. 2005. "Steady-State VEP-Based Brain-Computer Interface Control in an Immersive 3D Gaming Environment." *EURASIP Journal on Advances in Signal Processing* 2005 (19): 3156–3164. doi:10.1155/ASP.2005.3156.
- Lebedev, Mikhail A., and Miguel A.L. Nicolelis. 2006. "Brain-machine Interfaces: Past, Present and Future." *Trends in Neurosciences* 29 (9) (September): 536–46. doi:10.1016/j.tins.2006.07.004.
- Lecuyer, Anatole, Fabien Lotte, Richard B. Reilly, Robert Leeb, Michitaka Hirose, and Mel Slater. 2008. "Brain-Computer Interfaces, Virtual Reality, and Videogames." *Computer* 41 (10) (October): 66–72. doi:10.1109/MC.2008.410.

- Ledoit, Olivier, and Michael Wolf. 2004. "A Well-conditioned Estimator for Large-dimensional Covariance Matrices." *Journal of Multivariate Analysis* 88 (2) (February): 365–411. doi:10.1016/S0047-259X(03)00096-4.
- Lee, Hyekyung, and Seungjin Choi. 2003. "PCA+HMM+SVM for EEG Pattern Classification." In *Seventh International Symposium on Signal Processing and Its Applications, 2003. Proceedings.*, 541–544 vol.1. IEEE. doi:10.1109/ISSPA.2003.1224760.
- Leeb, Robert, Doron Friedman, Gernot R. Müller-Putz, Reinhold Scherer, Mel Slater, and Gert Pfurtscheller. 2007. "Self-paced (asynchronous) BCI Control of a Wheelchair in Virtual Environments: a Case Study with a Tetraplegic." *Computational Intelligence and Neuroscience* 2007 (January): 79642. doi:10.1155/2007/79642.
- Leeb, Robert, Doron Friedman, Mel Slater, and Gert Pfurtscheller. 2007. "A Tetraplegic Patient Controls a Wheelchair in Virtual Reality." *BRAINPLAY 07 Brain-Computer Interfaces and Games Workshop at ACE (Advances in Computer Entertainment)*: 37.
- Leeb, Robert, Miguel Gubler, Michele Tavella, Heather Miller, and Jose del. R. Millan. 2010. "On the Road to a Neuroprosthetic Hand: a Novel Hand Grasp Orthosis Based on Functional Electrical Stimulation." *Conference Proceedings : 2010 Annual International Conference of the IEEE Engineering in Medicine and Biology Society*. 2010 (January): 146–9. doi:10.1109/IEMBS.2010.5627412.
- Leeb, Robert, Felix Lee, Claudia Keinrath, Reinhold Scherer, Horst Bischof, and Gert Pfurtscheller. 2007. "Brain-computer Communication: Motivation, Aim, and Impact of Exploring a Virtual Apartment." *IEEE Transactions on Neural Systems and Rehabilitation Engineering : a Publication of the IEEE Engineering in Medicine and Biology Society* 15 (4) (December): 473–82. doi:10.1109/TNSRE.2007.906956.
- Leeb, Robert, and Jose del. R. Millan. 2013. *Towards Practical Brain-Computer Interfaces*. Edited by Brendan Z. Allison, Stephen Dunne, Robert Leeb, José Del R. Millán, and Anton Nijholt. Berlin, Heidelberg: Springer Berlin Heidelberg. doi:10.1007/978-3-642-29746-5.
- Lemm, Steven, Benjamin Blankertz, Gabriel Curio, and Klaus-Robert Müller. 2005. "Spatio-spectral Filters for Improving the Classification of Single Trial EEG." *IEEE Transactions on Bio-medical Engineering* 52 (9) (September): 1541–8. doi:10.1109/TBME.2005.851521.
- Lemm, Steven, Klaus-Robert Müller, and Gabriel Curio. 2009. "A Generalized Framework for Quantifying the Dynamics of EEG Event-related Desynchronization." *PLoS Computational Biology* 5 (8) (August): e1000453. doi:10.1371/journal.pcbi.1000453.
- Lemm, Steven, Christin Schäfer, and Gabriel Curio. 2004. "BCI Competition 2003--Data Set III: Probabilistic Modeling of Sensorimotor Mu Rhythms for Classification of Imaginary Hand Movements." *IEEE Transactions on Bio-medical Engineering* 51 (6) (June): 1077–80. doi:10.1109/TBME.2004.827076.

- Leuthardt, Eric C., Charles Gaona, Mohit Sharma, Nicholas Szrama, Jarod Roland, Zac Freudenberg, Jamie Solis, Jonathan Breshears, and Gerwin Schalk. 2011. "Using the Electrographic Speech Network to Control a Brain-computer Interface in Humans." *Journal of Neural Engineering* 8 (3) (June): 036004. doi:10.1088/1741-2560/8/3/036004.
- Levine, Simon P., David A. Bell, Lincoln A. Jaros, Richard C. Simpson, Yoram Koren, and Johann Borenstein. 1999. "The NavChair Assistive Wheelchair Navigation System." *IEEE Transactions on Rehabilitation Engineering : a Publication of the IEEE Engineering in Medicine and Biology Society* 7 (4) (December): 443–51.
- Lledo, Luis D., Jose M. Cano, Andres Ubeda, Eduardo Ianez, and Jose M. Azorin. 2012. "Neuro-fuzzy Classifier to Recognize Mental Tasks in a BCI." In *2012 4th IEEE RAS & EMBS International Conference on Biomedical Robotics and Biomechatronics (BioRob)*, 207–212. IEEE. doi:10.1109/BioRob.2012.6290302.
- Loo, Chu Kiong, Andrews Samraj, and Gin Chong Lee. 2011. "Evaluation of Methods for Estimating Fractal Dimension in Motor Imagery-Based Brain Computer Interface." *Discrete Dynamics in Nature and Society* 2011: 1–8. doi:10.1155/2011/724697.
- Lopes, Ana C., Gabriel Pires, and Urbano Nunes. 2013. "Assisted Navigation for a Brain-actuated Intelligent Wheelchair." *Robotics and Autonomous Systems* 61 (3) (March): 245–258. doi:10.1016/j.robot.2012.11.002.
- Lopes, Ana C., Gabriel Pires, Luis Vaz, and Urbano Nunes. 2011. "Wheelchair Navigation Assisted by Human-Machine Shared-control and a P300-based Brain Computer Interface." In *2011 IEEE/RSJ International Conference on Intelligent Robots and Systems*, 2438–2444. IEEE. doi:10.1109/IROS.2011.6094748.
- Lotte, Fabien. 2011. "Brain-computer Interfaces for 3D Games." In *Proceedings of the 6th International Conference on Foundations of Digital Games - FDG '11*, 325–327. New York, New York, USA: ACM Press. doi:10.1145/2159365.2159427.
- Lotte, Fabien, Marco Congedo, Anatole Lécuyer, Fabrice Lamarche, and Bruno Arnaldi. 2007. "A Review of Classification Algorithms for EEG-based Brain-computer Interfaces." *Journal of Neural Engineering* 4 (2) (June): R1–R13. doi:10.1088/1741-2560/4/2/R01.
- Lotte, Fabien, and Cuntai Guan. 2011. "Regularizing Common Spatial Patterns to Improve BCI Designs: Unified Theory and New Algorithms." *IEEE Transactions on Bio-medical Engineering* 58 (2) (February): 355–62. doi:10.1109/TBME.2010.2082539.
- Lotte, Fabien, Anatole Lecuyer, and Bruno Arnaldi. 2007. "FuRIA: A Novel Feature Extraction Algorithm for Brain-Computer Interfaces Using Inverse Models and Fuzzy Regions of Interest." In *2007 3rd International IEEE/EMBS Conference on Neural Engineering*, 175–178. IEEE. doi:10.1109/CNE.2007.369640.

- Mak, Joseph N., and Jonathan R. Wolpaw. 2009. "Clinical Applications of Brain-Computer Interfaces: Current State and Future Prospects." *IEEE Reviews in Biomedical Engineering* 2 (January): 187–199. doi:10.1109/RBME.2009.2035356.
- Makeig, Scott, Sgurd Enghoff, Tzyy-Ping Jung, and Terrence J. Sejnowski. 2000. "A Natural Basis for Efficient Brain-actuated Control." *IEEE Transactions on Rehabilitation Engineering : a Publication of the IEEE Engineering in Medicine and Biology Society* 8 (2) (June): 208–11.
- Mangold, S, T Keller, A Curt, and V Dietz. 2005. "Transcutaneous Functional Electrical Stimulation for Grasping in Subjects with Cervical Spinal Cord Injury." *Spinal Cord* 43 (1) (January): 1–13. doi:10.1038/sj.sc.3101644.
- Mano, Marsel, and Genci Capi. 2013. "A Novel Method to Navigate Robotic Wheelchair Using BMI Based Control and Assistive Information." *Research Notes in Information Science* 12 (April): 155–120. doi:10.4156/rnis.vol12.19.
- Mano, Marsel, Genci Capi, Norifumi Tanaka, and Shigenori Kawahara. 2013. "An Artificial Neural Network Based Robot Controller That Uses Rat's Brain Signals." *Robotics* 2 (2) (April 29): 54–65. doi:10.3390/robotics2020054.
- Marquand, Andre F., Sara De Simoni, Owen G. O'Daly, Steven C.R. Williams, Janaina Mourão-Miranda, and Mitul A. Mehta. 2011. "Pattern Classification of Working Memory Networks Reveals Differential Effects of Methylphenidate, Atomoxetine, and Placebo in Healthy Volunteers." *Neuropsychopharmacology : Official Publication of the American College of Neuropsychopharmacology* 36 (6) (May): 1237–47. doi:10.1038/npp.2011.9.
- Mason, Steven G., Ali Bashashati, Mehrdad Fatourehchi, Karla F. Navarro, and Gary E. Birch. 2007. "A Comprehensive Survey of Brain Interface Technology Designs." *Annals of Biomedical Engineering* 35 (2) (February): 137–69. doi:10.1007/s10439-006-9170-0.
- Mason, Steven G., and Gary E. Birch. 2003. "A General Framework for Brain-computer Interface Design." *IEEE Transactions on Neural Systems and Rehabilitation Engineering : a Publication of the IEEE Engineering in Medicine and Biology Society* 11 (1) (March): 70–85. doi:10.1109/TNSRE.2003.810426.
- Mason, Steven G., Julien Kronegg, Jane Huggins, Mehrdad Fatourehchi, and Alois Schlögl. 2006. "Evaluating the Performance of Self-paced Brain Computer Interface Technology." *Neil Squire Soc., ....* Vol. 0. Vancouver, BC, Canada.
- Mayaud, Louis, Sabine Filipe, Lucie Pétégnief, Oliver Rochecouste, and Marco Congedo. 2013. "Robust Brain-computer Interface for Virtual Keyboard (RoBIK): Project Results." *IRBM* 34 (2) (April): 131–138. doi:10.1016/j.irbm.2013.01.013.
- McCormick, Martin, Rui Ma, and Todd P. Coleman. 2010. "An Analytic Spatial Filter and a Hidden Markov Model for Enhanced Information Transfer Rate in EEG-based Brain Computer Interfaces." In *2010 IEEE International Conference on Acoustics,*

- Speech and Signal Processing*, 1:602–605. IEEE.  
doi:10.1109/ICASSP.2010.5495544.
- McFarland, Dennis J., Charles W. Anderson, Klaus-Robert Müller, Alois Schlögl, and Dean J. Krusienski. 2006. “BCI Meeting 2005--workshop on BCI Signal Processing: Feature Extraction and Translation.” *IEEE Transactions on Neural Systems and Rehabilitation Engineering : a Publication of the IEEE Engineering in Medicine and Biology Society* 14 (2) (June): 135–8. doi:10.1109/TNSRE.2006.875637.
- McFarland, Dennis J., Lynn M. McCane, Stephen V. David, and Jonathan R. Wolpaw. 1997. “Spatial Filter Selection for EEG-based Communication.” *Electroencephalography and Clinical Neurophysiology* 103 (3) (September): 386–94.
- Mellinger, Jürgen, Gerwin Schalk, Christoph Braun, Hubert Preissl, Wolfgang Rosenstiel, Niels Birbaumer, and Andrea Kübler. 2007. “An MEG-based Brain-computer Interface (BCI).” *NeuroImage* 36 (3) (July 1): 581–93.  
doi:10.1016/j.neuroimage.2007.03.019.
- Memberg, William D., Patrick E. Crago, and Michael W. Keith. 2003. “Restoration of Elbow Extension via Functional Electrical Stimulation in Individuals with Tetraplegia.” *Journal of Rehabilitation Research and Development* 40 (6): 477–86.
- Michel, Christoph M., Micah M. Murray, Göran Lantz, Sara Gonzalez, Laurent Spinelli, and Rolando Grave de Peralta. 2004. “EEG Source Imaging.” *Clinical Neurophysiology : Official Journal of the International Federation of Clinical Neurophysiology* 115 (10) (October): 2195–222. doi:10.1016/j.clinph.2004.06.001.
- Middendorf, Matthew, Grant McMillan, Gloria Calhoun, and Keith S. Jones. 2000. “Brain-computer Interfaces Based on the Steady-state Visual-evoked Response.” *IEEE Transactions on Rehabilitation Engineering : a Publication of the IEEE Engineering in Medicine and Biology Society* 8 (2) (June): 211–4.
- Millan, Jose del. R., Ferran Galan, D Vanhooydonck, Eileen Lew, Johan Philips, and Marnix Nuttin. 2009. “Asynchronous Non-invasive Brain-actuated Control of an Intelligent Wheelchair.” *Conference Proceedings : ... Annual International Conference of the IEEE Engineering in Medicine and Biology Society. IEEE Engineering in Medicine and Biology Society. Conference 2009* (January): 3361–4.  
doi:10.1109/IEMBS.2009.5332828.
- Millan, Jose del. R., Josep Mourino, Fabio Babiloni, Febo Cincotti, Markus Varsta, and Jukka Heikkonen. 2000. “Local Neural Classifier for EEG-based Recognition of Mental Tasks.” In *Proceedings of the IEEE-INNS-ENNS International Joint Conference on Neural Networks. IJCNN 2000. Neural Computing: New Challenges and Perspectives for the New Millennium*, 632–636 vol.3. IEEE.  
doi:10.1109/IJCNN.2000.861393.
- Millan, Jose del. R., Frédéric Renkens, Josep Mouriño, and Wulfram Gerstner. 2004. “Noninvasive Brain-actuated Control of a Mobile Robot by Human EEG.” *IEEE Transactions on Bio-medical Engineering* 51 (6) (June): 1026–33.  
doi:10.1109/TBME.2004.827086.

- Millan, Jose del. R., Rüdiger Rupp, Gernot R. Müller-Putz, Roderick Murray-Smith, Claudio Giugliemma, Michael Tangermann, Carmen Vidaurre, et al. 2010. "Combining Brain-Computer Interfaces and Assistive Technologies: State-of-the-Art and Challenges." *Frontiers in Neuroscience* 4 (September) (January): 1–15. doi:10.3389/fnins.2010.00161.
- Minati, Ludovico, Anna Nigri, Cristina Rosazza, and Maria Grazia Bruzzone. 2012. "Thoughts Turned into High-level Commands: Proof-of-concept Study of a Vision-guided Robot Arm Driven by Functional MRI (fMRI) Signals." *Medical Engineering & Physics* 34 (5) (June): 650–8. doi:10.1016/j.medengphy.2012.02.004.
- Mizuno, Yuji, Hiroshi Mabuchi, Goutam Chakraborty, and Masafumi Matsuhara. 2010. "Clustering of EEG Data Using Maximum Entropy Method and LVQ." *International Journal of Computers* 4 (4): 193–200.
- Montesano, Luis, Marta Díaz, Sonu Bhaskar, and Javier Minguez. 2010. "Towards an Intelligent Wheelchair System for Users with Cerebral Palsy." *IEEE Transactions on Neural Systems and Rehabilitation Engineering: a Publication of the IEEE Engineering in Medicine and Biology Society* 18 (2) (April): 193–202. doi:10.1109/TNSRE.2009.2039592.
- Moritz, Chet T., Steve I. Perlmuter, and Eberhard E. Fetz. 2008. "Direct Control of Paralysed Muscles by Cortical Neurons." *Nature* 456 (7222) (December 4): 639–42. doi:10.1038/nature07418.
- Mugler, Emily, Michael Bensch, Sebastian Halder, Wolfgang Rosenstiel, Niels Birbaumer, and Andrea Kübler. 2008. "Control of an Internet Browser Using the P300 Event-related Potential." *Control* 10 (1): 56–63.
- Mühl, Christian, Hayrettin Gürkök, Danny Plass-Oude Bos, Marieke E. Thurlings, Lasse Scherffig, Matthieu Duvinage, Alexandra A. Elbakyan, SungWook Kang, Mannes Poel, and Dirk Heylen. 2010. "Bacteria Hunt." *Journal on Multimodal User Interfaces* 4 (1) (August 14): 11–25. doi:10.1007/s12193-010-0046-0.
- Müller, Klaus-Robert, Matthias Krauledat, Guido Dornhege, Gabriel Curio, and Benjamin Blankertz. 2004. "Machine Learning Techniques for Brain-Computer Interfaces." *Machine Learning* 49 (x): 11–22.
- Müller-Gerking, Johannes, Gert Pfurtscheller, and Henrik Flyvbjerg. 1999. "Designing Optimal Spatial Filters for Single-trial EEG Classification in a Movement Task." *Clinical Neurophysiology* 110 (5) (May): 787–798. doi:10.1016/S1388-2457(98)00038-8.
- Müller-Putz, Gernot R, Reinhold Scherer, Gert Pfurtscheller, and Rüdiger Rupp. 2005. "EEG-based Neuroprosthesis Control: a Step Towards Clinical Practice." *Neuroscience Letters* 382 (1-2): 169–74. doi:10.1016/j.neulet.2005.03.021.
- Müller-Putz, Gernot R., Reinhold Scherer, Gert Pfurtscheller, and Rüdiger Rupp. 2006. "Brain-computer Interfaces for Control of Neuroprostheses: From Synchronous to

- Asynchronous Mode of Operation.” *Biomedizinische Technik. Biomedical Engineering* 51 (2) (July): 57–63. doi:10.1515/BMT.2006.011.
- Naeem, Muhammad, Clemens Brunner, Robert Leeb, Bernhard Graimann, and Gert Pfurtscheller. 2006. “Seperability of Four-class Motor Imagery Data Using Independent Components Analysis.” *Journal of Neural Engineering* 3 (3) (September): 208–16. doi:10.1088/1741-2560/3/3/003.
- Nawroj, Ahsan, Siyuan Wang, Ismail Jouny, Yih-Choung Yu, and Lisa Gabel. 2012. “An Event Classifier Using EEG Signals: An Artificial Neural Network Approach.” In *2012 38th Annual Northeast Bioengineering Conference (NEBEC)*, 386–387. IEEE. doi:10.1109/NEBC.2012.6207126.
- Nazarpour, K., J. Stastny, and R. C. Miall. 2009. “ssMRP State Detection for Brain Computer Interfacing Using Hidden Markov Models.” In *2009 IEEE/SP 15th Workshop on Statistical Signal Processing*, 29–32. IEEE. doi:10.1109/SSP.2009.5278648.
- Nelson, W. Todd, Lawrence J. Hettinger, James A. Cunningham, Merry M. Roe, Michael W. Haas, and Leon B. Dennis. 1997. “Navigating through Virtual Flight Environments Using Brain-body-actuated Control.” In *Proceedings of IEEE 1997 Annual International Symposium on Virtual Reality*, 30–37. IEEE Comput. Soc. Press. doi:10.1109/VRAIS.1997.583041.
- Nicolelis, Miguel A.L. 2001. “Actions from Thoughts.” *Nature* 409 (6818) (January 18): 403–7. doi:10.1038/35053191.
- Niedermeyer, Ernst, and Fernando H. Lopes da Silva. 2005. *Electroencephalography: Basic Principles, Clinical Applications and Related Fields*. Wolters Kluwer Health.
- Nijholt, Anton, Danny Plass-Oude Bos, and Boris Reuderink. 2009. “Turning Shortcomings into Challenges: Brain–computer Interfaces for Games.” *Entertainment Computing* 1 (2) (April): 85–94. doi:10.1016/j.entcom.2009.09.007.
- Noirhomme, Quentin, Richard I. Kitney, and Benoît Macq. 2008. “Single-trial EEG Source Reconstruction for Brain-computer Interface.” *IEEE Transactions on Bio-medical Engineering* 55 (5) (May): 1592–601. doi:10.1109/TBME.2007.913986.
- Nudo, Randolph J. 2006. “Mechanisms for Recovery of Motor Function Following Cortical Damage.” *Current Opinion in Neurobiology* 16 (6) (December): 638–44. doi:10.1016/j.conb.2006.10.004.
- Obermaier, Bernhard, Christoph Guger, Christa Neuper, and Gert Pfurtscheller. 2001. “Hidden Markov Models for Online Classification of Single Trial EEG Data.” *Pattern Recognition Letters* 22 (12) (October): 1299–1309. doi:10.1016/S0167-8655(01)00075-7.
- Odom, J. Vernon, Michael Bach, Colin Barber, Mitchell Brigell, Michael F. Marmor, Alma Patrizia Tormene, Graham E. Holder, and Vaegan. 2004. “Visual Evoked

- Potentials Standard (2004).” *Documenta Ophthalmologica. Advances in Ophthalmology* 108 (2) (March): 115–23.
- Oppenheim, Alan V., Ronald W. Schafer, and John R. Buck. 1999. *Discrete-time Signal Processing*. 2nd ed. New Jersey 07458: Prentice Hall.
- Palaniappan, Ramaswamy. 2005. “Brain Computer Interface Design Using Band Powers Extracted During Mental Tasks.” In *Conference Proceedings. 2nd International IEEE EMBS Conference on Neural Engineering, 2005.*, 321–324. IEEE. doi:10.1109/CNE.2005.1419622.
- Palaniappan, Ramaswamy, Raveendran Paramesran, Shogo Nishida, and Naoki Saiwaki. 2002. “A New Brain-computer Interface Design Using Fuzzy ARTMAP.” *IEEE Transactions on Neural Systems and Rehabilitation Engineering : a Publication of the IEEE Engineering in Medicine and Biology Society* 10 (3) (September): 140–8. doi:10.1109/TNSRE.2002.802854.
- Parikh, Sarangi P., Valdir Grassi Jr., R. Vijay Kumar, and Jun Okamoto Jr. 2004. “Incorporating User Inputs in Motion Planning for a Smart Wheelchair.” In *IEEE International Conference on Robotics and Automation, 2004. Proceedings. ICRA '04. 2004*, 2043–2048 Vol.2. IEEE. doi:10.1109/ROBOT.2004.1308124.
- Patel, Salil H., and Pierre N. Azzam. 2005. “Characterization of N200 and P300: Selected Studies of the Event-Related Potential.” *International Journal of Medical Sciences* 2 (4) (January): 147–54.
- Penny, William D., Stephen J. Roberts, Eleanor A. Curran, and Maria J. Stokes. 2000. “EEG-based Communication: a Pattern Recognition Approach.” *IEEE Transactions on Rehabilitation Engineering* 8 (2) (June): 214–215. doi:10.1109/86.847820.
- Perez, Jose Luis Martinez, and Antonio Barrientos Cruz. 2007. “Linear Discriminant Analysis on Brain Computer Interface.” In *2007 IEEE International Symposium on Intelligent Signal Processing*, 1–6. IEEE. doi:10.1109/WISP.2007.4447590.
- Perrin, Xavier, Ricardo Chavarriaga, Francis Colas, Roland Siegwart, and Jose del. R. Millan. 2010. “Brain-coupled Interaction for Semi-autonomous Navigation of an Assistive Robot.” *Robotics and Autonomous Systems* 58 (12) (December 31): 1246–1255. doi:10.1016/j.robot.2010.05.010.
- Pfurtscheller, Gert, and Andrea Berghold. 1989. “Patterns of Cortical Activation During Planning of Voluntary Movement.” *Electroencephalography and Clinical Neurophysiology* 72 (3) (March): 250–8.
- Pfurtscheller, Gert, Bernhard Graimann, and Christa Neuper. 2006. “EEG-Based Brain-Computer Interface System.” In *Encyclopedia of Biomedical Engineering*. John Wiley & Sons, Inc. doi:10.1002/9780471740360.
- Pfurtscheller, Gert, and Fernando Lopes da Silva. 1999. “Event-related EEG/MEG Synchronization and Desynchronization: Basic Principles.” *Clinical*

*Neurophysiology : Official Journal of the International Federation of Clinical Neurophysiology* 110 (11) (November): 1842–57.

- Pfurtscheller, Gert, Gernot R. Müller, Jörg Pfurtscheller, Hans Jürgen Gerner, and Rüdiger Rupp. 2003. “‘Thought’ – Control of Functional Electrical Stimulation to Restore Hand Grasp in a Patient with Tetraplegia.” *Neuroscience Letters* 351 (1) (November): 33–36. doi:10.1016/S0304-3940(03)00947-9.
- Pfurtscheller, Gert, Gernot R. Müller-Putz, Jörg Pfurtscheller, and Rüdiger Rupp. 2005. “EEG-Based Asynchronous BCI Controls Functional Electrical Stimulation in a Tetraplegic Patient.” *EURASIP Journal on Advances in Signal Processing* 2005 (19): 3152–3155. doi:10.1155/ASP.2005.3152.
- Pfurtscheller, Gert, and Christa Neuper. 2001. “Motor Imagery and Direct Brain-computer Communication.” *Proceedings of the IEEE* 89 (7) (July): 1123–1134. doi:10.1109/5.939829.
- Pfurtscheller, Gert, Christa Neuper, Doris Flotzinger, and Martin Pregenzer. 1997. “EEG-based Discrimination Between Imagination of Right and Left Hand Movement.” *Electroencephalography and Clinical Neurophysiology* 103 (6) (December): 642–651. doi:10.1016/S0013-4694(97)00080-1.
- Pfurtscheller, Gert, Christa Neuper, Alois Schlögl, and Klaus Lugger. 1998. “Separability of EEG Signals Recorded During Right and Left Motor Imagery Using Adaptive Autoregressive Parameters.” *IEEE Transactions on Rehabilitation Engineering : a Publication of the IEEE Engineering in Medicine and Biology Society* 6 (3) (September): 316–25.
- Pfurtscheller, Gert, Teodoro Solis-Escalante, Rupert Ortner, Patricia Linortner, and Gernot R. Müller-Putz. 2010. “Self-paced Operation of an SSVEP-Based Orthosis with and Without an Imagery-based ‘Brain Switch:’ a Feasibility Study Towards a Hybrid BCI.” *IEEE Transactions on Neural Systems and Rehabilitation Engineering : a Publication of the IEEE Engineering in Medicine and Biology Society* 18 (4) (August): 409–14. doi:10.1109/TNSRE.2010.2040837.
- Philips, Johan, Jose del. R. Millan, Gerolf Vanacker, Eileen Lew, Ferran Galan, Pierre W Ferrez, Hendrik Van Brussel, and Marnix Nuttin. 2007. “Adaptive Shared Control of a Brain-Actuated Simulated Wheelchair.” In *2007 IEEE 10th International Conference on Rehabilitation Robotics*, 00:408–414. IEEE. doi:10.1109/ICORR.2007.4428457.
- Piccione, F, F Giorgi, P Tonin, K Priftis, S Giove, S Silvoni, G Palmas, and F Beverina. 2006. “P300-based Brain Computer Interface: Reliability and Performance in Healthy and Paralyzed Participants.” *Clinical Neurophysiology : Official Journal of the International Federation of Clinical Neurophysiology* 117 (3) (March): 531–7. doi:10.1016/j.clinph.2005.07.024.
- Popescu, Florin, Siamac Fazli, Yakob Badower, Benjamin Blankertz, and Klaus-Robert Müller. 2007. “Single Trial Classification of Motor Imagination Using 6 Dry EEG Electrodes.” *PloS One* 2 (7) (January): e637. doi:10.1371/journal.pone.0000637.

- Prassler, Erwin, Jens Scholz, and Paolo Fiorini. 2001. "A Robotics Wheelchair for Crowded Public Environment." *IEEE Robotics & Automation Magazine* 8 (1) (March): 38–45. doi:10.1109/100.924358.
- Qin, Lei, Lei Ding, and Bin He. 2004. "Motor Imagery Classification by Means of Source Analysis for Brain-computer Interface Applications." *Journal of Neural Engineering* 1 (3) (September): 135–41. doi:10.1088/1741-2560/1/3/002.
- Rakotomamonjy, Alain, Vincent Guigue, Gregory Mallet, and Victor Alvarado. 2005. "Ensemble of SVMs for Improving Brain Computer Interface P300 Speller Performances." In *International Conference on Artificial Neural Networks: Biological Inspirations*, 45–50. Springer Berlin Heidelberg. doi:10.1007/11550822\_8.
- Ramoser, Herbert, Johannes Müller-Gerking, and Gert Pfurtscheller. 2000. "Optimal Spatial Filtering of Single Trial EEG During Imagined Hand Movement." *IEEE Transactions on Rehabilitation Engineering : a Publication of the IEEE Engineering in Medicine and Biology Society* 8 (4) (December): 441–6.
- Rebsamen, Brice, Etienne Burdet, Cuntai Guan, Haihong Zhang, Chee Leong Teo, Qiang Zeng, Christian Laugier, and Marcelo H. Ang Jr. 2007. "Controlling a Wheelchair Indoors Using Thought." *IEEE Intelligent Systems* 22 (2) (March): 18–24. doi:10.1109/MIS.2007.26.
- Rockstroh, Brigitte, Niels Birbaumer, Thomas Elbert, and Werner Lutzenberger. 1984. "Operant Control of EEG and Event-related and Slow Brain Potentials." *Biofeedback and Self-regulation* 9 (2) (June): 139–60.
- Rodrak, Supassorn, and Yodchanan Wongsawat. 2012. "On the Classification of EEG / HEG-based Attention Levels via Time-frequency Selective Multilayer Perceptron for BCI-based Neurofeedback System." In *Signal & Information Processing Association Annual Summit and Conference (APSIPA ASC)*, 1–4. Hollywood, CA.
- Röfer, Thomas, and Alex Lankenau. 2000. "Architecture and Applications of the Bremen Autonomous Wheelchair." *Information Sciences* 126 (1-4) (July): 1–20. doi:10.1016/S0020-0255(00)00020-7.
- Rugg, Michael D., and Michael G.H. Coles. 1996. *Electrophysiology of Mind*. Oxford University Press. doi:10.1093/acprof:oso/9780198524168.001.0001.
- Sagara, Kazuhiko, Kunihiro Kido, and Kuniaki Ozawa. 2009. "Portable Single-channel NIRS-based BMI System for Motor Disabilities' Communication Tools." *Conference Proceedings : 31st Annual International Conference of the IEEE Engineering in Medicine and Biology Society* 2009 (January): 602–5. doi:10.1109/IEMBS.2009.5333071.
- Sajda, Paul, Adam Gerson, Klaus-Robert Müller, Benjamin Blankertz, and Lucas Parra. 2003. "A Data Analysis Competition to Evaluate Machine Learning Algorithms for Use in Brain-computer Interfaces." *IEEE Transactions on Neural Systems and*

*Rehabilitation Engineering : a Publication of the IEEE Engineering in Medicine and Biology Society* 11 (2) (June): 184–5. doi:10.1109/TNSRE.2003.814453.

Sanei, Saeid, and Jonathon. A. Chambers. 2007. *EEG Signal Processing. Chemistry & Biodiversity*. Vol. 1. Wiley-Interscience.

Schäfer, Juliane, and Korbinian Strimmer. 2005. “A Shrinkage Approach to Large-scale Covariance Matrix Estimation and Implications for Functional Genomics.” *Statistical Applications in Genetics and Molecular Biology* 4 (1) (January): Article32. doi:10.2202/1544-6115.1175.

Scherer, Reinhold, Felix Lee, Alois Schlogl, Robert Leeb, Horst Bischof, and Gert Pfurtscheller. 2008. “Toward Self-paced Brain-computer Communication: Navigation through Virtual Worlds.” *IEEE Transactions on Bio-medical Engineering* 55 (2 Pt 1) (February): 675–82. doi:10.1109/TBME.2007.903709.

Scherer, Reinhold, Gernot R. Müller-Putz, Christa Neuper, Bernhard Graimann, and Gert Pfurtscheller. 2004. “An Asynchronously Controlled EEG-based Virtual Keyboard: Improvement of the Spelling Rate.” *IEEE Transactions on Bio-medical Engineering* 51 (6) (June): 979–84. doi:10.1109/TBME.2004.827062.

Scherer, Reinhold, Alois Schloegl, Felix Lee, Horst Bischof, Janez Jansa, and Gert Pfurtscheller. 2007. “The Self-paced Graz Brain-computer Interface: Methods and Applications.” *Computational Intelligence and Neuroscience* 2007 (i) (January): 79826. doi:10.1155/2007/79826.

Schlögl, Alois, Felix Lee, Horst Bischof, and Gert Pfurtscheller. 2005. “Characterization of Four-class Motor Imagery EEG Data for the BCI-competition 2005.” *Journal of Neural Engineering* 2 (4) (December): L14–22. doi:10.1088/1741-2560/2/4/L02.

Schwartz, Andrew B., X. Tracy Cui, Douglas J. Weber, and Daniel W. Moran. 2006. “Brain-controlled Interfaces: Movement Restoration with Neural Prosthetics.” *Neuron* 52 (1) (October 5): 205–20. doi:10.1016/j.neuron.2006.09.019.

Sellers, Eric W., and Emanuel Donchin. 2006. “A P300-based Brain-computer Interface: Initial Tests by ALS Patients.” *Clinical Neurophysiology : Official Journal of the International Federation of Clinical Neurophysiology* 117 (3) (March): 538–48. doi:10.1016/j.clinph.2005.06.027.

Shih, Jerry J., Dean J. Krusienski, and Jonathan R. Wolpaw. 2012. “Brain-computer Interfaces in Medicine.” *Mayo Clinic Proceedings. Mayo Clinic* 87 (3) (March): 268–79. doi:10.1016/j.mayocp.2011.12.008.

Silvia Chiappa, Nicolas Donckers, Samy Bengio, and Frédéric Vrins. 2004. “HMM and IOHMM Modeling of EEG Rhythms for Asynchronous BCI Systems.” *The European Symposium on Artificial Neural Networks* (April): 193–204.

Smith Lindsay I. 2002. “A Tutorial on Principal Components Analysis Introduction.” *Statistics*. USA: Cornell University.

- Solhjo, S., and M. H. Moradi. 2004. "Mental Task Recognition: A Comparison Between Some of Classification Methods." In *In BIOSIGNAL 2004 International EURASIP Conference*, 24–26.
- Squires, Nancy K., Kenneth C. Squires, and Steven A. Hillyard. 1975. "Two Varieties of Long-latency Positive Waves Evoked by Unpredictable Auditory Stimuli in Man." *Electroencephalography and Clinical Neurophysiology* 38 (4) (April): 387–401.
- Stone, James V. 2005. "Independent Component Analysis." In *The Encyclopedia of Statistics in Behavioral Science*, edited by Brian S Everitt and David C Howell. Wiley. doi:10.1002/0470013192.bsa297.
- Tavakolian, Kouhyar, and Simak Rezaei. 2004. "Classification of Mental Tasks Using Gaussian Mixture Bayesian Network Classifiers." In *IEEE International Workshop on Biomedical Circuits and Systems, 2004.*, 347–349. IEEE. doi:10.1109/BIOCAS.2004.1454169.
- Tavella, Michele, Robert Leeb, Rüdiger Rupp, and Jose del. R. Millan. 2010. "Towards Natural Non-invasive Hand Neuroprostheses for Daily Living." In *Conference Proceedings : 2010 Annual International Conference of the IEEE Engineering in Medicine and Biology Society*, 2010:126–9. doi:10.1109/IEMBS.2010.5627178.
- Tomioka, Ryota, Guido Dornhege, Kazuyuki Aihara, and Klaus-Robert Muller. 2006. "An Iterative Algorithm for Spatio-Temporal Filter Optimization". In Verlag der Technischen Universität Graz.
- Tomioka, Ryota, Guido Dornhege, Guido Nolte, Benjamin Blankertz, Kazuyuki Aihara, and Klaus-Robert Muller. 2006. "Spectrally Weighted Common Spatial Pattern Algorithm for Single Trial EEG Classification". Tokyo, Japan.
- Tonin, Luca, Robert Leeb, Michele Tavella, Serafeim Perdikis, and Jose del. R. Millan. 2010. "The Role of Shared-control in BCI-based Telepresence." In *2010 IEEE International Conference on Systems, Man and Cybernetics*, 1462–1466. IEEE. doi:10.1109/ICSMC.2010.5642338.
- Trung, Le, Dat Tran, Tuan Hoang, and Dharmendra Sharma. 2012. "Maximal Margin Approach to Kernel Generalised Learning Vector Quantisation for Brain-Computer Interface." In *19th International Conference on Neural Information Processing*, 191–198. Qatar. doi:10.1007/978-3-642-34487-9\_24.
- Tsui, Chun Sing Louis, John Q Gan, and Huosheng Hu. 2011. "A Self-paced Motor Imagery Based Brain-computer Interface for Robotic Wheelchair Control." *Clinical EEG and Neuroscience : Official Journal of the EEG and Clinical Neuroscience Society (ENCS)* 42 (4) (October): 225–9.
- Ullsperger, P., A. -M. Metz, and H. -G. Gille. 1988. "The P300 Component of the Event-related Brain Potential and Mental Effort." *Ergonomics* 31 (8) (August): 1127–37. doi:10.1080/00140138808966752.

- Urdiales, Cristina, Manuel Fernández-Carmona, José M Peula, Ulises Cortés, Roberta Annichiarico, Carlo Caltagirone, and Francisco Sandoval. 2011. "Wheelchair Collaborative Control for Disabled Users Navigating Indoors." *Artificial Intelligence in Medicine* 52 (3) (July): 177–91. doi:10.1016/j.artmed.2011.05.002.
- Vanacker, Gerolf, Jose del. R. Millan, Eileen Lew, Pierre. W. Ferrez, Ferran Galán Moles, Johan Philips, Hendrik Van Brussel, and Marnix Nuttin. 2007. "Context-based Filtering for Assisted Brain-actuated Wheelchair Driving." *Computational Intelligence and Neuroscience* 2007 (January): 25130. doi:10.1155/2007/25130.
- Vaughan, Theresa M., Dennis J. McFarland, Gerwin Schalk, William A. Sarnacki, Dean J. Krusienski, Eric W. Sellers, and Jonathan R. Wolpaw. 2006. "The Wadsworth BCI Research and Development Program: At Home with BCI." *IEEE Transactions on Neural Systems and Rehabilitation Engineering : a Publication of the IEEE Engineering in Medicine and Biology Society* 14 (2) (June): 229–33. doi:10.1109/TNSRE.2006.875577.
- Velliste, Meel, Sagi Perel, M. Chance Spalding, Andrew S. Whitford, and Andrew B. Schwartz. 2008. "Cortical Control of a Prosthetic Arm for Self-feeding." *Nature* 453 (7198) (June 19): 1098–101. doi:10.1038/nature06996.
- Vialatte, François-Benoît, Monique Maurice, Justin Dauwels, and Andrzej Cichocki. 2010. "Steady-state Visually Evoked Potentials: Focus on Essential Paradigms and Future Perspectives." *Progress in Neurobiology* 90 (4) (April): 418–38. doi:10.1016/j.pneurobio.2009.11.005.
- Vidal, Jacques J. 1973. "Toward Direct Brain-computer Communication." *Annual Review of Biophysics and Bioengineering* 2 (January): 157–80. doi:10.1146/annurev.bb.02.060173.001105.
- Wang, Yijun, Bo Hong, Xiaorong Gao, and Shangkai Gao. 2007. "Implementation of a Brain-computer Interface Based on Three States of Motor Imagery." In *Conference Proceedings : 29th Annual International Conference of the IEEE Engineering in Medicine and Biology Society, 2007*:5059–62. doi:10.1109/IEMBS.2007.4353477.
- Wang, Yijun, Zhiguang Zhang, Yong Li, Xiaorong Gao, Shangkai Gao, and Fusheng Yang. 2004. "BCI Competition 2003--Data Set IV: An Algorithm Based on CSSD and FDA for Classifying Single-trial EEG." *IEEE Transactions on Bio-medical Engineering* 51 (6) (June): 1081–6. doi:10.1109/TBME.2004.826697.
- Ward, Nick S., and Leonardo G. Cohen. 2004. "Mechanisms Underlying Recovery of Motor Function after Stroke." *Archives of Neurology* 61 (12) (December): 1844–8. doi:10.1001/archneur.61.12.1844.
- Weiskopf, Nikolaus, Klaus Mathiak, Simon W. Bock, Frank Scharnowski, Ralf Veit, Wolfgang Grodd, Rainer Goebel, and Niels Birbaumer. 2004. "Principles of a Brain-computer Interface (BCI) Based on Real-time Functional Magnetic Resonance Imaging (fMRI)." *IEEE Transactions on Bio-medical Engineering* 51 (6) (June): 966–70. doi:10.1109/TBME.2004.827063.

- Wolpaw, Jonathan R, Niels Birbaumer, Dennis J. McFarland, Gert Pfurtscheller, and Theresa M. Vaughan. 2002. "Brain-computer Interfaces for Communication and Control." *Clinical Neurophysiology : Official Journal of the International Federation of Clinical Neurophysiology* 113 (6) (June): 767–91.
- Wolpaw, Jonathan R. 2007. "Brain-computer Interfaces as New Brain Output Pathways." *The Journal of Physiology* 579 (Pt 3) (March 15): 613–9. doi:10.1113/jphysiol.2006.125948.
- Wolpaw, Jonathan R., Niels Birbaumer, William J. Heetderks, Dennis J. McFarland, Hunter Peckham, Gerwin Schalk, Emanuel Donchin, Louis A. Quatrano, Charles J. Robinson, and Theresa M. Vaughan. 2000. "Brain-computer Interface Technology: a Review of the First International Meeting." *IEEE Transactions on Rehabilitation Engineering* 8 (2) (June): 164–173. doi:10.1109/TRE.2000.847807.
- Wolpaw, Jonathan R., Gerald E. Loeb, Brendan Z. Allison, Emanuel Donchin, Omar Feix do Nascimento, William J. Heetderks, Femke Nijboer, William G. Shain, and James N. Turner. 2006. "BCI Meeting 2005--workshop on Signals and Recording Methods." *IEEE Transactions on Neural Systems and Rehabilitation Engineering : a Publication of the IEEE Engineering in Medicine and Biology Society* 14 (2) (June): 138–41. doi:10.1109/TNSRE.2006.875583.
- Wolpaw, Jonathan R., and Dennis J. McFarland. 2004. "Control of a Two-dimensional Movement Signal by a Noninvasive Brain-computer Interface in Humans." *Proceedings of the National Academy of Sciences of the United States of America* 101 (51) (December 21): 17849–54. doi:10.1073/pnas.0403504101.
- Wolpaw, Jonathan R., Dennis J. McFarland, Gregory W. Neat, and Catherine A. Forneris. 1991. "An EEG-based Brain-computer Interface for Cursor Control." *Electroencephalography and Clinical Neurophysiology* 78 (3) (March): 252–9.
- Yanagisawa, Takufumi, Masayuki Hirata, Youichi Saitoh, Haruhiko Kishima, Kojiro Matsushita, Tetsu Goto, Ryohei Fukuma, Hiroshi Yokoi, Yukiyasu Kamitani, and Toshiki Yoshimine. 2012. "Electrocorticographic Control of a Prosthetic Arm in Paralyzed Patients." *Annals of Neurology* 71 (3) (March): 353–61. doi:10.1002/ana.22613.
- Yanco, Holly A. 1998. "Wheelesley: A Robotic Wheelchair System: Indoor Navigation and User Interface." *Assistive Technology and Artificial Intelligence* 1458: 256–268. doi:10.1007/BFb0055983.
- Zhang, Dan, Yijun Wang, Xiaorong Gao, Bo Hong, and Shangkai Gao. 2007. "An Algorithm for Idle-state Detection in Motor-imagery-based Brain-computer Interface." *Computational Intelligence and Neuroscience* (January): 39714. doi:10.1155/2007/39714.
- Zhang, Haihong, Cuntai Guan, Kai Keng Ang, and Chuanchu Wang. 2012. "BCI Competition IV - Data Set I: Learning Discriminative Patterns for Self-Paced EEG-Based Motor Imagery Detection." *Frontiers in Neuroscience* 6 (February) (January): 7. doi:10.3389/fnins.2012.00007.

Zhao, QiBin, LiQing Zhang, and Andrzej Cichocki. 2009. "EEG-based Asynchronous BCI Control of a Car in 3D Virtual Reality Environments." *Chinese Science Bulletin* 54 (1) (January 11): 78–87. doi:10.1007/s11434-008-0547-3.

Zimmermann, Raphael, Laura Marchal-Crespo, Janis Edelmann, Olivier Lambercy, Marie-Christine Fluet, Robert Riener, Martin Wolf, and Roger Gassert. 2013. "Detection of Motor Execution Using a Hybrid fNIRS-biosignal BCI: a Feasibility Study." *Journal of Neuroengineering and Rehabilitation* 10 (January): 4. doi:10.1186/1743-0003-10-4.